AN ABSTRACT OF THE THESIS OF

Tim Mefford for the degree of Doctor of Philosophy in Physics presented on May 2, 1995.

Title: A Parallel Numerical Computation of Nucleon Scattering from Nuclei, Including Full Spin Coupling and Coulomb Forces

Abstract approved: Redacted for Privacy

Rubin H. Landau

The microscopic, momentum space, optical potential description of spin $\frac{1}{2} \times \frac{1}{2}$ scattering is extended to include the coupling of the singlet-triplet spin channels and the exact handling of the Coulomb force. Computing performance in constructing the optical potential and in solving the coupled-channels Lippmann-Schwinger equations is enhanced by parallelization via the PVM library. Cross sections and spin observables are predicted for $p - {}^{13}C$ and $p - {}^{3}$He elastic scattering at 500 MeV. The complete set of nucleon-trinucleon reactions is calculated to investigate the sensitivity of these reactions to charge-symmetry breaking effects.

A Parallel Numerical Computation of Nucleon Scattering from Nuclei, Including Full Spin Coupling and Coulomb Forces

by

Tim Mefford

A Dissertation

submitted to

Oregon State University

in partial fulfillment of
the requirements for the
degree of

Doctor of Philosophy

Completed May 2, 1995
Commencement June 1996

Doctor of Philosophy thesis of Tim Mefford presented on May 2, 1995

APPROVED:

Redacted for Privacy

Major Professor, representing Physics

Redacted for Privacy

Head of Department of Physics

Redacted for Privacy

Dean of Graduate School

I understand that my thesis will become part of the permanent collection of Oregon State University libraries. My signature below authorizes release of my thesis to any reader upon request.

Redacted for Privacy

Tim Mefford, Author

ACKNOWLEDGEMENT

Many people have assisted me over the years, and I wish I could thank all of them. My teachers and fellow students were of great value, particularly Dinghui Lu and Guangliang He. I would like to thank my committee members and their substitutes, Dr. Adel Faridani, Dr. David Griffiths, Dr. Victor Madsen, Dr. Albert Stetz, Dr. Allen Wasserman, and Dr. Pat Welch. I am especially grateful to my advisor, Dr. Rubin Landau, for his support over the years. His advice and encouragement has been constant and irreplaceable in the long process of completing this degree. My greatest thanks go to my parents, who sacrificed much so that I might reach my goals.

CONTRIBUTION OF AUTHORS

Lindsey Berge and Ken Amos contributed to the groundwork which led to chapter 2. Section 3.2 is the work of Dinghui Lu in collaboration with Dr. Landau, building on a foundation laid with Dr. Song. Dr. Lu also contributed to sections 3.1 and 3.4. Dr. Landau, has, of course, guided all the work presented here.

TABLE OF CONTENTS

TABLE OF CONTENTS (Continued)

TABLE OF CONTENTS (Continued)

LIST OF FIGURES

LIST OF FIGURES (Continued)

LIST OF TABLES

A PARALLEL NUMERICAL COMPUTATION OF NUCLEON SCATTERING FROM NUCLEI, INCLUDING FULL SPIN COUPLING AND COULOMB FORCES

1. INTRODUCTION

Increasingly sophisticated measurements of nuclear scattering reactions have made intermediate energy elastic collisions a demanding test of theory. New and sophisticated techniques for polarizing targets and beams have expanded the number of physical observables beyond cross-sections and analyzing powers, which were the rule only a few years ago. [1,2] Even these quantities are now measured with increasing accuracy. Predicting the results of these experiments accordingly requires more precise and complete calculations using more accurate theories. This increasing precision and completeness demands a more powerful computing approach. This thesis attempts to provide these advances.

New observables require new theory. Initial analyses of the spin $\frac{1}{2} \times \frac{1}{2}$ scattering problem limited themselves to the nucleon- nucleon problem. In that case, the generalized Pauli principle permits the neglect of the f term in the scattering amplitude, which would otherwise mix the spin singlet and spin triplet states. Singlet-triplet coupling occurs, for instance, when a projectile and target pair whose spins are counter-aligned prior to reacting end the reaction with their spins aligned. Inclusion of this f term correctly is a necessary prerequisite to predicting the spin observables in polarized nuclear target-polarized nucleon beam experiments because

the beam and target are not identical particles and so singlet- triplet coupling may occur.

A long standing challenge in nuclear physics has been the simultaneous treatment of the Coulomb and nuclear forces in momentum space. This is largely because the Coulomb potential becomes infinite at zero momentum, yet falls off slowly at infinite momentum, where the nuclear potential falls off rapidly. An accurate handling of the Coulomb force is necessary not only because of the magnitude of the potential, but also because it is a source of charge-symmetry violation which must be fully included in the calculation before more fundamental sources can be investigated. Because the of the extreme behavior of the Coulomb potential, as well as the need to simultaneously treat the strong potential accurately, the Coulomb and nuclear problem require high accuracy and great computer resources to predict its complete effect.

Once in place, a sufficiently accurate theory of scattering, and a code to predict it, can be used to test the assumptions which underlie it. For instance, charge symmetry is an approximate symmetry of the strong force. If all other elements of the theory are sufficiently accurate, the degree of violation should manifest itself in differences with the results of precise experiments. We attempt to make such predictions, noting the reliability of the results and the conclusions which may be drawn.

PPP is a code to predict these spin $\frac{1}{2} \times \frac{1}{2}$ reactions. It has been developed over many years by many people. [3,4] It solves the Lippman-Schwinger equation for a microscopic momentum space optical model and predicts the scattering cross section and spin observables. Developed from a code originally written to predict pion scattering, it has been modified many times over the years. Only through continued modification will it be able to keep up with the advances made in experiment. The

increased number of observables and increased numerical complexity has made the calculation larger and more time consuming. Any further advances will, presumably, continue to do so. Therefore, a new version of the code, one faster and capable of handling larger numbers of variables is a necessity. Hopefully, this thesis provides for these requirements. Parallel computing is fast, modular, and increasingly becoming the standard for high performance computing.

2. A SCHRÖDINGER OPTICAL-POTENTIAL CALCULATION OF 500 MEV POLARIZED PROTON SCATTERING FROM POLARIZED ^{13}C

T. Mefford and R.H. Landau

Physics Department, Oregon State University, Corvallis, OR

L.Berge and K. Amos

School of Physics, University of Melbourne, Parkville, Victoria 3052, Australia

(Published in Physical Review C **50** 1648, 1994.)

Spin observables for elastic $p - {}^{13}C$ scattering at 500 and 547 MeV are calculated using a microscopic, momentum-space optical potential in a relativistic Schrödinger equation. Included are the full spin dependences, off-energy-shell kinematics and dynamics, several models for the nuclear structure, exact treatment of the Coulomb force, and spin singlet-triplet mixing. Agreements with data are good for some observables but, in other observables, indicate the need for additional physics.

2.1. INTRODUCTION

Recent experimental advances have combined polarized nuclear targets with polarized proton beams to measure more and more of the 36 possible spin observables describing the elastic scattering of two spin 1/2 particles [5–8]. Most of these observables have never been measured before at intermediate energies, and it is of basic interest to understand what aspects of nuclear spin dynamics may be revealed by them. This is a challenging problem because, on the one hand, the connection between an observable and dynamics is often not direct [9], and, on the other hand, a spin observable often arises from delicate interferences within the scattering amplitude. Accordingly, it is not surprising to find a theory that is fine for predicting differential cross sections and analyzing powers has problems with the spin observables.

In the present work we report on a microscopic, optical-potential calculation of polarized-proton scattering from a polarized ^{13}C nucleus. We use a microscopic,

first order potential in momentum space, including the full spin structure of the proton-nucleon and proton-carbon interactions, spin singlet–triplet mixing, and an exact treatment of the Coulomb potential via an extension of the Vincent-Phatak matching procedure. We solve a relativistic Lippmann-Schwinger equation and make comparisons to available data near 500 MeV. While we find good agreement between our predictions and experiment for some observables, we also find poor agreement, for no apparent reason, with others.

As part of the present work we have extended the Stapp phase-shift analysis of nucleon-nucleon scattering [10,11] to the more general case of nonidentical spin 1/2 particles in the angular momentum basis. The requisite coupling of the spin singlet and triplet channels is equivalent to including isospin-symmetry breaking effects in the NN problem. Related extensions have been made by Gersten et al. [12] in the helicity basis with specialization to one-boson exchange potentials, and by Williams et al. [13] in Born approximation.

In contrast to the full solutions of the p-^{13}C Lippmann-Schwinger equation reported here, the calculations by Seestrom–Morris et al. [5], Ray et al. [6], Hoffmann, Barlett, Ciskowski et al. [7], and Hoffmann, Barlett, Kielhorn et al. [8] are based on a relativistic distorted wave impulse approximation. While the basic physics in the impulse approximation and optical potential is similar, cancellation effects and the large number of partial waves involved make the predictions sensitive to the theoretical differences. On a more phenomenological level, the DWIA studies first adjust the optical potential to obtain a best fit to the $p - {}^{12}$C scattering data, and then use the corresponding distorted wave to predict $p - {}^{13}$C scattering. Our calculations, in contrast, are independent of $p - {}^{12}$C scattering data, contain different multiple scattering processes, use different assumptions for off-energy-shell kinematics and dynamics, and, although relativistic, contain no negative-energy degrees of freedom.

2.2. SPIN PHENOMENOLOGY

2.2.1. The T Matrix

The $p - {}^{13}\mathrm{C}$ spin $1/2 \times 1/2$ elastic scattering observables all derive from a T matrix which has a spin-space structure much like that for the NN system. If we assume rotation invariance, parity conservation, and time reversal invariance, this structure is [10,14–16]:

$$2\,T(\mathbf{k}',\mathbf{k}) = a + b + (a-b)\vec{\sigma}_n^p\vec{\sigma}_n^C + (c+d)\vec{\sigma}_m^p\vec{\sigma}_m^C + (c-d)\vec{\sigma}_l^p\vec{\sigma}_l^C + e(\vec{\sigma}_n^p + \vec{\sigma}_n^C) + f(\vec{\sigma}_n^p - \vec{\sigma}_n^C), \tag{2.1}$$

where we have suppressed the $(\mathbf{k}',\mathbf{k})$ dependence of a–f. The superscripts "p" and "C" in Eq. (2.1) indicate the projectile and target respectively, while the subscripts indicates a dot product of σ with one of the three independent unit vectors:

$$\hat{\mathbf{n}} = \frac{\mathbf{k}\times\mathbf{k}'}{|\mathbf{k}\times\mathbf{k}'|}, \quad \hat{\mathbf{m}} = \frac{\mathbf{k}-\mathbf{k}'}{|\mathbf{k}-\mathbf{k}'|}, \quad \hat{\mathbf{l}} = \frac{\mathbf{k}+\mathbf{k}'}{|\mathbf{k}+\mathbf{k}'|}, \tag{2.2}$$

where the vectors $\mathbf{k}$ and $\mathbf{k}'$ are the incident and scattered proton momenta in the COM frame and define the scattering plane. The vector $\hat{\mathbf{n}}$ is *normal* to the scattering plane, the vector $\hat{\mathbf{m}}$ is in the scattering plane along the *momentum* transfer $\mathbf{q} = \mathbf{k}' - \mathbf{k}$ direction (*sideways* to the beam direction), and $\hat{\mathbf{l}}$ is in the scattering plane (*longitudinal* to the beam direction). For on-shell ($k' = k$) scattering, the vectors $\hat{\mathbf{l}}$ and $\hat{\mathbf{m}}$ are orthogonal.

In terms of conventional nuclear forces, the $(a+b)$ term in Eq. (2.1) arises from a "central" force, the e and f terms from "spin-orbit" forces, and $(a-b)$, $(c+d)$, and $(c-d)$ from "tensor" forces. In NN scattering the particles are identical, and if the generalized exclusion principle (including isospin) holds true, the f term vanishes. In p-^{13}C scattering, no symmetry principle forbids f and this results in the spin singlet and triplet states being coupled.

2.2.2. Polarization Observables

There are 36 spin observables for the scattering of two spin-1/2 particles which can be formed from the amplitudes in Eq. (2.1) [14,15,17]. The observables recently measured [5,7,8] are related to the amplitudes in Eq. (2.1) by:

$$\frac{d\sigma^{(1)}}{d\Omega} = \frac{1}{2}(|a|^2 + |b|^2 + |c|^2 + |d|^2 + |e|^2 + |f|^2), \tag{2.3}$$

$$A^{(2)}_{oono} = \frac{1}{\sigma} Re(a^* e + b^* f), \tag{2.4}$$

$$A^{(2')}_{ooon} = \frac{1}{\sigma} Re(a^* e - b^* f), \tag{2.5}$$

$$D^{(3)}_{nono} = \frac{1}{2\sigma}(|a|^2 + |b|^2 - |c|^2 - |d|^2 + |e|^2 + |f|^2), \tag{2.6}$$

$$D^{(4)}_{loso} = \frac{1}{\sigma} Im(b^* e + a^* f), \tag{2.7}$$

$$D^{(5)}_{soso} = \frac{1}{\sigma} Re(a^* b + c^* d - e^* f), \tag{2.8}$$

$$A^{(11)}_{oonn} = \frac{1}{2\sigma}(|a|^2 - |b|^2 - |c|^2 + |d|^2 + |e|^2 - |f|^2). \tag{2.9}$$

Here we use the traditional Wolfenstein notation as analyzing powers, polarizations, and depolarizations, as well as the tensor notation $X^{(n)}_{p't'pt}$ with the subscripts p and t denoting the direction of the initial-state projectile and target polarizations, the primes denoting the corresponding final-state quantities, and a subscript o signifies zero or undetected polarization. The superscript (n) refers to the variable number that is tabulated in reference [17], a redundancy we find useful when dealing with difficult-to-pronounce and easy-to-confuse variables.

2.3. OPTICAL POTENTIAL

Our theoretical input is a microscopic, first order, momentum-space optical potential [17,3,18]:

$$V(\mathbf{k}',\mathbf{k}) \simeq N\left\{(t^{pn}_{a+b} + t^{pn}_{e}\vec{\sigma}^{p}_{n})\rho^{n}_{mt}(q)\right.$$

$$
\begin{aligned}
&+\left[t^{pn}_{a-b}\vec{\sigma}^p_n\vec{\sigma}^C_n + t^{pn}_e\vec{\sigma}^C_n + t^{pn}_{c+d}\vec{\sigma}^p_m\vec{\sigma}^C_m + t^{pn}_{c-d}\vec{\sigma}^p_l\vec{\sigma}^C_l + t^{pn}_{c+d}(\vec{\sigma}^p_m\vec{\sigma}^C_l + \vec{\sigma}^p_l\vec{\sigma}^C_m)\right]\rho^n_{sp}(q)\Big\} \\
&+Z\Big\{(t^{pp}_{a+b} + t^{pp}_e\vec{\sigma}^p_n)\rho^p_{mt}(q) \\
&+\left[t^{pp}_{a-b}\vec{\sigma}^p_n\vec{\sigma}^C_n + t^{pp}_e\vec{\sigma}^C_n + t^{pp}_{c+d}\vec{\sigma}^p_m\vec{\sigma}^C_m + t^{pp}_{c-d}\vec{\sigma}^p_l\vec{\sigma}^C_l + t^{pp}_{c+d}(\vec{\sigma}^p_m\vec{\sigma}^C_l + \vec{\sigma}^p_l\vec{\sigma}^C_m)\right]\rho^p_{sp}(q)\Big\} \\
&\stackrel{def}{=} \frac{1}{2}\Big[V_{a+b}(\vec{k}',\vec{k}) + V_{a-b}(\vec{k}',\vec{k})\vec{\sigma}^p_n\vec{\sigma}^C_n + V_{c+d}(\vec{k}',\vec{k})\vec{\sigma}^p_m\vec{\sigma}^C_m \\
&+ V_{c-d}(\vec{k}',\vec{k})\vec{\sigma}^p_l\vec{\sigma}^C_l + V_e(\vec{k}',\vec{k})(\vec{\sigma}^p_n + \vec{\sigma}^C_n) + V_f(\vec{k}',\vec{k})(\vec{\sigma}^p_n - \vec{\sigma}^C_n)\Big], \qquad (2.10)
\end{aligned}
$$

where the subscripts on t indicate their origins in terms of the elementary NN amplitudes. This potential manifestly contains the spin $1/2 \times 1/2$ dependence of nucleon-nucleon scattering weighted by four, possibly different, form factors describing the distributions of spin (sp) and matter (mt) for point protons and neutrons within the nucleus. The finite size of the nucleon is included in the pN t matrices, and thus must be removed from the form factors. To improve upon this theory one could include antisymmetrization of the projectile nucleon with the unstruck nucleons in the nucleus, NN correlations within the nucleus, intermediate nuclear excitations, Dirac-like relativity, and meson or quark currents.

If the charge and magnetic form factors of the mirror nuclei ^{13}C and ^{13}N were known, if isospin were a perfect symmetry, and if we could remove the meson-exchange currents from the electromagnetic form factors, then we could deduce the strong interaction form factors from these electromagnetic ones. While such is the case for the three-nucleon system, it is not yet possible for the 13-nucleon system. Instead we assume an independent particle shell model description of ^{13}C as a $1p_{\frac{1}{2}}$ valence neutron outside of a ^{12}C core of closed $1s_{\frac{1}{2}}$ and $1p_{\frac{3}{2}}$ shells. While it is known that the ^{12}C core is not spherical, and that core excitations play an important role in reactions with ^{12}C, we remain consistent with the assumptions of a first order

optical potential that ignores virtually excited intermediate states. For a harmonic oscillator shape for the nucleus [19], the corresponding form factors are:

$$\rho^p_{mt}(r) = \rho_0 \left[1 + \frac{N-2}{3}\frac{r^2}{a^2}\right] e^{-r^2/a^2}, \tag{2.11}$$

$$\rho^p_{mt}(q) = \left[1 - \frac{Z-2}{6}q^2a^2\right] \frac{e^{-q^2a^2/4}}{f(q)}, \quad \rho^p_{sp}(q) = 0, \tag{2.12}$$

$$\rho^n_{sp}(q) = \left[1 - \frac{q^2a^2}{6}\right] \frac{e^{-q^2a^2/4}}{3Nf(q)}, \tag{2.13}$$

$$\rho^n_{mt} = \left[1 - \frac{(N-2)q^2a^2}{6}\right] \frac{e^{-q^2a^2/4}}{f(q)} e^{-q^2a^2/4}, \tag{2.14}$$

$$f(q) = \left(1 + q^2/18.2\ \mathrm{fm}^{-2}\right)^{-2}, \quad a = 1.58\mathrm{fm}. \tag{2.15}$$

For ^{13}C, the parameters $(N, Z) = (7, 6)$, the 3 in Eq. (2.13) arises from the spin-angle function describing the $1p_{\frac{1}{2}}$ valence neutron, and the $f(q)$ is the form factor for the elementary nucleon [20]. Because ^{12}C and ^{13}C have root-mean-square radii which differ by only 0.02fm [19], we took the parameters of the charge distribution of ^{12}C [19] as the proton parameters for ^{13}C parameters, and, there being no strong evidence to the contrary, we assume the parameters for the neutron and proton matter distributions are equal. In contrast, Hoffmann et al. [7] and Ray et al. [6] vary the neutron size to obtain a better fit the elastic $p - {}^{12}$C data.

The same assumptions for the form factors are made when we parameterize them with the Fermi or Wood-Saxon shape,

$$\rho(r) = \frac{\rho_0(1 - 0.149\, r^2/R^2)}{1 + e^{(r-R)/a}}, \tag{2.16}$$

$$(R, a, r_{rms}) = (2.172, 0.5690, 2.38)\mathrm{fm}. \tag{2.17}$$

We calculate the $\rho(q)$ by a numerical Fourier transform. First we determine the partial wave expansion of $\rho(q)$ at a large value of the momentum transfer $q = q_{max} = 5.2\mathrm{fm}^{-1} \stackrel{def}{=} 2k_m$:

$$\rho(q) \simeq \sum_{l=0}^{48} \rho_l(k_m, k_m) P_l(1 - q^2/2k_m^2), \tag{2.18}$$

$$\rho_l(k_m, k_m) = 4\pi(2l+1) \int_0^\infty dr r^2 \rho(r) j_l(k_m) j_l(k_m) \ , \tag{2.19}$$

where we use 96 integration points in Eq. (2.19). The numerics were checked by reproducing over five decades the form factor published by Frosch et al [21]. For momentum transfers larger than q_{max} we use an analytic expression which falls off exponentially in q^2 and which matches the magnitude and slope of our numeric one at q_{max}:

$$\rho(q) = \rho(q_{max}) e^{-(q^2 - q_{max}^2)/\alpha} \qquad (q > q_{max}). \tag{2.20}$$

Because there are no electron scattering measurements for these large values of q, Eq. (2.20) provides a well-behaved extrapolation with insignificant influence upon our computed cross sections. The off-energy-shell nucleon-nucleon T matrices (t) in the optical potential Eq. (2.10) are transformed to the p-^{13}C COM with a Lorentz covariant prescription, and an impulse approximation is made which optimizes the factorization approximation [3,18]:

$$t^{pN} \ = \ \langle \mathbf{k}', \mathbf{p}_0 - \mathbf{q} |\ t^{pN}(\omega[E])\ | \mathbf{k}, \mathbf{p}_0 \rangle \ , \tag{2.21}$$

$$\mathbf{p}_0 \ = \ -\frac{\mathbf{k}}{A} + \frac{A-1}{2A}\,\mathbf{q}. \tag{2.22}$$

We take ω in Eq. (2.21) to be the "3-body energy",

$$\omega^2 \ = \ \omega_{3B}^2 \ = \ (k_p^\mu + k_A^\mu - P^\mu)^2, \tag{2.23}$$

$$P^2 \ \simeq \ \frac{A-1}{A}(k^2 + \frac{q^2}{4p_f^2} + \mathbf{q}\cdot\mathbf{k}), \quad p_f = 185\mathrm{MeV/c}, \tag{2.24}$$

which clearly includes some recoil and binding effects into the first order potential. This procedure leads to a different momentum and NN energy for each p-nucleus scattering angle.

The off-shell variation of the NN t matrices in each eigenchannel $\alpha = (JlS)$ is described with a separable potential,

$$\langle \kappa' \,|\, t_\alpha(\omega) \,|\, \kappa' \rangle \;=\; \frac{g_\alpha(\kappa') g_\alpha(\kappa)}{g_\alpha^2(\kappa_0)} \langle \kappa_0 |\; t_\alpha(\omega) \,|\, \kappa_0 \rangle \,, \tag{2.25}$$

where $\langle \kappa_0 |\; t_\alpha(\omega) \,|\, \kappa_0 \rangle$ is the on-shell amplitude determined from the phase-shift analyses of Arndt [22] (see Ref. [18] for a demonstration of the NN phase shift sensitivity). We use the Graz NN potential [23] because its off-shell behavior closely approximates that of the Paris potential and provides consistent relativistic propagators in the two- and many-body systems. Because these elementary amplitudes are antisymmetrized, our optical potential inherently includes the exchange of the projectile and struck nucleon, but not with the other nucleons in the nucleus.

While not obvious from the form of the optical potential Eq. (2.10), the terms arising from the NN spin-orbit amplitude t_e, when converted to the standard form of equation Eq. (2.1), generate the V_e and V_f terms in the carbon potential:

$$\begin{aligned} &V_e(\vec{\sigma}_n^p + \vec{\sigma}_n^C) + V_f(\vec{\sigma}_n^p - \vec{\sigma}_n^C) \equiv \\ &\quad N\left[t_e^{pn}\vec{\sigma}_n^p \rho_{mt}^n + t_e^{pn}\vec{\sigma}_n^C \rho_{sp}^n\right] + Z\left[t_e^{pp}\vec{\sigma}_n^p \rho_{mt}^p + t_e^{pp}\vec{\sigma}_n^C\right], \end{aligned} \tag{2.26}$$

and this implies:

$$V_e = \frac{1}{2}\left[N t_e^{pn}(\rho_{mt}^n + \rho_{sp}^n) + Z t_e^{pp}(\rho_{mt}^p + \rho_{sp}^p)\right], \tag{2.27}$$

$$V_f = \frac{1}{2}\left[N t_e^{pn}(\rho_{mt}^n - \rho_{sp}^n) + Z t_e^{pp}(\rho_{mt}^p - \rho_{sp}^p)\right]. \tag{2.28}$$

Accordingly, V_f vanishes only if the distributions of neutron spin and neutron matter are the same, as well as the distributions of proton matter and spin (equalities not realized for ^{13}C).

2.4. COUPLED-CHANNELS LIPPMANN SCHWINGER EQUATION

Many-body effects and relativity leads to a potential V incorporating complicated nonlocalities. Rather than treat such a potential in coordinate space and solve an integro-differential Schrödinger equation, we solve the Lippmann-Schwinger equation in momentum space:

$$T(\vec{k}',\vec{k}) = V(\vec{k}',\vec{k}) + \int \frac{d^3p}{E^+ - E(p)} V(\vec{k}',\vec{p})\, T(\vec{p},\vec{k}), \tag{2.29}$$

where $E(p) = E_p(p) + E_C(p)$ is the projectile plus target energy and the $+$ superscript indicates a positive $i\epsilon$ has been added to the on-shell energy. To obtain one-dimensional integral equations, we expand T and V in spin-angle functions and substitute into this equation. A complication arises in our problem from the ability of the $V_f(\vec{\sigma}_n^p - \vec{\sigma}_n^C)$ term in the optical potential Eq. (2.10) to mix singlet and triplet states:

$$\langle 0,0|V|1,1\rangle \;= -\frac{i}{\sqrt{2}} V_f(\vec{k}',\vec{p}). \tag{2.30}$$

Accordingly, an extension of the phase shift analysis used for NN scattering [10,11] is needed and is given in the Appendix. We show there that the integral equations in the partial-wave basis have form:

$$\begin{bmatrix} T^{j(s_1s_1)}_{l_a\,l_a} \\ T^{j(s_2s_1)}_{l_b\,l_a} \end{bmatrix} = \begin{bmatrix} V^{j(s_1s_1)}_{l_a\,l_a} \\ V^{j(s_2s_1)}_{l_b\,l_a} \end{bmatrix} + \int_0^\infty \frac{p^2dp}{E^+ - E(p)} \begin{bmatrix} V^{j(s_1s_1)}_{l_a\,l_a}(k'p)\; V^{j(s_1s_2)}_{l_a\,l_b}(k',p) \\ V^{j(s_2s_1)}_{l_b\,l_a}(k',p)\; V^{j(s_2s_2)}_{l_b\,l_b}(k',p) \end{bmatrix} \begin{bmatrix} T^{j(s_1s_1)}_{l_a\,l_a}(p,k) \\ T^{j(s_2s_1)}_{l_b\,l_a}(p,k) \end{bmatrix} \tag{2.31}$$

where we leave off the (k',k) dependence of the leftmost T's and V's, and use l, s, and j to denote the orbital, spin, and total angular momenta. We solve these equations on a grid of 40 momentum values for 48 angular momentum (l) values, which is large enough to avoid numerical noise.

The Vincent-Phatak technique for including the Coulomb potential in momentum-space calculations was formulated originally for uncoupled channels and low energies [24]. For the present calculation we have extended it [25] to coupled angular-momentum channels and to much larger numbers of partial waves and grid points. The Coulomb potential which we add to the optical potential is the Fourier transform of a potential arising from the actual nuclear charge distribution cut-off at some radius R_{cut}:

$$V_{coul}^{cut}(\mathbf{k}', \mathbf{k}) = \frac{Z_P Z_T e^2}{2\pi^2 q^2} \left[\rho(q) - \cos(qR_{cut})\right] . \tag{2.32}$$

In the present calculations we take $R_{cut} = 8$ fm, and have verified that our predictions are insensitive to a $1 - 2$ fm variation around this value. In this way the short-range nuclear force and the finite-range corrections to the Coulomb force are included directly in the Lippmann-Schwinger equation. The scattering from the point-Coulomb potential is included by adding the amplitude for scattering from a point-Coulomb potential f_{pt}^c to the a and b amplitudes:

$$\begin{pmatrix} a(\theta) \\ b(\theta) \end{pmatrix} \rightarrow \begin{pmatrix} a(\theta) + f_{pt}^c(\theta) \\ b(\theta) + f_{pt}^c(\theta) \end{pmatrix}. \tag{2.33}$$

2.5. RESULTS

The $p - {}^{13}$C experimental observables are determined by computing the a–f amplitudes and then substituting them into Eqs. (2.3)–(2.9). In trying to understand the observables it is helpful to have a picture of the behavior of these $p - {}^{13}$C amplitudes as a function of scattering angle. We present such a picture in Fig. 2.1, where we set the scale by dividing the amplitudes by the square root of the cross section. Note that these amplitudes are for $p - {}^{13}$C, and accordingly have more oscillations and a greater falloff with momentum transfer than the elementary NN a-e amplitudes from which they derive.

We see in Fig. 2.1, that a and b are approximately equal in magnitude and in phase with each other, that e and f are also approximately equal in magnitude and in phase with each other, but that c and d are much smaller than the other amplitudes and of opposite phase to each other. Because the observables in Eq. (2.3)-(2.9) are the sums of products of these amplitudes, we generally expect an observable to be large if it contains the product of two large amplitudes and to be small if it contains only c and d. However, the converse is not true, cancellation between large amplitudes can produce small values for an observable.

In Fig. 2.2 we compare the predicted cross-sections to cross sections measured by Hoffmann et al. [7] at 500 MeV and by Seestrom-Morris et al. [5] at 547 MeV. We see that the theory produces good agreement with the forward peak of the 547 MeV data, is slightly too low for the 500 MeV data, and slightly too high for the larger-angle data. The locations of the minima and maxima in the 500 MeV data appear to be predicted well, which is important because the spin observables, being inversely proportional to $d\sigma/d\Omega$, are sensitive to the locations of these minima.

Although at first we believed the discrepancy in the 500 MeV forward differential cross sections showed the need to include Coulomb or channel coupling effects more correctly, the disagreement persists even with an exact treatment of the Coulomb force in a full coupled-channels formalism [25]. To see if the discrepancy is a size effect, in the top part of Fig. 2.3 we present predictions for $d\sigma/d\Omega$ using slightly smaller rms sizes (0.07 fm) and the harmonic oscillator form for the nuclear densities, Eqs. (2.11)-(2.15). We conclude that no simple size or shape change provides agreement with the forward peak of the 500 MeV data, and that there may be a small inconsistency between the 500 and 547 MeV data sets.

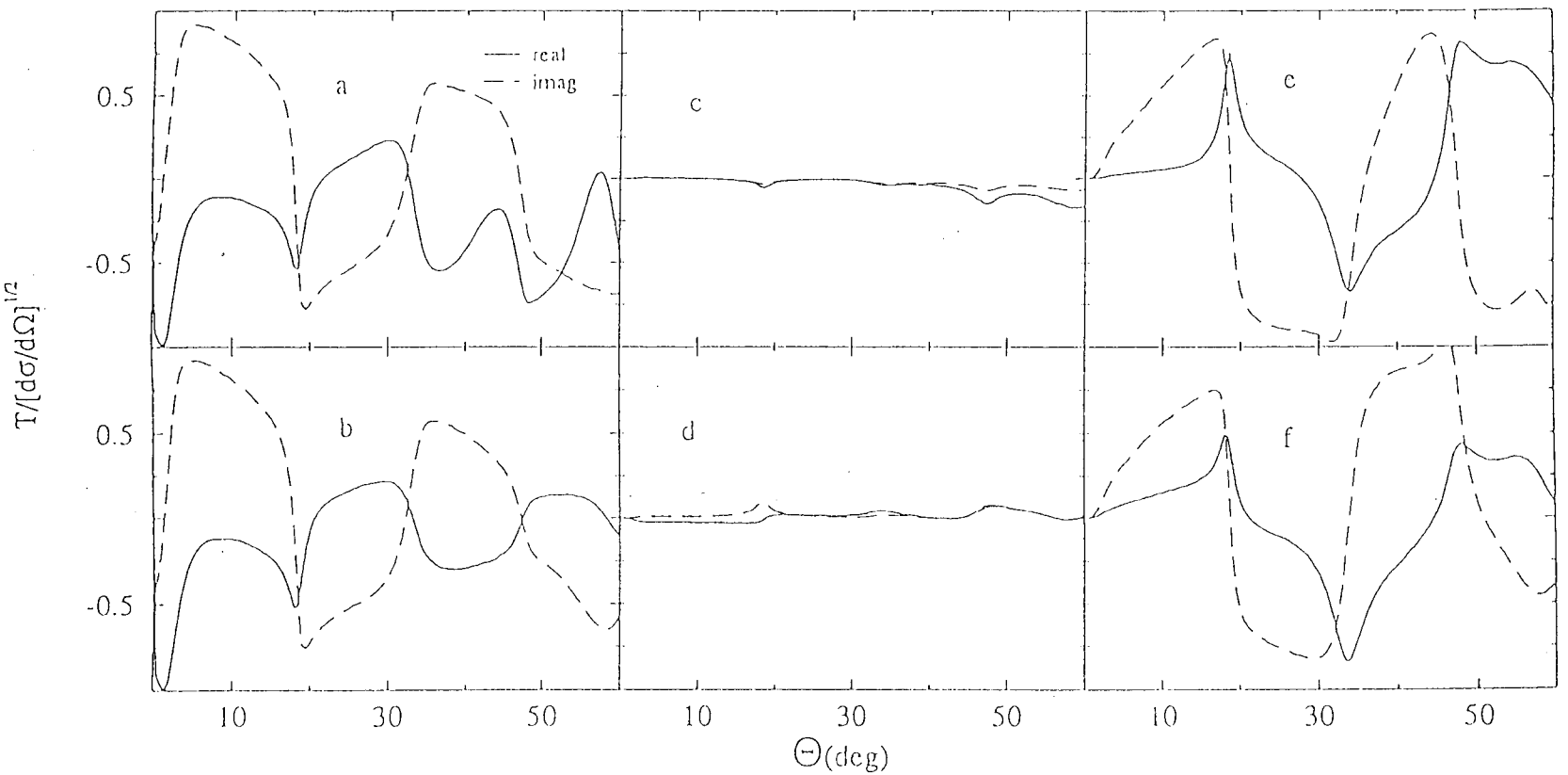

Figure 2.1. The $p - {}^{13}\mathrm{C}$ spin amplitudes a-f of equation (2.1) as a function of scattering angle at 500 MeV. The amplitudes are divided by the square root of the differential cross sections to match the way they contribute to the spin observables in (2.3)-(2.9).

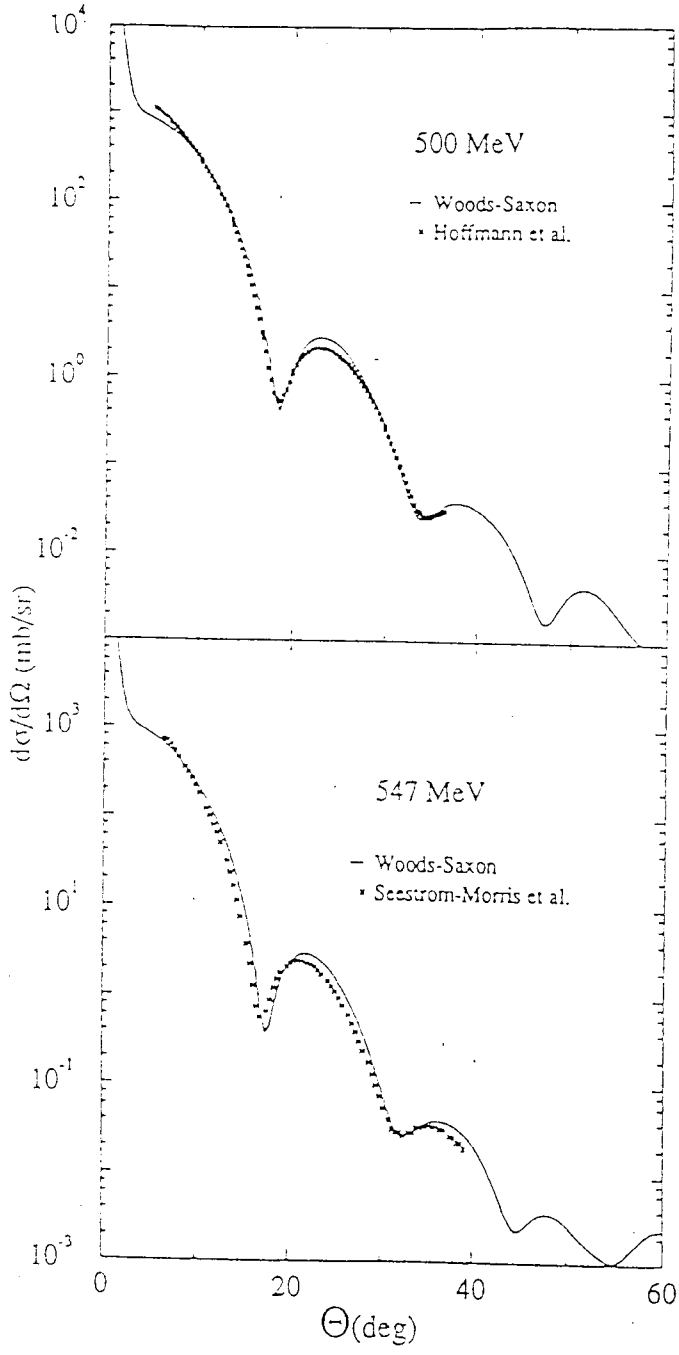

Figure 2.2. Predictions for the $p - {}^{13}C$ differential cross section at 500 MeV (top) and 547 MeV (bottom) compared, respectively, with the data of Hoffmann et al. [7] and Seestrom–Morris et al. [5]. The nucleus is described with the Wood-Saxon shape (2.16).

We have already indicated that a new aspect of the present study is its exact treatment of spin singlet-triplet coupling and the ensuing generation of the $f(\vec{\sigma}_n^P - \vec{\sigma}_n^C)$ term of the scattering amplitude Eq. (2.1). In Fig. 2.3 we show the importance of this f amplitude in the differential cross section (top) and analyzing power (bottom). As expected from Eq. (2.3), since the modulus squared of all amplitudes add to form $d\sigma/d\Omega$ (with four of the amplitudes being large), the f contribution is significant but not dominating. However, as may be expected from Eq. (2.9), since these same six amplitudes contribute to $A_{00nn}^{(11)}$ with cancellations (bottom of Fig. 2.3), f is more important there. Indeed, the dramatic improvement in the prediction of $A_{00nn}^{(11)}$ once f is included (bottom of Fig. 2.3), builds confidence in our treatment of the f term. However, the almost complete cancellation of amplitudes occurring in our prediction of $A_{00nn}^{(11)}$ (we are essentially predicting zero) warns that the spin observables may well be very sensitive to otherwise small effects in the theory.

In Fig. 2.4 we show predictions and data for the projectile analyzing power $A_{oono}^{(2)}$ (top) and the polarized target asymmetry $A_{ooon}^{(2')}$ (bottom). As we see from comparing the phenomenological forms Eqs. (2.4) and (2.5), $A_{oono}^{(2),(2')} \propto Re(a^* e \pm b^* f)$, and so involve identical combinations of amplitudes with only the sign of the $b^* f$ term differing. The fact that the computed observables differ significantly indicates that the f amplitude is large. Further, as we see by comparing the top and bottom of Fig. 2.4, there is slightly too much *constructive* interference in the forward $A_{oono}^{(2)}$ and slightly too much *destructive* interference in the forward $A_{ooon}^{(2')}$. Because Fig. 2.1 shows that a and b tend to be in phase with each other, and that e and f tend to be in phase with each other, we suspect that our $a - e$ relative phase is not quite correct. In a non coupled-channels, spin $0 \times 1/2$ Schrödinger equation calculation, Arellano et al. [26] find a small forward peak in $A_{oono}^{(2)}$ when

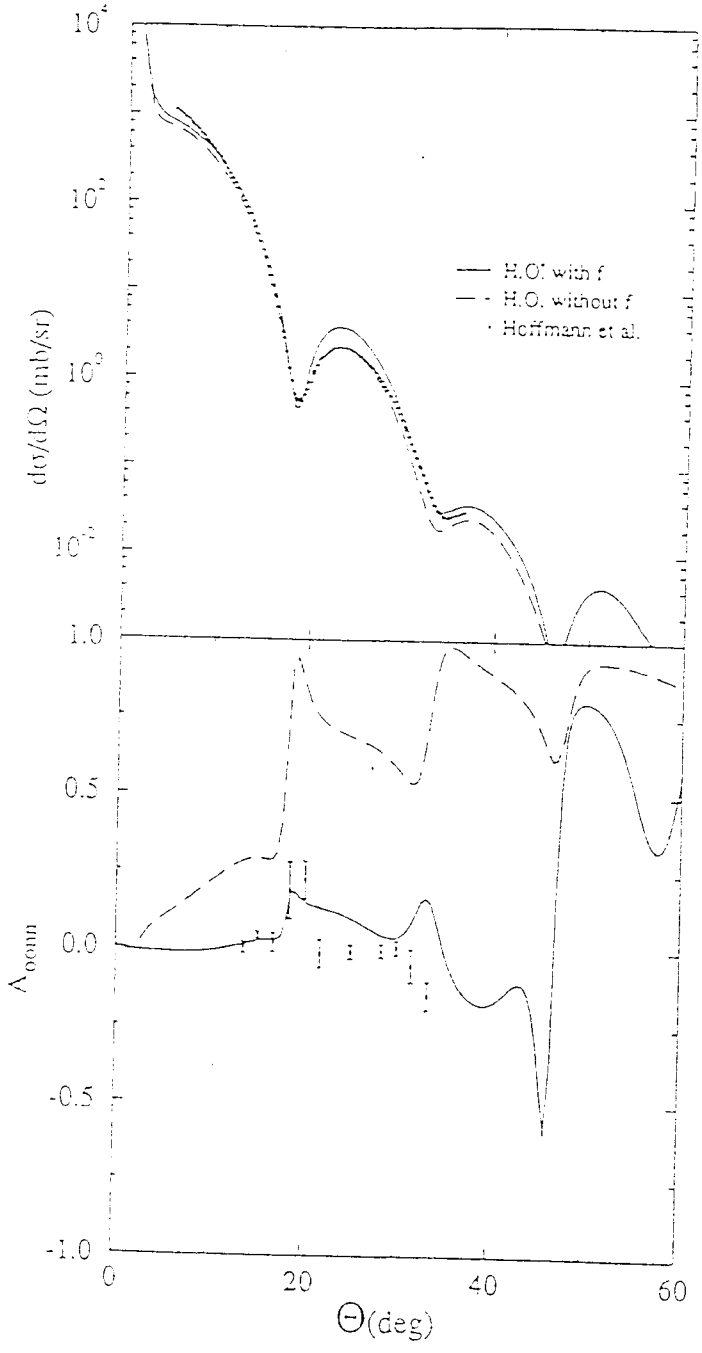

Figure 2.3. The 547 MeV $p - {}^{13}C$ differential cross section (top) and polarized target-polarized beam analyzing power $A^{(11)}_{oonn}$ (bottom) compared to the data of Seestrom-Morris et al. [5]. The nucleus is described with the harmonic oscillator shape, (2.11)-(2.15). The dashed curves are the predictions with no f amplitude.

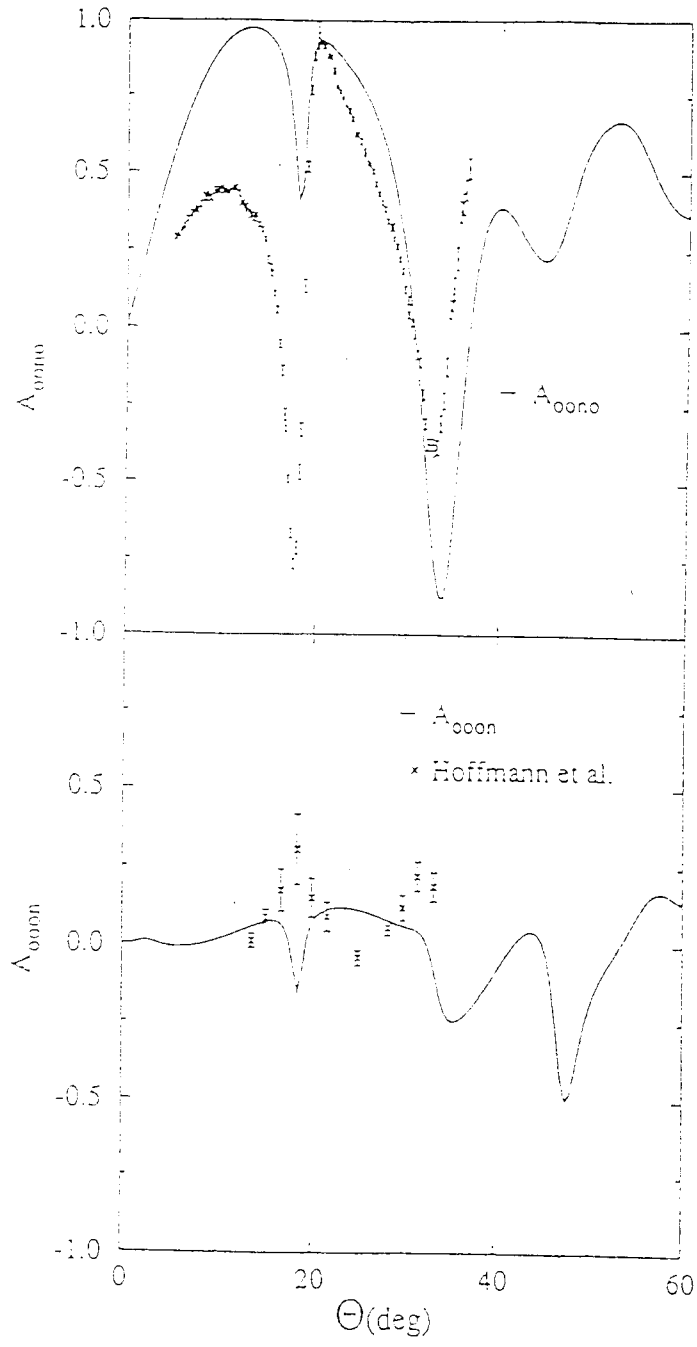

Figure 2.4. The projectile analyzing power $A^{(2)}_{0ono}$ (top), and the polarized target asymmetry $A^{(2')}_{0oon}$ (bottom), compared with the 500 MeV data of Hoffmann et al. [7].

full Fermi average is performed; others [6], however, obtain good agreement without full-folding but with the Dirac equation.

In the top part of Fig. 2.5 we compare theoretical and experimental values for the depolarization in the normal direction $D^{(3)}_{nono}$. The deviation of this observable from 1 measures spin-flip scattering which is interesting because it should be sensitive to the valence neutron in ^{13}C. However, as we see from its phenomenological form Eq. (2.6), all the large amplitude which enter into $D^{(3)}_{nono}$ are added together in moduli and then the small amplitudes are subtracted. Accordingly, and as is (all too) clear in the top part of Fig. 2.5, although our predictions for $D^{(3)}_{nono}$ agree well with the data, the small deviation from 1 renders the comparison nonrevealing.

In the middle and bottom parts of Fig. 2.5 we compare theoretical and experimental values for the sideways to longitudinal depolarization $D^{(4)}_{loso}$ and the sideways depolarization $D^{(5)}_{soso}$. Whereas the phenomenological forms for both observables, Eqs. (2.7)-(2.8), indicate they should be large in the forward direction, we see that $D^{(4)}_{loso}$ starts off with a strong destructive interference, while $D^{(5)}_{soso}$ commences with a strong constructive interference. As we see in Fig. 2.5, the theory does a very good job at predicting the sharp destructive interference in $D^{(4)}_{loso}$ (which also contains a large contribution from the f amplitude), but does not contain enough constructive interference for agreement with the forward part of $D^{(5)}_{soso}$ (although the location of the precipitous interference minimum in $D^{(5)}_{soso}$ is predicted accurately). Clearly, the relative phases of the amplitudes are important here.

2.6. SUMMARY AND CONCLUSION

We have examined how well a first order, theoretical optical potential can describe the cross sections and spin observables measured in elastic proton scattering from ^{13}C near 500 MeV. The theory includes the full spin dependences for two

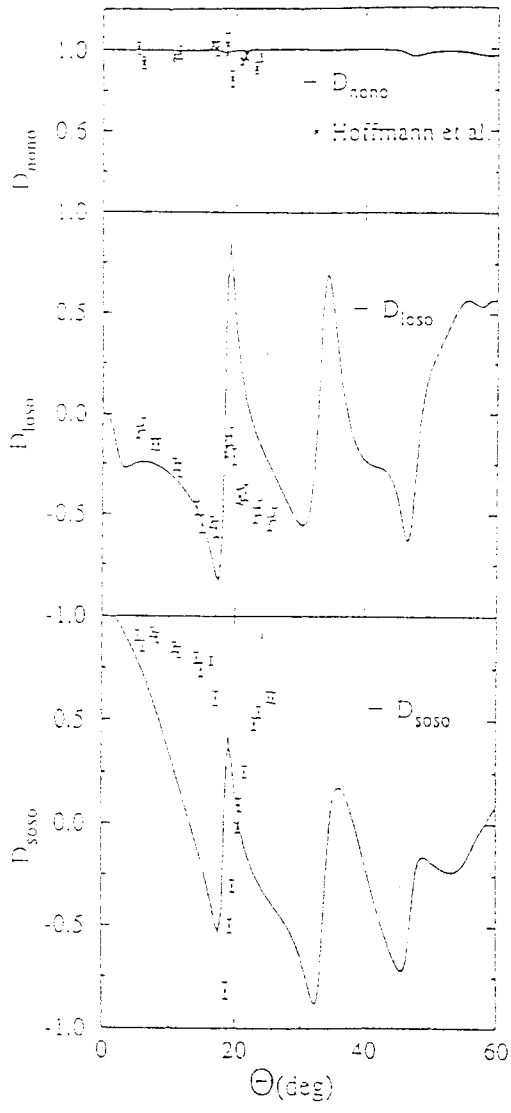

Figure 2.5. The depolarization in the normal direction $D^{(3)}_{nono}$ (top), the sideways to longitudinal depolarization $D^{(4)}_{loso}$ (middle), and the sideways depolarization $D^{(5)}_{soso}$ (bottom) compared with the 500 MeV data of Hoffmann et al. [7].

spin 1/2 particles, singlet-triplet mixing, nonlocalities arising from off-energy-shell behavior of the NN interaction, and Lorentz covariant, off-shell kinematics. When the resulting optical potential is used in a relativistic Schrödinger equation, multiple scattering and exchange effects are included.

These are our first results including the exact singlet-triplet mixing and the inclusion of the Coulomb force for coupled-channels. We find that attaining agreement with the new data is quite a challenge. The theory is basically parameterless (we did however explore the sensitivity to nuclear size), and the spin observables are often the result of delicate interference between as many as six complex amplitudes, with slight variation of the amplitudes leading to significantly different predictions. To be expected, our agreement is not as good as that found in models whose parameters are adjusted to the ^{12}C data as a prerequisite to predicting ^{13}C [5–8,29]. Nevertheless, the level of agreement is comparable with that found by Arellano et al. [26] in a similar study of proton scattering from the simpler spin-0 light nuclei.

Clearly, improvements are needed and we believe the theory is advanced to the stage where they are worthwhile. We have omitted effects known to be important at lower energies such as nuclear correlations, virtual nuclear excitations, Pauli exclusion, and the density dependence of the effective interaction. Probably most important, our theory does not include effects known to be important at intermediate energies, namely the negative energy degrees of freedom present in the Dirac equation [6,28,29], and the full folding over Fermi motion [26].

2.7. ACKNOWLEDGMENTS

We wish to thank Lanny Ray, Victor Madsen, Sid Coon, Otto Häuser, Charlie Drake, and Richard Woloshyn for stimulating and illuminating discussions. We also wish to gratefully acknowledge support from the U.S. Department of Energy under

Grant DE-FG06-86ER40283. In addition, we wish to thank the peoples at the National Institute for Nuclear Theory, Seattle, and in the Physics Department of Melbourne University for their hospitality during part of this work.

2.8. APPENDIX: SPIN DECOMPOSITION

We extend the spin $1/2 \times 1/2$ phase shift analysis [10,11] used for the NN problem in order to include the effect of the V_f potential's mixing of singlet and triplet states. We assume the conventional expansion of T and V in spin-angle functions:

$$V(\vec{k}', \vec{k}) = \frac{2}{\pi} \sum_{jm_j ll' ss'} i^{(l'-l)} V^{j(s's)}_{l'l}(k', k) \mathcal{Y}^{jm_j}_{l's'}(\hat{k}') \mathcal{Y}^{\dagger jm_j}_{ls}(\hat{k}), \tag{2.34}$$

$$T(\vec{k}', \vec{k}) = \frac{2}{\pi} \sum_{jm_j ll' ss'} i^{(l'-l)} T^{j(s's)}_{l'l}(k', k) \mathcal{Y}^{jm_j}_{l's'}(\hat{k}') \mathcal{Y}^{\dagger jm_j}_{ls}(\hat{k}). \tag{2.35}$$

where l, s, and j are the orbital, spin, and total angular momenta for the target plus projectile:

$$\vec{j} = \vec{l} + \vec{s}, \quad \vec{s} = \frac{1}{2}(\vec{\sigma^p} + \vec{\sigma^C}), \quad s = 0(s), 1(t). \tag{2.36}$$

The $\mathcal{Y}$'s in Eq. (2.34)-(2.35) are orthonormal spin-angle functions with the definition and properties [28]:

$$\mathcal{Y}^{jm}_{ls}(\hat{k}) = \sum_{m_s m_l} \langle l m_l s m_s | jm \rangle \, Y^{m_l}_l(\theta, \phi) \, | s m_s \rangle, \tag{2.37}$$

$$Y^m_l(\theta, \phi) = (-1)^m \sqrt{\frac{(2l+1)(l-m)!}{4\pi(l+m)!}} \, P^m_l(\cos\theta) e^{im\phi}, \tag{2.38}$$

$$P^m_l(x) = (1-x^2)^{m/2} \frac{d^m P_l(x)}{dx^m}. \tag{2.39}$$

To evaluate the spin matrix elements, we adopt the Madison Convention in which the z axis is taken as the beam direction $\vec{k}$ ($\phi_i = \theta_i = 0$), and the scattered momentum $\vec{k}'$ is placed in the xz plane ($\theta_f = \theta, \phi_f = 0$). We then follow a two-step

procedure in which we first evaluate [10] the potential Eq. (2.10) in the spin basis $|s, m_s\rangle$, and then invert the angular momentum decomposition of the spin-basis matrix elements. The potential in the spin basis is:

$$V_{s1}(\vec{k}', \vec{k}) \equiv \langle 0,0|V|1,1\rangle = -V_{1s}(\vec{k}', \vec{k}) = V_{s-1}(\vec{k}', \vec{k}) \;=\; \frac{-i}{\sqrt{2}} V_f(\vec{k}', \vec{k}), \tag{2.40}$$

$$\begin{aligned} V_{ss}(\vec{k}', \vec{k}) &\equiv \langle 0,0|V|0,0\rangle \\ &= V_{a+b}(\vec{k}', \vec{k}) - V_{a-b}(\vec{k}', \vec{k}) - V_{c+d}(\vec{k}', \vec{k}) - V_{c-d}(\vec{k}', \vec{k}), \end{aligned} \tag{2.41}$$

$$\begin{aligned} V_{00}(\vec{k}', \vec{k}) &\equiv \langle 1,0|V|1,0\rangle \\ &= V_{a+b}(\vec{k}', \vec{k}) + V_{a-b}(\vec{k}', \vec{k}) + \Big(V_{c+d}(\vec{k}', \vec{k}) - V_{c-d}(\vec{k}', \vec{k})\Big)\cos\theta, \end{aligned} \tag{2.42}$$

$$V_{11}(\vec{k}', \vec{k}) = V_{-1-1} = V_{a+b}(\vec{k}', \vec{k}) + V_{c+d}(\vec{k}', \vec{k})\sin^2\frac{\theta}{2} + V_{c-d}(\vec{k}', \vec{k})\cos^2\frac{\theta}{2}, \tag{2.43}$$

$$\begin{aligned} V_{10}(\vec{k}', \vec{k}) &= -V_{-10} \\ &= \frac{-i}{\sqrt{2}} V_e(\vec{k}', \vec{k}) - \frac{1}{\sqrt{2}} V_{c+d}(\vec{k}', \vec{k})\sin\theta + \frac{1}{\sqrt{2}} V_{c-d}(\vec{k}', \vec{k})\sin\theta, \end{aligned} \tag{2.44}$$

$$\begin{aligned} V_{01}(\vec{k}', \vec{k}) &= -V_{0-1} \\ &= \frac{i}{\sqrt{2}} V_e(\vec{k}', \vec{k}) - \frac{1}{\sqrt{2}} V_{c+d}(\vec{k}', \vec{k})\sin\theta + \frac{1}{\sqrt{2}} V_{c-d}(\vec{k}', \vec{k})\sin\theta, \end{aligned} \tag{2.45}$$

$$V_{1,-1}(\vec{k}', \vec{k}) = V_{-11} = -V_{a-b}(\vec{k}', \vec{k}) + V_{c+d}(\vec{k}', \vec{k})\cos^2\frac{\theta}{2} + V_{c-d}(\vec{k}', \vec{k})\sin^2\frac{\theta}{2}. \tag{2.46}$$

Next we expand the spin matrix elements in angular momentum states:

$$\begin{aligned} \langle s'''m_s'''|V(\vec{k}', \vec{k})|s''m_s''\rangle = \frac{2}{\pi} \sum_{js's'lm_s m_{s'} m_l m_{l'}} & \langle s'''m_s'''|s'm_s'\rangle\, i^{l-l'}\, \langle l'm_l's'm_s'|jm\rangle \\ & \times \langle jm|lm_l sm_s\rangle Y_{l'}^{m_{l'}}(\theta_f, \phi_f)\, V_{l'l}^{js's}(k', k)\, Y_l^{m_l^*}(\theta_i, \phi_i)\, \langle sm_s|s'', m_s''\rangle, \end{aligned} \tag{2.47}$$

where (k, θ_i, ϕ_i) and (k', θ_f, ϕ_f) are the spherical coordinates of the initial and final momenta. The Clebsch-Gordon coefficients vanish unless $l = l' \pm 1, l'$ and $m_j = m_l + m_s = m_l' + m_s'$, and parity conservation requires $|l - l'| = 0, 2$. In the Madison convention the projectile has no angular momentum in its propagation direction and so $m_l = 0$, in which case

$$Y_l^{m_l^*}(\theta_i, \phi_i) = Y_l^0(0,0) = \sqrt{\frac{2l+1}{4\pi}}. \tag{2.48}$$

As an example we consider the V_{s1} term Eq. (2.40) which couples the singlet state to triplet state. Because j is a constant and $s' = 0$ in the final state, the total angular momentum j must equal l'. Parity conservation requires $l = l'$, and because m_s and m_l are 1 and 0, we must have $m_j = 1$, and $m_{l'} = 1$. The sum in Eq. (2.47) then reduces to a simple sum in the final orbital angular momentum l'. In this way we obtain the partial wave decompositions:

$$V_{s1}(\vec{k'}, \vec{k}) = \frac{-\sqrt{2}}{4\pi^2} \sum_{l=1} P_l^1(x = \cos\theta_{k'k}) \frac{2l+1}{\sqrt{l(l+1)}} V_{ll}^{l(st)}(k', k), \tag{2.49}$$

$$V_{ss}(\vec{k'}, \vec{k}) = \frac{1}{2\pi^2} \sum_{l=0} P_l(x)(2l+1)\, V_{ll}^{l(ss)}(k', k), \tag{2.50}$$

$$\begin{aligned} V_{11}(\vec{k'}, \vec{k}) = \frac{1}{4\pi^2} \sum_{l=0} P_l(x) \Big\{ & (l+2) V_{ll}^{l+1(tt)}(k', k) - \sqrt{(l+1)(l+2)}\, V_{ll+2}^{l+1(tt)}(k', k) \\ & + (2l+1) V_{ll}^{l(tt)}(k', k) + (l-1) V_{ll}^{l-1(tt)}(k', k) - \sqrt{(l-1)l}\, V_{ll-2}^{l-1(tt)}(k', k) \Big\}, \end{aligned} \tag{2.51}$$

$$\begin{aligned} V_{00}(\vec{k'}, \vec{k}) = \frac{1}{2\pi^2} \sum_{l=0} P_l(x) \Big\{ & (l+1) V_{ll}^{l+1(tt)}(k', k) + l V_{ll}^{l-1(tt)}(k', k) \\ & + \sqrt{(l+1)(l+2)}\, V_{ll+2}^{l+1(tt)}(k', k) + \sqrt{(l-1)l}\, V_{ll-2}^{l-1(tt)}(k', k) \Big\}, \end{aligned} \tag{2.52}$$

$$\begin{aligned} V_{10}(\vec{k'}, \vec{k}) = \frac{\sqrt{2}}{4\pi^2} \sum_{l=1} P_l^1(x) \Big\{ & -V_{ll}^{l-1(tt)}(k', k) + V_{ll}^{l+1(tt)}(k', k) \\ & + \sqrt{\frac{l+2}{l+1}} V_{ll+2}^{l+1(tt)}(k', k) - \sqrt{\frac{l-1}{l}} V_{ll-2}^{l-1(tt)}(k', k) \Big\}, \end{aligned} \tag{2.53}$$

$$\begin{aligned} V_{01}(\vec{k'}, \vec{k}) = \frac{\sqrt{2}}{4\pi^2} \sum_{l=1} P_l^1(x) \Big\{ & -\frac{l+2}{l+1} V_{ll}^{l+1(tt)}(k', k) + \frac{2l+1}{l(l+1)} V_{ll}^{l(tt)}(k', k) \\ & + \frac{l-1}{l} V_{ll}^{l-1(tt)}(k', k) + \sqrt{\frac{l+2}{l+1}} V_{ll+2}^{l+1(tt)}(k', k) - \sqrt{\frac{l-1}{l}} V_{ll-2}^{l-1(tt)}(k', k) \Big\}, \end{aligned} \tag{2.54}$$

$$\begin{aligned} V_{1-1}(\vec{k'}, \vec{k}) = \frac{1}{4\pi^2} \sum_{l=2} P_l^2(x) \Big\{ & \frac{1}{l+1} V_{ll}^{l+1(tt)}(k', k) - \frac{1}{\sqrt{(l+1)(l+2)}} V_{ll+2}^{l+1(tt)}(k', k) \\ & - \frac{2l+1}{l(l+1)} V_{ll}^{l(tt)}(k', k) + \frac{1}{l} V_{ll}^{l-1(tt)}(k', k) - \frac{1}{\sqrt{l(l-1)}} V_{ll-2}^{l-1(tt)}(k', k) \Big\}. \end{aligned} \tag{2.55}$$

Note that the sums are over the orbital angular momentum of the final state, and that we have combined matrix elements of different j values if they multiply the

same Legendre polynomial (the Lippmann-Schwinger equations couple states with the same j only).

We invert Eqs. (2.49)-(2.55) for the partial wave potentials $V_{l'l}^{j(s's)}(k',k)$ by multipling the equation for each $V_{m'm}$ by $P_l^{|m'-m|}$, and numerically evaluating the integral:

$$I_{m'm}(k',k) = \int_{-1}^{1} dx\, V_{m'm}(\vec{k'},\vec{k})\, P_l^{|m'-m|}(\cos\theta_{k'k}). \tag{2.56}$$

For Eq. (2.49) and Eq. (2.50) the inversion is simple because only one $V_{l'l}^{j(s's)}$ is involved:

$$V_{ll}^{l(st)}(k',k) = V_{ll}^{l(ts)}(k',k) = \frac{-\sqrt{2}\pi^2}{\sqrt{l(l+1)}} I_{s1}(k',k), \tag{2.57}$$

$$V_{ll}^{l(ss)}(k',k) = \pi^2 I_{ss}(k',k). \tag{2.58}$$

The Eqs. (2.51)-(2.55) contain $V_{l'l}^{j(tt)}$'s intermixed for differing j and l values, and so the projection results in five, coupled equations:

$$\vec{I} = B\vec{V} \tag{2.59}$$

$$\begin{pmatrix} I_{11}(k',k) \\ I_{00}(k',k) \\ I_{10}(k',k) \\ I_{01}(k',k) \\ I_{1-1}(k',k) \end{pmatrix} = \begin{pmatrix} \\ \\ B_{l'l}^{m'm} \\ \\ \\ \end{pmatrix} \begin{pmatrix} V_{ll}^{l+1(tt)}(\vec{k'},\vec{k}) \\ V_{ll}^{l(tt)}(\vec{k'},\vec{k}) \\ V_{ll}^{l-1(tt)}(\vec{k'},\vec{k}) \\ V_{ll+2}^{l+1(tt)}(\vec{k'},\vec{k}) \\ V_{ll-2}^{l-1(tt)}(\vec{k'},\vec{k}) \end{pmatrix} \tag{2.60}$$

where $B_{l'l}^{m'm}$ makes up a matrix of coefficients multiplying the V's in Eq. (2.51)-(2.55). We solve the matrix equation (2.60) by matrix inversion,

$$\vec{V} = B^{-1}\vec{I}. \tag{2.61}$$

Finally, we check the procedure by recombining the potential according to Eq. (2.49)-(2.55) and comparing to the original.

The substitution of the partial wave expansions into the three-dimensional Lippmann-Schwinger equation leads to the coupled integral equations:

$$\begin{bmatrix} T_{jj}^{j(ss)} \\ T_{jj}^{j(ts)} \end{bmatrix} = \begin{bmatrix} V_{jj}^{j(ss)} \\ V_{jj}^{j(ts)} \end{bmatrix} + \int_0^\infty \frac{p^2 dp}{E^+ - E(p)} \begin{bmatrix} V_{jj}^{j(ss)}(k',p)\ V_{jj}^{j(st)}(k',p) \\ V_{jj}^{j(ts)}(k',p)\ V_{jj}^{j(tt)}(k',p) \end{bmatrix} \begin{bmatrix} T_{jj}^{j(ss)}(p,k) \\ T_{jj}^{j(ts)}(p,k) \end{bmatrix}, \quad (2.62)$$

$$\begin{bmatrix} T_{jj}^{j(tt)} \\ T_{jj}^{j(st)} \end{bmatrix} = \begin{bmatrix} V_{jj}^{j(tt)} \\ V_{jj}^{j(st)} \end{bmatrix} + \int_0^\infty \frac{p^2 dp}{E^+ - E(p)} \begin{bmatrix} V_{jj}^{j(tt)}(k',p)\ V_{jj}^{j(ts)}(k',p) \\ V_{jj}^{j(st)}(k',p)\ V_{jj}^{j(ss)}(k',p) \end{bmatrix} \begin{bmatrix} T_{jj}^{j(tt)}(p,k) \\ T_{jj}^{j(st)}(p,k) \end{bmatrix}, \quad (2.63)$$

$$\begin{bmatrix} T_{j-1j-1}^{j(tt)} \\ T_{j+1j-1}^{j(tt)} \end{bmatrix} = \begin{bmatrix} V_{j-1j-1}^{j(tt)} \\ V_{j+1j-1}^{j(tt)} \end{bmatrix} + \int_0^\infty \frac{p^2 dp}{E^+ - E(p)} \begin{bmatrix} V_{j-1j-1}^{j(tt)}(k',p)\ V_{j-1j+1}^{j(tt)}(k',p) \\ V_{j+1j-1}^{j(tt)}(k',p)\ V_{j+1j+1}^{j(tt)}(k',p) \end{bmatrix} \begin{bmatrix} T_{j-1j-1}^{j(tt)}(p,k) \\ T_{j+1j-1}^{j(tt)}(p,k) \end{bmatrix} \quad (2.64)$$

$$\begin{bmatrix} T_{j+1j+1}^{j(tt)} \\ T_{j-1j+1}^{j(tt)} \end{bmatrix} = \begin{bmatrix} V_{j+1j+1}^{j(tt)} \\ V_{j-1j+1}^{j(tt)} \end{bmatrix} + \int_0^\infty \frac{p^2 dp}{E^+ - E(p)} \begin{bmatrix} V_{j+1j+1}^{j(tt)}(k',p)\ V_{j+1j-1}^{j(tt)}(k',p) \\ V_{j-1j+1}^{j(tt)}(k',p)\ V_{j-1j-1}^{j(tt)}(k',p) \end{bmatrix} \begin{bmatrix} T_{j+1j+1}^{j(tt)}(p,k) \\ T_{j-1j+1}^{j(tt)}(p,k) \end{bmatrix} \quad (2.65)$$

Eqs. (2.62)-(2.63) describe singlet-triplet coupling arising from the V_f term in the optical potential Eq. (2.10), which in turn produces an f term in the scattering amplitude Eq. (2.1). Eqs. (2.64)-(2.65) describe mixing within the triplet state arising from the tensor-force terms $V_{a-b}, V_{c+d}, V_{c-d}$ in the potential Eq. (2.10). Because the total angular momentum j is a conserved quantity, all coupled states have the same j superscript.

Once the $T_{l'l}^{j(s's)}$'s have been solved for, the matrix elements in the spin basis $\langle s'm_{s'}|T|sm_s\rangle$ are computed via Eqs. (2.49)-(2.55) with the V's replaced by T's. The $a - f$ amplitudes are then:

$$a = \frac{1}{2}\left(T_{11} + T_{00} - T_{1-1}\right), \quad (2.66)$$

$$b = \frac{1}{2}\left(T_{11} + T_{ss} + T_{1-1}\right), \tag{2.67}$$

$$c = \frac{1}{2}\left(T_{11} - T_{ss} + T_{1-1}\right), \tag{2.68}$$

$$d = \frac{1}{2}\left(T_{00} + T_{1-1} - T_{11}\right)/(2\cos\theta_{kk}), \tag{2.69}$$

$$= -\left(T_{10} + T_{01}\right)/(\sqrt{2}\sin\theta_{k'k}), \tag{2.70}$$

$$e = \frac{i}{\sqrt{2}}\left(T_{10} - T_{01}\right), \tag{2.71}$$

$$f = i\sqrt{2}T_{s1}. \tag{2.72}$$

The on-energy-shell T matrix elements in the partial-wave basis are related to the bar phase shifts [12,11]:

$$-2i\rho T^{j(ss)}_{jj}(k_0, k_0) = \cos 2\bar{\gamma}_l e^{2i\bar{\delta}_j} - 1, \tag{2.73}$$

$$-2i\rho T^{j(tt)}_{jj}(k_0, k_0) = \cos 2\bar{\gamma}_l e^{2i\bar{\delta}_{jj}} - 1, \tag{2.74}$$

$$-2i\rho T^{j\,(tt)}_{j\pm1\,j\pm1}(k_0, k_0) = \cos 2\bar{\epsilon}_j e^{2i\bar{\delta}_{j\pm1\,j}} - 1, \tag{2.75}$$

$$-2i\rho T^{j\,(tt)}_{j\pm1\,j\mp1}(k_0, k_0) = -i\sin 2\bar{\epsilon}_j\, e^{i(\bar{\delta}_{j-1\,j}+\bar{\delta}_{j+1\,j})}, \tag{2.76}$$

$$-2i\rho T^{j(ts)}_{jj}(k_0, k_0) = -i\sin 2\bar{\gamma}_l\, e^{i(\bar{\delta}_j+\bar{\delta}_{jj})}, \tag{2.77}$$

$$\rho = 2k_0 \frac{E_p(k_0)E_t(k_0)}{E_p(k_0) + E_t(k_0)}, \tag{2.78}$$

where the parameter $\bar{\gamma}_l$ is the mixing angle between the $|0,0\rangle$ singlet and $|1,1\rangle$ triplet state and the parameter $\bar{\epsilon}_l$ is the mixing angle between the l and $l+2$ triplet states. In Table 2.1 we give the connection to the α notation of Stapp [11] and the N_{spin} notation used in our computer code *Lpotp2*.

Table 2.1. Notations for spin $1/2 \times 1/2$ amplitudes.

$T_{ll'}^{j(ss')}$	$T_{jj}^{j(ss)}$	$T_{jj}^{j(ts)}$	$T_{j-1j-1}^{j(tt)}$	$T_{j+1j-1}^{j(tt)}$	$T_{j+1j+1}^{j(tt)}$	$T_{j-1j+1}^{j(tt)}$	$T_{jj}^{j(tt)}$	$T_{jj}^{j(st)}$
Spin	0	$1 \leftarrow 0$	1	1	1	1	1	$0 \leftarrow 1$
Δl	0	0	0	2	0	-2	0	0
Stapp	α_l	–	$\alpha_{l,l+1}$	α^{l-1}	$\alpha_{l,l-1}$	α^{l+1}	α_{ll}	–
N_{spin}	1	2	3	4	5	6	7	8

[a] $T_{00}^{0(tt)} = T_{-1-1}^{0(tt)} = T_{1-1}^{0(tt)} = T_{-11}^{0(tt)} = 0.$

2.9. REFERENCES

[1] S.J. Seestrom–Morris, M.A. Franey, D. Dehnhard, D.B. Holtkamp, R.L. Bourdie, J.F. Amann, G.C. Idzorek, and C.A. Goulding, Phys. Rev. C **30**, 270 (1984).

[2] L. Ray, G.W. Hoffmann, M.L. Barlett, J.D. Lumpe, B.C. Clark, S. Hama, and R.L. Mercer, Phys. Rev C **37**,1169 (1988).

[3] G.W. Hoffmann, M.L. Barlett, D. Ciskowski, G. Pauletta, M. Purcell, L. Ray, J.F. Amann, J.J. Jarmer, K.W. Jones, S. Penttilä, N. Tanaka, M.M.Gazzaly, J.R. Comfort, B.C. Clark,and S. Hama, Phys. Rev. C **41**, 1651 (1990).

[4] G.W. Hoffmann, M.L. Barlett, W. Kielhorn, G. Pauletta, M. Purcell, L. Ray, J.F. Amann, J.J. Jarmer, K.W. Jones, S. Penttilä, N. Tanaka, G. Burleson, J. Faucett, M. Gilani, G. Kyle, L. Stevens, A.M. Mack, D. Mihailidis, T. Averett, J. Comfort, J. Görgen, J. Tinsley, B.C. Clark, S. Hama, and R.L. Mercer, Phys. Phys. Rev. Letters, **65**, 3096 (1990).

[5] G.R. Goldstein and M.J. Moravcsik, Ann. Phys. (N.Y.) **142**, 219 (1982).

[6] M. Goldberger and K. Watson *Collision Theory*, Wiley, New York, 1964.

[7] H.P. Stapp, T.J. Ypsilantis, and N. Metropolis, Physical Review, **105**, 302 (1957).

[8] A. Gersten, Phys. Rev. C **18**, 2252 (1978); Phys. Rev. C **24**, 2174 (1981).

[9] A.G. Williams, A.W. Thomas, and G.A. Miller, Phys. Rev. C **36**, 1956 (1987).

[10] J. Bystricky, F. Lehar, and P. Winternitz, Le Journal de Physique,**39**,1, (1978).

[11] P. La France and P. Winternitz, Le Journal de Physique, **41**,1391 (1980); correction in [6].

[12] P.L. Csonka, Rev. Mod. Phys **37**, 177 (1965).

[13] R.H. Landau, M. Sagen, and G. He, Phys. Rev. C **41**, 50 (1990).

[14] Although neither T nor V is a wave, we refer to their angular momentum decomposition as a "partial-wave" expansion.

[15] M.J. Paez and R. H. Landau, Phys. Rev. C **29**,2267 (1984); **30**, 1757 (1984); Phys. Lett. **142B**, 235 (1984).

[16] R.H. Landau and M. Sagen, Phys. Rev. C **33**, 447 (1986).

[17] C.W. DeJager, H.DeVries, and C. DeVries, Atomic Data and Nuclear Data Tables **14**, 479 (1974).

[18] B.Bartoli, F. Felicetti, and V.S. Silvestrini, Rev. Nuov. Cim. **2**, 241 (1972).

[19] R.F. Frosch, R. Hofstadter, J.S. McCarthy, G.K. Nöldeke, K.J. vanOostrum, M.R. Yearian, B.C. Clark, R. Herman, and D.G. Ravenhall, Phys. Rev. **174**, 1380 (1968).

[20] R.A. Arndt, L.D. Roper, R.A. Bryan, R.B. Clark, B.J. VerWest, and P. Signell, SAID dial up system, IP no. 128.173.176.61, userid=physics, password=quantum.

[21] K. Schwarz, J. Haidenbauer, and J. Frohlich, Phys. Rev. C **86**, 456 (1986).

[22] C.M. Vincent and S.C. Phatak, Phys. Rev. **10**, 391 (1974).

[23] D. Lu, T. Mefford, G. Song, and R.H. Landau, *Coulomb plus Nuclear Scattering in Momentum Space for Coupled Angular-Momentum States*, OSU preprint, Feb. 1994.

[24] H.F. Arellano, F.A. Brieva, and W.G. Love, Phys. Rev C **41**, 2188 (1990); H.F. Arellano, F.A. Brieva, W.G. Love, and K. Nakayama, *ibid* **43**, 1875 (1991).

[25] L. Ray, Phys. Rev. C 41, 2816 (1990).

[26] L. Ray, Phys. Rev. C 47, 2990 (1993).

[27] B.C. Clark, *Relativstic Dynamics and Quark-Nuclear Physics*, M.B. Johnson and A. Pickelseimer, eds., New York, Wiley, p.302 (1986).

[28] This is the sign convention of Messiah and Goldberger and Watson. It differs by $(-1)^m$ from Abramowitz and Stegun, Jackson, and some unpublished work of Goddard.

3. COULOMB PLUS NUCLEAR SCATTERING IN MOMENTUM SPACE FOR COUPLED ANGULAR-MOMENTUM STATES

Dinghui H. Lu, Tim Mefford, Rubin H. Landau, and Guilian Song*

Department of Physics, Oregon State University, Corvallis, OR 97331

(Published in Physical Review C **50** 3037, (1994).)

---

* Current address: Physics Department, Harbin Normal University, P.R. China.

The Vincent–Phatak procedure for solving the momentum-space Schrödinger equation with combined Coulomb-plus-short-range potentials is extended to angular momentum states coupled by an optical potential—as occurs in spin $1/2 \times 1/2$ scattering. A generalization of the Blatt–Biedenharn phase shift parameterization is derived and applied to 500 MeV polarized-proton scattering from ^{3}He. The requisite high-precision partial-wave expansions and integrations are described.

3.1. INTRODUCTION

The theory and equations of quantum mechanics are represented equally well in coordinate or momentum space. Bound states problems, which by definition deal with normalizable wavefunctions, can actually be solved equally well in either space, while scattering problems, which in the time-independent Schrödinger theory deal with non-normalizable states, are more challenging in momentum space. This challenge arises, in part, because boundary conditions are more naturally imposed in coordinate space, and, in part, because non-normalizable states contain singularities in momentum space and, accordingly, have no Fourier transforms [31]. In spite of the difficulties, momentum-space calculations are important because momentum space is where one derives the nonlocal potentials of many-body and field theories, and because there are fewer approximations needed in momentum space to handle them.

The Coulomb problem in momentum space has actually been "solved" a number of times—possibly starting with Fock's study of the hydrogen atom [33]—yet no one numerical approach appears to provides the requisite precision for all

applications. The real "problem" is that the Coulomb potential between a point projectile (P) and a target (T),

$$V_c(\mathbf{k}', \mathbf{k}) = \frac{Z_P Z_T e^2}{2\pi^2 q^2} \rho(q), \tag{3.1}$$

has a $1/q^2$ singularity arising from the infinite range of the Coulomb potential, and this singularity must somehow be regularized before a numerical solution is implemented. In (3.1), $\mathbf{q} = \mathbf{k}' - \mathbf{k}$ is the difference between the final and initial momenta $\mathbf{k}'$ and $\mathbf{k}$, and $\rho(q)$ is a form factor which accounts for the finite size of the target's charge distribution and makes the potential well-behaved at large q (but not at $q = 0$).

Kwon and Tabakin [34] solved the bound-state problem with the potential (3.1) by using Landé's technique of subtracting a term from (3.1) which makes its integral finite, and then adding in a correction. Alternatively, Cieplý et al. [36] solved the bound-state problem by using a modification of the Vincent–Phatak (VP) procedure [24]. This procedure gives the Coulomb potential a finite range by cutting it off beyond some radius R_{cut}, as shown in Fig. 3.1, and then corrects the asymptotic behavior of the resulting wavefunctions. If the procedure is successful, the calculated scattering will be independent of R_{cut}.

The VP cutoff procedure was originally formulated for intermediate-energy pion scattering from light nuclei [24] where it provided sufficient accuracy for the small number of partial waves involved [4]. However, the accuracy has become a concern for intermediate-energy proton scattering where the proton's much larger mass leads to correspondingly larger momentum transfers and correspondingly greater numbers of partial waves. Crespo and Tostevin [39] and Picklesimer et al. [40] have documented difficulties with the VP procedure, difficulties which appear as a sensitivity of the computed phase shifts to the cutoff radius, or as a several-

percent error in the phase shift when compared to coordinate-space calculations. Both references [39] and [40] suggest algorithms to reduce the errors. Alternatively, Elster et al. [41] applied the two-potential formula to the Coulomb and nuclear potentials and outlined an approach requiring multiple, numeric Fourier transforms between coordinate and momentum spaces. In contrast, Arrellano et al.'s study of intermediate-energy proton scattering from spinless nuclei [10] simply made the VP procedure sufficiently precise by using the high-precision partial wave expansions developed by Eisenstein and Tabakin [43] (as a check, they transformed the potentials to coordinate space and solved the equivalent integro-differential equation).

In this paper we generalize the VP procedure so that it can be applied to intermediate-energy proton scattering from spin 1/2 nuclei in which states of differing orbital or spin angular momentum are coupled. In the process, we also generalize the Blatt–Biedenharn phase shift parameterization of the scattering of two spin 1/2 particles so that it can describe channel coupling with a nonsymmetric or nonunitary S matrix, as occurs when scattering from an optical potential or when the phase shifts are complex. Although our generalizations of the VP procedure and computations emphasize working directly with S or T matrix elements, the connection to phase shifts is indicated.

In Sec. 3.2 we derive and reformulate the VP procedure for uncoupled channels. Since the basic physics can get obscured in the multiple steps of the VP procedure for coupled channels, it is important to understand the physics and notation of Sec. 3.2 before proceeding to the couple-channels case. In Sec. 3.3 we present our formulation for coupled channels, and in Sec. 3.4 we give some sample calculations of 500 MeV proton scattering from ^{3}He.

3.2. UNCOUPLED STATES (0×0, $0 \times 1/2$)

Consider scattering from a short-ranged, but nonlocal, nuclear potential $V_n(\mathbf{r}', \mathbf{r})$ and the infinite-ranged Coulomb potential $V_c(r)$. Because the nuclear potential V_n is nonlocal, the preferred method to obtain the scattering amplitude is to solve the Lippmann-Schwinger equation,

$$T_j(k', k) = V_j(k', k) + \frac{2}{\pi} \int_0^\infty p^2 \, dp \frac{V_j(k', p) T_j(p, k)}{E(k_0) + i\epsilon - E(p)}, \tag{3.2}$$

with $V_{j=l\pm}(k', k)$ the partial-wave matrix element of the momentum-space potential $V_n(\mathbf{k}', \mathbf{k})$. Here l is the orbital angular momentum and $j = l \pm 1/2 \stackrel{def}{=} l\pm$ is the total angular momentum. For spin 0 scattering from a spin 0 or spin 1/2 target, there is no coupling of different channels in (3.2).

Eq. (3.2) is valid as long as the coordinate-space potential is of finite range—which in practice means that at some radius the potential is small enough to be ignored without significantly changing the predicted scattering observables. We indicate by the shaded area in Fig. 3.1 the region in which the nuclear potential V_n acts, and the range for the nuclear potential by R. The coordinate-space Coulomb potential does not vanish rapidly enough to be considered as having a finite range, and although its strength may be weaker than the nuclear potential, it cannot be included with the nuclear potential in (3.2).

The Vincent-Phatak procedure sets the coordinate-space Coulomb potential to zero (cuts it off) for all radii r greater than some fixed value R_{cut}:

$$V_c^{cut}(r) = V_c(r) \, \theta(R_{cut} - r). \tag{3.3}$$

The coordinate-space regions are illustrated in Fig. 3.1 where we assume that R_{cut} is larger than the range R of the nuclear potential. Since the momentum-space transform,

$$V_c^{cut}(\mathbf{k}',\mathbf{k}) = \frac{Z_P Z_T e^2}{2\pi^2 q^2}\left[\rho(q) - \cos(qR_{cut})\right], \tag{3.4}$$

of the truncated Coulomb potential (3.3), has the $q \to 0$ limit of $Z_P Z_T e^2 R_{cut}^2/(6\pi^2)$, we see that the $q = 0$ singularity of (3.1) has indeed been removed. Because the cutoff Coulomb potential is of finite range (in coordinate space) and without singularities in momentum space, its partial-wave decomposition can be added to that of the nuclear potential,

$$V_{l\pm}(k',k) = V_{n,l\pm}(k',k) + V_{c,l}^{cut}(k',k), \tag{3.5}$$

and when inserted in the Lippmann-Schwinger equation (3.2), this combined potential produces a well-defined solution.

The solutions $T_{l\pm}(k',k)$ of the Lippmann-Schwinger equation in momentum space (3.2) can readily be transformed into coordinate-space wavefunctions for all values of r [12]. Alternatively, just the on-shell element $T_{l\pm}(k_0,k_0)$ can be used to obtain the wavefunction anyplace outside of the shaded region in Fig. 3.1. In the "outer" region $r > R_{cut}$, both the nuclear and cutoff Coulomb potentials vanish, and so the (unnormalized) wavefunction there is expressed as a linear combination of the regular plus either irregular or outgoing solutions [$F_l(k_0r)$ plus either $G_l(k_0r)$ or $H_l^{(+)}(k_0r)$] of the potential-free Schrödinger equation [44]:

$$\hat{u}_{j=l\pm1/2}(r) = \begin{cases} e^{i\delta_{l\pm}(k_0)}\left[\sin\delta_{l\pm}(k_0)\, G_l(k_0r) + \cos\delta_{l\pm}(k_0)\, F_l(k_0r)\right] & r > R_{cut} \\ F_l(k_0r) + \hat{T}_{l\pm}(k_0)\, H_l^{(+)}(k_0r) & r > R_{cut} \\ \sin[k_0r - l\pi/2 + \delta_{l\pm}(k_0)] & r(> R_{cut}) \to \infty \end{cases} . \tag{3.6}$$

In (3.6) we have used two equivalent forms for the free partial wavefunctions as well as the asymptotic limit. The reduced T matrix element $\hat{T}_{l\pm}(k_0)$ in (3.6) is related to the "preliminary" phase shift $\delta_{l\pm}$ by:

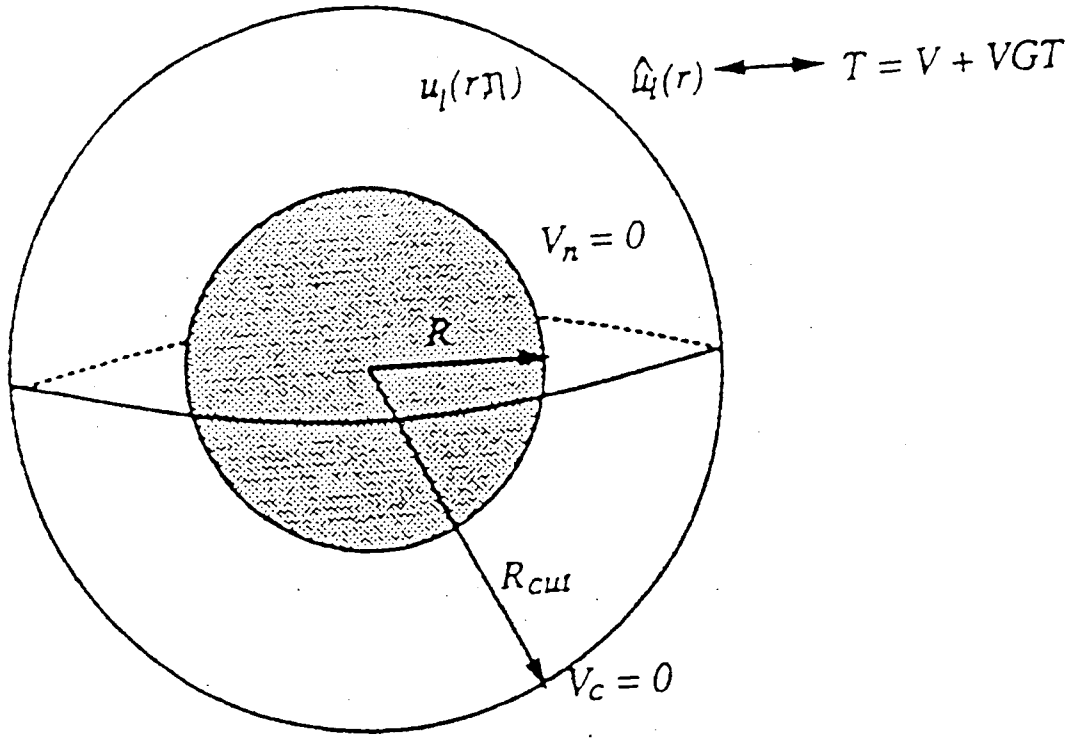

Figure 3.1. The VP procedure's partition of coordinate space into a region $r > R$ in which the nuclear potential vanishes, and a region $r > R_{cut}$ in which the Coulomb potential is set equal to zero. The wavefunction in the outer region is denoted by $\hat{u}_l(r)$ and that in the intermediate region by $u_l(\eta, r)$.

$$\hat{T}_{l\pm}(k_0) = e^{i\delta_{l\pm}(k_0)} \sin \delta_{l\pm}(k_0), \tag{3.7}$$

and to the solution $T_{l\pm}(k', k)$ of the Lippmann-Schwinger equation (3.2) by:

$$\hat{T}_{l\pm}(k_0) = -\rho_E T_{l\pm}(k_0, k_0), \quad \rho_E = 2k_0 \frac{E_P(k_0) E_T(k_0)}{E_P(k_0) + E_T(k_0)}. \tag{3.8}$$

Note again, we solve the Lippmann-Schwinger equation with a potential which is the sum of nuclear and cutoff Coulomb. Accordingly, the preliminary or unmatched phase shift $\delta_{j=l\pm}$ [which describes the wavefunction (3.6) in the outer region of Fig. 3.1], incorporates the effects of the naturally finite-range nuclear potential and of the artificially truncated Coulomb potential. In particular, effects arising from the finite extent of the target's charge distribution is included in the charge form factor $\rho(q)$ in (3.1), and consequently is included in the preliminary phase shift $\delta_{j=l\pm}$.

To describe physical scattering observables we need a wavefunction which incorporates the full extent of the Coulomb force (or at least one with a cutoff of atomic dimensions, which is essentially at infinity in Fig. 3.1). This, in turn, requires that the preliminary phase shifts δ_j be corrected for the artificial cutoff. The heart of the VP procedure is the observation that while there is no nuclear potential acting in the intermediate region between R and R_{cut} of Fig. 3.1, there is the Coulomb potential there, and that means the wavefunction in the intermediate region must be a linear combination of regular and irregular Coulomb waves:

$$u_{l\pm}(\eta, r) = \begin{cases} F_l(\eta, k_0 r) + \hat{T}^c_{l\pm}(k_0)\, H_l^{(+)}(\eta, k_0 r) & R \le r \le R_{cut} \\ \sin\left[k_0 r - l\pi/2 + \delta^c_{l\pm} + \sigma_l - \eta \ln(2k_0 r)\right] & r(\le R_{cut}) \to \infty \end{cases}. \tag{3.9}$$

Here $\eta = Z_P Z_T e^2/v$ is the Sommerfeld parameter, $F_l(\eta, kr)$ is the regular Coulomb function, and $H_l^{(+)}(\eta, kr)$ is the outgoing Coulomb function.

The Coulomb-modified T matrix,

$$\hat{T}^c_{l\pm}(k_0) \stackrel{def}{=} e^{i\delta^c_{l\pm}} \sin\delta^c_{l\pm}, \tag{3.10}$$

is unknown, and the purpose of the VP procedure is to determine it, or equivalently the phase shift $\delta^c_{l\pm}$. This is done by the requiring that at $r = R_{cut}$, the intermediate region's wavefunction $u_{l\pm}(\eta, r)$ (a linear combination of Coulomb waves) has a logarithmic derivative which matches that of the exterior wavefunction $\hat{u}_{l\pm}(r)$ (a linear combination of free waves):

$$\left.\frac{u'_{l\pm}(\eta,r)}{u_{l\pm}(\eta,r)}\right|_{r\to R_{cut}-} = \left.\frac{\hat{u}'_{l\pm}(r)}{\hat{u}_{l\pm}(r)}\right|_{r\to R_{cut}+}. \tag{3.11}$$

While r is not large enough to match the phases of the asymptotic wavefunctions in (3.6) and (3.9), we can match the linear combination of free and Coulomb waves. This yields

$$\hat{T}^c_{l\pm}(k) = \frac{\hat{T}_{l\pm}(k)[F_l(\eta,kr), H^{(+)}_l(kr)] + [F_l(\eta,kr), F_l(kr)]}{[F_l(kr), H^{(+)}_l(\eta,kr)] + \hat{T}_{l\pm}(k)[H^{(+)}_l(kr), H^{(+)}_l(\eta,kr)]}, \tag{3.12}$$

where the brackets indicate Wronskians evaluated at $r = R_{cut}$ [14].

As we expand the intermediate region by taking $R_{cut} \to \infty$, the intermediate region's wavefunction $u_{l\pm}(k_0 r, \eta)$ becomes the final physical wavefunction from which we can extract the experimental scattering observables. Consequently, we can now use the standard expression for the scattering amplitude describing scattering from a short-range potential in the presence of the Coulomb potential. It is informative to note that if, instead of matching, we had set the phase of the asymptotic limit of the intermediate-region wavefunction $u_{l\pm}(k_0 r, \eta)$ (3.9) equal to that of the asymptotic limit of the exterior wavefunction $\hat{u}_{j=l\pm 1/2}(r)$ (3.6), we would have obtained

$$\delta_{l\pm} \sim \delta^c_{l\pm} + \sigma_l - \eta \ln(2kR_{cut}). \tag{3.13}$$

The $\ln(2kR_{cut})$ term, which arises from the specific distortion of wavefunctions caused by the point Coulomb force, is problematic in the $R_{cut} \to \infty$ limit. The

detailed analysis [44,45] shows that for all but the most forward of scatterings, the standard expansion of the scattering amplitude can be used with

$$\delta_{l\pm} \simeq \delta^c_{l\pm} + \sigma_l. \tag{3.14}$$

When we determine the Coulomb-modified phase shift via matching the wavefunctions' logarithmic derivatives (3.12), we explicitly subtract the $\ln(2kR_{cut})$ term.

Substitution of (3.14) into the usual partial-wave expansion of the scattering amplitude, and some rearrangement, leads to the final expression for the (spin-nonflip) amplitude for scattering:

$$f(\theta) = f^c_{pt}(\theta) + f^{nc}(\theta), \tag{3.15}$$

$$f^c_{pt}(\theta) = -\frac{\eta}{2k_0 \sin^2(\theta/2)} \exp\{2i\left[\sigma_0 - \eta \ln \sin(\theta/2)\right]\}, \tag{3.16}$$

$$f^{nc}(\theta) = \frac{1}{2ik_0} \sum_{l=0}^{\infty} (2l+1) e^{2i\sigma_l} \left(e^{2i\delta^c_l} - 1\right) P_l(\cos\theta) \tag{3.17}$$

$$= \frac{1}{k_0} \sum_{l=0}^{\infty} (2l+1) e^{2i\sigma_l} \hat{T}^c_{l\pm} P_l(\cos\theta), \tag{3.18}$$

where f^c_{pt} is the scattering amplitude for a point Coulomb potential, and f^{nc} is the amplitude for nuclear scattering in the presence of the Coulomb [46]. Note, that since the Coulomb-modified phase shift $\delta^c_{l\pm}$ is defined in (3.9) relative to Coulomb waves which are already shifted by the point Coulomb phase σ_l, the amplitude f^{nc} also include the effect of Coulomb scattering from the finite extent of the charge distribution.

3.3. COUPLED STATES ($\frac{1}{2} \times \frac{1}{2}$)

3.3.1. Basic Analysis

If the strong interaction couples orbital or spin angular-momentum states, we must generalize the VP method—even though we assume the Coulomb interaction

remains central and does not couple states. We assume rotation invariance, parity conservation, and time reversal invariance, in which case the spin-space structure of the nucleon-nucleus T matrix is [14,15]:

$$2\,T(\mathbf{k}',\mathbf{k}) = a + b + (a-b)\vec{\sigma}_n^P\vec{\sigma}_n^T + (c+d)\vec{\sigma}_m^P\vec{\sigma}_m^T \\ +(c-d)\vec{\sigma}_l^P\vec{\sigma}_l^T + e(\vec{\sigma}_n^P + \vec{\sigma}_n^T) + f(\vec{\sigma}_n^P - \vec{\sigma}_n^T). \tag{3.19}$$

Although not indicated in (3.19), a–f are functions of the initial and final momenta $\mathbf{k}$ and $\mathbf{k}'$. The superscripts "P" and "T" in Eq. (3.19) indicate the projectile and target respectively, while the subscripts n, l, and m indicates a dot product of P or T's σ with one of the three independent unit vectors:

$$\hat{\mathbf{n}} = \frac{\mathbf{k}\times\mathbf{k}'}{|\mathbf{k}\times\mathbf{k}'|}, \quad \hat{\mathbf{m}} = \frac{\mathbf{k}-\mathbf{k}'}{|\mathbf{k}-\mathbf{k}'|}, \quad \hat{\mathbf{l}} = \frac{\mathbf{k}+\mathbf{k}'}{|\mathbf{k}+\mathbf{k}'|}. \tag{3.20}$$

Once the a–f amplitudes are known, it is straightforward to calculate the experimental scattering observables [14,15,17]. For example, the differential cross section, beam analyzing power, target analyzing power, and depolarization parameter are:

$$\sigma = \frac{1}{2}(|a|^2 + |b|^2 + |c|^2 + |d|^2 + |e|^2 + |f|^2), \tag{3.21}$$

$$A_{oono} = \frac{1}{\sigma}\Re(a^*e + b^*f), \tag{3.22}$$

$$A_{ooon} = \frac{1}{\sigma}\Re(a^*e - b^*f), \tag{3.23}$$

$$D_{nono} = \frac{1}{2\sigma}(|a|^2 + |b|^2 - |c|^2 - |d|^2 + |e|^2 + |f|^2). \tag{3.24}$$

Here we use the tensor notation $X_{p't'pt}$ with the subscripts p and t denoting the direction of the initial-state projectile and target polarizations, the primes denoting the corresponding final-state quantities, and a subscript o denoting zero or undetected polarization. Accordingly, only P is polarized in the n direction in (3.22) while only T is polarized in the n direction in (3.23).

The origin of the partial-wave analysis [20] is the expansion of the T and V matrices in spin-angle functions:

$$\begin{pmatrix} T(\mathbf{k}',\mathbf{k}) \\ V(\mathbf{k}',\mathbf{k}) \end{pmatrix} = \frac{2}{\pi} \sum_{jm_j ll' ss'} i^{(l'-l)} \begin{pmatrix} T^{j(s's)}_{l'l}(k',k) \\ V^{j(s's)}_{l'l}(k',k) \end{pmatrix} \times \mathcal{Y}^{jm_j}_{l's'}(\hat{k}')\, \mathcal{Y}^{\dagger jm_j}_{ls}(\hat{k}). \tag{3.25}$$

In (3.25), l, s, and j are the orbital, spin, and total angular momenta of the target plus projectile, and $\mathcal{Y}^{jm_j}_{ls}$ is the spin-angle function. When we substitute the expansions (3.25) into the three-dimensional Lippmann-Schwinger equation, we obtain the integral equations coupling states with spin 0 and 1 (the singlet "s" and triplet "t" states), as well as those coupling triplet states with differing orbital angular momenta:

$$\begin{bmatrix} T^{j(ss)}_{jj} \\ T^{j(ts)}_{jj} \end{bmatrix} = \begin{bmatrix} V^{j(ss)}_{jj} \\ V^{j(ts)}_{jj} \end{bmatrix} + \int_0^\infty \frac{p^2 dp}{E^+ - E(p)} \begin{bmatrix} V^{j(ss)}_{jj}(k'p)\; V^{j(st)}_{jj}(k',p) \\ V^{j(ts)}_{jj}(k',p)\; V^{j(tt)}_{jj}(k',p) \end{bmatrix} \begin{bmatrix} T^{j(ss)}_{jj}(p,k) \\ T^{j(ts)}_{jj}(p,k) \end{bmatrix} \tag{3.26}$$

$$\begin{bmatrix} T^{j(tt)}_{jj} \\ T^{j(st)}_{jj} \end{bmatrix} = \begin{bmatrix} V^{j(tt)}_{jj} \\ V^{j(st)}_{jj} \end{bmatrix} + \int_0^\infty \frac{p^2 dp}{E^+ - E(p)} \begin{bmatrix} V^{j(tt)}_{jj}(k',p)\; V^{j(ts)}_{jj}(k',p) \\ V^{j(st)}_{jj}(k',p)\; V^{j(ss)}_{jj}(k',p) \end{bmatrix} \begin{bmatrix} T^{j(tt)}_{jj}(p,k) \\ T^{j(st)}_{jj}(p,k) \end{bmatrix}, \tag{3.27}$$

$$\begin{bmatrix} T^{j(tt)}_{j-1j-1} \\ T^{j(tt)}_{j+1j-1} \end{bmatrix} = \begin{bmatrix} V^{j(tt)}_{j-1j-1} \\ V^{j(tt)}_{j+1j-1} \end{bmatrix} + \int_0^\infty \frac{p^2 dp}{E^+ - E(p)} \begin{bmatrix} V^{j(tt)}_{j-1j-1}(k',p)\; V^{j(tt)}_{j-1j+1}(k',p) \\ V^{j(tt)}_{j+1j-1}(k',p)\; V^{j(tt)}_{j+1j+1}(k',p) \end{bmatrix} \begin{bmatrix} T^{j(tt)}_{j-1j-1}(p,k) \\ T^{j(tt)}_{j+1j-1}(p,k) \end{bmatrix}, \tag{3.28}$$

$$\begin{bmatrix} T^{j(tt)}_{j+1j+1} \\ T^{j(tt)}_{j-1j+1} \end{bmatrix} = \begin{bmatrix} V^{j(tt)}_{j+1j+1} \\ V^{j(tt)}_{j-1j+1} \end{bmatrix} + \int_0^\infty \frac{p^2 dp}{E^+ - E(p)} \begin{bmatrix} V^{j(tt)}_{j+1j+1}(k',p)\; V^{j(tt)}_{j+1j-1}(k',p) \\ V^{j(tt)}_{j-1j+1}(k',p)\; V^{j(tt)}_{j-1j-1}(k',p) \end{bmatrix} \begin{bmatrix} T^{j(tt)}_{j+1j+1}(p,k) \\ T^{j(tt)}_{j-1j+1}(p,k) \end{bmatrix}, \tag{3.29}$$

For the sake of compactness, we leave off the (k',k) dependences of the leftmost T and V in (3.26)–(3.29), and use E^+ as a shorthand for $E(k_0) + i\epsilon$.

Once these partial-wave Lippmann-Schwinger equations are solved, the on-energy-shell matrix elements $T_{l'l}^{j(s's)}(k_0,k_0)$ can be converted to phase shifts or summed to form scattering amplitudes. In Sec. 3.3.2 we show how to extend the spin $1/2\times 1/2$ phase shift analysis used for two nucleons [11]- [49] to nucleon-nucleus scattering with complex potentials. The summation of the partial-wave T matrices to form the spin-basis matrix element, $\langle s'm_{s'}|T|sm_s\rangle$, is derived in [20] for the pure nuclear case. As discussed in Sec. 3.3.3, when the Coulomb force is present, there is a point Coulomb scattering amplitude added to the nonflip spin matrix elements, and a Coulomb phase factor $\Phi_l = \exp(2i\sigma_l)$ multiplying some of the partial wave matrix elements:

$$T_{s1}(\mathrm{k}',\mathrm{k}) \equiv \langle 0,0|T|1,1\rangle = \frac{-\sqrt{2}}{4\pi^2}\sum_{l=1} P_l^1(x=\cos\theta_{k'k})\,\frac{2l+1}{\sqrt{l(l+1)}}\,T_{ll}^{l(st)}(k',k) \tag{3.30}$$

$$T_{ss}(\mathrm{k}',\mathrm{k}) \equiv \langle 0,0|T|0,0\rangle = \frac{1}{2\pi^2}\sum_{l=0} P_l(x)(2l+1)\,\Phi_l T_{ll}^{l(ss)}(k',k) \tag{3.31}$$

$$\begin{aligned} T_{11}(\mathrm{k}',\mathrm{k}) = \frac{1}{4\pi^2}\sum_{l=0} P_l(x)\Big\{&(l+2)\Phi_l T_{ll}^{l+1(tt)}(k',k) - \sqrt{(l+1)(l+2)}\,T_{ll+2}^{l+1(tt)}(k',k) \\ &+(2l+1)\Phi_l T_{ll}^{l(tt)}(k',k) + (l-1)\Phi_l T_{ll}^{l-1(tt)}(k',k) - \sqrt{(l-1)l}\,T_{ll-2}^{l-1(tt)}(k',k)\Big\} \end{aligned} \tag{3.32}$$

$$\begin{aligned} T_{00}(\mathrm{k}',\mathrm{k}) \equiv \langle 0,0|T|0,0\rangle = \frac{1}{2\pi^2}\sum_{l=0} P_l(x)\Big\{&(l+1)\Phi_l T_{ll}^{l+1(tt)}(k',k) + l\Phi_l T_{ll}^{l-1(tt)}(k',k) \\ &+\sqrt{(l+1)(l+2)}\,T_{ll+2}^{l+1(tt)}(k',k) + \sqrt{(l-1)l}\,T_{ll-2}^{l-1(tt)}(k',k)\Big\} \end{aligned} \tag{3.33}$$

$$\begin{aligned} T_{10}(\mathrm{k}',\mathrm{k}) = \frac{\sqrt{2}}{4\pi^2}\sum_{l=1} P_l^1(x)\Big\{&-T_{ll}^{l-1(tt)}(k',k) + T_{ll}^{l+1(tt)}(k',k) \\ &+\sqrt{\frac{l+2}{l+1}}T_{ll+2}^{l+1(tt)}(k',k) - \sqrt{\frac{l-1}{l}}T_{ll-2}^{l-1(tt)}(k',k)\Big\} \end{aligned} \tag{3.34}$$

$$\begin{aligned} T_{01}(\mathrm{k}',\mathrm{k}) = \frac{\sqrt{2}}{4\pi^2}\sum_{l=1} P_l^1(x)\Big\{&-\frac{l+2}{l+1}T_{ll}^{l+1(tt)}(k',k) + \frac{2l+1}{l(l+1)}T_{ll}^{l(tt)}(k',k) \\ &+\frac{l-1}{l}T_{ll}^{l-1(tt)}(k',k) + \sqrt{\frac{l+2}{l+1}}T_{ll+2}^{l+1(tt)}(k',k) - \sqrt{\frac{l-1}{l}}T_{ll-2}^{l-1(tt)}(k',k)\Big\} \end{aligned} \tag{3.35}$$

$$\begin{aligned} T_{1\,-1}(\mathrm{k}',\mathrm{k}) = \frac{1}{4\pi^2}\sum_{l=2} P_l^2(x)\Big\{&\frac{1}{l+1}T_{ll}^{l+1(tt)}(k',k) - \frac{1}{\sqrt{(l+1)(l+2)}}T_{ll+2}^{l+1(tt)}(k',k) \\ &-\frac{2l+1}{l(l+1)}T_{ll}^{l(tt)}(k',k) + \frac{1}{l}T_{ll}^{l-1(tt)}(k',k) - \frac{1}{\sqrt{l(l-1)}}T_{ll-2}^{l-1(tt)}(k',k)\Big\} \end{aligned} \tag{3.36}$$

The a–f amplitudes needed to calculate the spin observables (3.21)-(3.24) are then constructed from the T matrices in the spin basis:

$$a(\mathbf{k}',\mathbf{k}) = \frac{1}{2}\left(T_{11} + T_{00} - T_{1-1}\right), \tag{3.37}$$

$$b(\mathbf{k}',\mathbf{k}) = \frac{1}{2}\left(T_{11} + T_{ss} + T_{1-1}\right), \tag{3.38}$$

$$c(\mathbf{k}',\mathbf{k}) = \frac{1}{2}\left(T_{11} - T_{ss} + T_{1-1}\right), \tag{3.39}$$

$$d(\mathbf{k}',\mathbf{k}) = \frac{1}{2}\left(T_{00} + T_{1-1} - T_{11}\right)/(2\cos\theta_{kk}), \tag{3.40}$$

$$e(\mathbf{k}',\mathbf{k}) = \frac{i}{\sqrt{2}}\left(T_{10} - T_{01}\right), \tag{3.41}$$

$$f(\mathbf{k}',\mathbf{k}) = i\sqrt{2}T_{s1}. \tag{3.42}$$

The partial-wave potential matrix elements used as input to (3.26)-(3.29) are obtained by first evaluating the potentials in the spin basis $\langle s'm_{s'}|V|sm_s\rangle$, and then expanding these spin-basis matrix elements in partial waves. The expansions are the same as those of the T matrix, (3.30)–(3.36), but with no Coulomb phase factors. These expansions are then inverted to obtain the partial wave potentials $V_{l'l}^{j(s's)}(k',k)$ by numerically projecting out the different $P_l^m(x)$ dependences and then solving the resulting linear equations [20].

3.3.2. Extensions for Optical Potentials

Blatt and Biedenharn were the first to give the extension to the phase shift analysis needed to describe the scattering of two spin 1/2 particles in the presence of a tensor force which mixes the orbital angular momentum states [48,49]. They assumed that the $j = l \pm 1$ states within the nucleon-nucleon spin triplet have the asymptotic forms:

$$\lim_{r\to\infty} u_{j=l+1}(r) = A_+ e^{-i[kr-(j-1)\frac{\pi}{2}]} - B_+ e^{i[kr-(j-1)\frac{\pi}{2}]}, \tag{3.43}$$

$$\lim_{r\to\infty} u_{j=l'-1}(r) = A_- e^{-i[kr-(j+1)\frac{\pi}{2}]} - B_- e^{i[kr-(j+1)\frac{\pi}{2}]}. \tag{3.44}$$

The S matrix for the coupled system is then defined by the relation among the A's and B's:

$$\begin{bmatrix} B_+ \\ B_- \end{bmatrix} = \begin{bmatrix} S_{++} & S_{+-} \\ S_{-+} & S_{--} \end{bmatrix} \begin{bmatrix} A_+ \\ A_- \end{bmatrix}, \tag{3.45}$$

where we use the shorthand notation:

$$\pm \stackrel{def}{=} (j = l \pm 1). \tag{3.46}$$

For NN scattering below pion production threshold, the S matrix must be unitary since flux is conserved, and symmetric since all terms in the Schrödinger equation are real. For that case, the most general form for S, a unitary and symmetric 2×2 matrix, is given by a similarity transformation with a "mixing" parameter ϵ:

$$[S] = [U]^{-1}[e^{2i\Delta}][U], \tag{3.47}$$

$$[U] = \begin{bmatrix} \cos\epsilon_j & \sin\epsilon_j \\ -\sin\epsilon_j & \cos\epsilon_j \end{bmatrix}, \tag{3.48}$$

$$[e^{2i\Delta}] = \begin{bmatrix} e^{2i\delta_{++}} & 0 \\ 0 & e^{2i\delta_{--}} \end{bmatrix}. \tag{3.49}$$

When dealing with nonidentical particles scattering through an optical potential, the S matrix is no longer unitary (which means the phases shifts become complex), and, as well, the S matrix is no longer symmetric (which means there are now two mixing parameters). To describe this more general case, we assume (3.47) to be valid but with a more general transformation matrix:

$$[U] = \begin{bmatrix} \cos\epsilon_{+-} & \sin\epsilon_{-+} \\ -\sin\epsilon_{+-} & \cos\epsilon_{-+} \end{bmatrix}, \tag{3.50}$$

$$[U]^{-1} = \frac{1}{\det U} \begin{bmatrix} \cos\epsilon_{-+} & -\sin\epsilon_{-+} \\ \sin\epsilon_{+-} & \cos\epsilon_{+-} \end{bmatrix}, \tag{3.51}$$

$$\det U = \cos\epsilon_{+-}\cos\epsilon_{-+} + \sin\epsilon_{+-}\sin\epsilon_{-+}. \tag{3.52}$$

This leads to the S matrix elements $S_{\pm\pm} \equiv S_{j=l'\pm1,j=l\pm1}(k_0)$ having the form:

$$S_{++} = \frac{1}{\det U}(\cos\epsilon_{+-}\cos\epsilon_{-+}e^{2i\delta_{++}} + \sin\epsilon_{+-}\sin\epsilon_{-+}e^{2i\delta_{--}}), \tag{3.53}$$

$$S_{+-} = \frac{1}{\det U}(\sin\epsilon_{-+}\cos\epsilon_{-+}e^{2i\delta_{++}} - \cos\epsilon_{-+}\sin\epsilon_{-+}e^{2i\delta_{--}}), \tag{3.54}$$

$$S_{-+} = \frac{1}{\det U}(\sin\epsilon_{+-}\cos\epsilon_{+-}e^{2i\delta_{++}} - \cos\epsilon_{+-}\sin\epsilon_{+-}e^{2i\delta_{--}}), \tag{3.55}$$

$$S_{--} = \frac{1}{\det U}(\cos\epsilon_{+-}\cos\epsilon_{-+}e^{2i\delta_{--}} + \sin\epsilon_{+-}\sin\epsilon_{-+}e^{2i\delta_{++}}). \tag{3.56}$$

The T matrix elements used in the VP procedure and computations are simply related to the S matrix elements via (3.7) and (3.8):

$$2i\rho_E T_{ll'}(k_0,k_0) = \delta_{ll'} - S_{l'=j\mp1,l=j\mp1}(k_0). \tag{3.57}$$

We note that (3.53)-(3.56) reduce to the standard, coupled case [48,49] if $\epsilon_{+-} = \epsilon_{-+}$, and to the standard uncoupled case if $\epsilon_{+-} = \epsilon_{-+} = 0$. For the symmetric S matrix case, Stapp [11] also gave a parameterization of the S matrix in terms of the "bar" phase shifts, which in some cases is more convenient for the phenomenological parameterization of data. Note, however, the bar phases are not the ones introduced here, and even for the NN case, the bar phases do not provide a diagonal representation of the S matrix as do the Blatt-Biedenharn phases.

3.3.3. VP Procedure for Coupled Channels

The general approach we take for applying the VP procedure to channels coupled by an optical potential has three steps. First, we transform the states to

a new basis in which there is no channel coupling. Second, we match the exterior wavefunction in this basis $\hat{u}(kr)$, to an intermediate region wavefunction $u(r,\eta)$ (a linear combination of Coulomb waves). Finally, we return to the original, nondiagonal basis to calculate the scattering observables.

A possible implementation of these steps would be to take our S matrix elements computed via (3.26)-(3.29) and (3.57), assume they have the forms (3.53)–(3.56) in terms of phase shifts and coupling parameters, and then search for the $(\delta_{--},\delta_{++},\epsilon_{+-},\epsilon_{-+})$ which satisfy these transcendental equations. The δ's would then be the phase shifts in the basis in which S is diagonal and we could use them for matching. Instead, we have adopted a more direct—but equivalent—approach in which we explicitly diagonalize the S matrix, do the VP matching of the wavefunctions in the diagonal basis to obtain the Coulomb-modified T matrix elements, and then transform the matrix elements back to the original basis where we calculate the observables.

Considering the complexity of the procedure, we enumerate the steps followed in a realistic calculation.

1. Start with a microscopic, first order, momentum-space optical potential [3,17,18]:

$$\begin{aligned} V_n(\mathbf{k}',\mathbf{k}) \;=\; & N\Big\{(t^{Pn}_{a+b}+t^{Pn}_{e}\vec{\sigma}^{P}_{n})\rho^{n}_{mt}(q)+\Big[t^{Pn}_{a-b}\vec{\sigma}^{P}_{n}\vec{\sigma}^{T}_{n}+t^{Pn}_{e}\vec{\sigma}^{T}_{n} \\ & +t^{Pn}_{c+d}\vec{\sigma}^{P}_{m}\vec{\sigma}^{T}_{m}+t^{Pn}_{c-d}\vec{\sigma}^{P}_{l}\vec{\sigma}^{T}_{l}+t^{Pn}_{c+d}(\vec{\sigma}^{P}_{m}\vec{\sigma}^{T}_{l}+\vec{\sigma}^{P}_{l}\vec{\sigma}^{T}_{m})\Big]\rho^{n}_{sp}(q)\Big\} \\ & +Z\Big\{(t^{Pp}_{a+b}+t^{Pp}_{e}\vec{\sigma}^{P}_{n})\rho^{p}_{mt}(q)+\Big[t^{Pp}_{a-b}\vec{\sigma}^{P}_{n}\vec{\sigma}^{T}_{n}+t^{Pp}_{e}\vec{\sigma}^{t}_{n} \\ & +t^{Pp}_{c+d}\vec{\sigma}^{P}_{m}\vec{\sigma}^{T}_{m}+t^{Pp}_{c-d}\vec{\sigma}^{P}_{l}\vec{\sigma}^{P}_{l}+t^{Pp}_{c+d}(\vec{\sigma}^{P}_{m}\vec{\sigma}^{T}_{l}+\vec{\sigma}^{P}_{l}\vec{\sigma}^{T}_{m})\Big]\rho^{p}_{sp}(q)\Big\}. \end{aligned} \tag{3.58}$$

Here the subscripts a–e indicate that these terms originate from nucleon-nucleon (NN) t's with the same spin-space structure as (3.19). The potential

(3.58) manifestly contains the spin $1/2 \times 1/2$ dependence of NN scattering weighted by form factors describing the distributions of spin (sp) and matter (mt) for protons and neutrons within the nucleus. The off-energy-shell NN t's in (3.58) are transformed to the projectile-target center of momentum frame with a Lorentz covariant prescription which also optimizes the impulse and factorization approximations, and the off-shell variation is described with a separable potential [3,18].

2. Add the regularized Coulomb potential $V_c^{cut}(\mathbf{k}', \mathbf{k})$ (3.22) to the optical potential $V_n(\mathbf{k}', \mathbf{k})$ (3.58). Since the Coulomb potential is central, this effectively modifies the central potential term arising from t_{a+b}^{Pp} and t_{a+b}^{Pn}. The Coulomb potential is accordingly added to the diagonal spin-basis potentials V_{ss}, V_{00}, and V_{11}:

$$\begin{pmatrix} V_{ss}(\mathbf{k}', \mathbf{k}) \\ V_{00}(\mathbf{k}', \mathbf{k}) \\ V_{11}(\mathbf{k}', \mathbf{k}) \end{pmatrix} \rightarrow \begin{pmatrix} V_{ss}(\mathbf{k}', \mathbf{k}) \\ V_{00}(\mathbf{k}', \mathbf{k}) \\ V_{11}(\mathbf{k}', \mathbf{k}) \end{pmatrix} + V_c^{cut}(\mathbf{k}', \mathbf{k}). \tag{3.59}$$

3. Project out the partial wave potentials from the spin-basis potentials using the V versions of (3.30)-(3.36). The spin-independent Coulomb potential is thereby included in $V_{ll}^{j(ss)}(k', k)$ and $V_{ll}^{j(tt)}(k', k)$.

4. Solve the coupled Lippmann-Schwinger equations (3.26)-(3.29) for $T_{l'l}^{j(s's)}(k', k)$. This is equivalent to solving for the wavefunction in the outer region.

5. Convert the T matrix elements into S matrix elements via (3.57), and construct the nondiagonal S matrix,

$$[S] = \begin{bmatrix} S_{++} & S_{+-} \\ S_{-+} & S_{--} \end{bmatrix}. \tag{3.60}$$

6. Explicitly diagonalize the S matrix elements with the similarity transformation:

$$[S'] = [U][S][U]^{-1} = \begin{pmatrix} e^{2i\delta'_{++}} & 0 \\ 0 & e^{2i\delta'_{--}} \end{pmatrix}, \tag{3.61}$$

$$[U] = \begin{pmatrix} 1 & \frac{S_{+-}}{\lambda_- - S_{--}} \\ \frac{S_{-+}}{\lambda_+ - S_{++}} & 1 \end{pmatrix}, \tag{3.62}$$

$$[U]^{-1} = \frac{1}{\det U} \begin{pmatrix} 1 & \frac{-S_{+-}}{\lambda_- - S_{--}} \\ \frac{-S_{-+}}{\lambda_+ - S_{++}} & 1 \end{pmatrix}, \tag{3.63}$$

$$2\lambda_\pm = S_{++} + S_{--} \pm \sqrt{(S_{++} - S_{--})^2 + 4S_{+-}S_{-+}}. \tag{3.64}$$

We now know the diagonal elements $\exp(2i\delta'_{\pm\pm})$.

7. Extract the preliminary phase shift $\delta'_{\pm\pm}$ (for the outer-region's wavefunction), or equivalently, the normalized preliminary T' matrix (3.7):

$$\hat{T}'_{\pm\pm} = e^{i\delta'_{\pm\pm}} \sin \delta'_{\pm\pm}. \tag{3.65}$$

Since we are in a basis in which there is no coupling, we can match the outer wavefunctions to the linear combination of Coulomb waves of the intermediate region.

8. Do the VP matching as in (3.12) to obtain the Coulomb-modified amplitude $\hat{T}'^{c}_{\pm\pm}$ (or, equivalently, the phase shift $\delta'^{c}_{\pm\pm}$) from the $\hat{T}'_{\pm\pm}$:

$$\hat{T}'^{c}_{\pm\pm}(k) = \frac{\hat{T}'_{\pm\pm}(k)[F_l(\eta, kr), H_l^{(+)}(kr)] + [F_l(\eta, kr), F_l(kr)]}{[F_l(kr), H_l^{(+)}(\eta, kr)] + \hat{T}'_{\pm\pm}(k)[H_l^{(+)}(kr), H_l^{(+)}(\eta, kr)]}. \tag{3.66}$$

9. Now that we know the wavefunction in the intermediate region, we transform back to the original basis to extract the scattering amplitude. Form a Coulomb-modified S' matrix in the diagonal basis,

$$[S'^c] = \begin{pmatrix} e^{2i\delta'^c_{++}} & 0 \\ 0 & e^{2i\delta'^c_{--}} \end{pmatrix}, \tag{3.67}$$

and use the U matrix of (3.61) to transform S'^c back to the basis in which we calculate the observables:

$$[S^{nc}] = [U]^{-1}[S'^c][U]. \tag{3.68}$$

10. Even though the method is guaranteed to diagonalize the S matrix, as an independent test, check that the unitarity constraint is preserved throughout:

$$|S^{nc}_{ll'}| \leq 1, \quad \left|S'_{ll'}\right| \leq 1. \tag{3.69}$$

11. We have split the total phase shift into the sum of the point Coulomb phase σ_l plus the Coulomb-modified phase shift $\delta^c_{\pm\pm}$. As done for the spinless case, we separate out the point-Coulomb scattering amplitude from the nuclear amplitude, leaving behind the Coulomb-phase factor, $\Phi_l = \exp(2i\sigma_l)$, in the diagonal ($m'_s = m_s$) spin-basis amplitudes $T_{m'_s m_s}(\mathbf{k}', \mathbf{k})$. Form the partial-wave expansions of these amplitudes via (3.30)–(3.36).

12. Add the point Coulomb amplitude to the diagonal spin-basis amplitudes:

$$\begin{pmatrix} T_{ss}(\mathbf{k},\mathbf{k}') \\ T_{00}(\mathbf{k},\mathbf{k}') \\ T_{11}(\mathbf{k},\mathbf{k}') \end{pmatrix} \rightarrow \begin{pmatrix} T_{ss}(\mathbf{k},\mathbf{k}') \\ T_{00}(\mathbf{k},\mathbf{k}') \\ T_{11}(\mathbf{k},\mathbf{k}') \end{pmatrix} + f^c_{pt}(\theta). \tag{3.70}$$

13. Calculate the scattering amplitudes a–f via (3.37)–(3.42), and from these the experimental observables, for example, via (3.21)– (3.24).

3.4. SAMPLE CALCULATIONS

As a first test of our precision with the VP method, we solved the Lippmann-Schwinger equation with only a point-Coulomb potential. We confirmed that our computations reproduced the point-Coulomb phase shifts σ_l [after removal of the $\eta \ln(2kR_{cut})$ term in (3.9)]. We concluded from this severe test that factoring out the overall phase factor of $e^{2i\sigma_0}$ is helpful, and that 48–64 grid points are required in order for our solution of the Lippmann-Schwinger equation to yield four–five place precision in σ_l. That precision in σ_l is needed to obtain a point-Coulomb scattering amplitude f_c^{pt} which is indistinguishable from the analytic expression on a five-decade semi-logarithmic plot.

As the next test, we computed pure-Coulomb scattering of 500 MeV protons from the finite charge distribution of ^{3}He. While in this case we have no exact answer to compare with, we do have the first Born approximation amplitude,

$$f_c^{finite}(\theta) \simeq f_c^{pt}(\theta)\rho(q) + O[(Z\alpha)^2]. \tag{3.71}$$

We obtained essentially perfect reproduction of (3.71). This means we can include finite Coulomb effects, in addition to the long-range Coulomb force, to at least this level of precision [$(Z\alpha)^2 \simeq 0.02\%$]. To obtain this agreement we used 48 grid points in the solution of the Lippmann–Schwinger equations (3.26)-(3.29), and increased the number of Gaussian integration points used in our partial-wave projection,

$$V_l(k',k) = \pi^2 \int_{-1}^{1} V(\mathbf{k}',\mathbf{k})\, P_l(\cos\theta'_{kk})\, d(\cos\theta'_{kk}), \tag{3.72}$$

until the partial-wave summation,

$$V(\mathbf{k}',\mathbf{k}) \simeq \frac{1}{2\pi^2} \sum_{l}^{l_{max}} (2l+1) V_l(k',k) P_l(\cos\theta_{k'k}), \tag{3.73}$$

reproduced all oscillations present in $V_c^{cut}(\mathbf{k}',\mathbf{k})$. We show a reproduction of this type in Fig. 3.2 where the many oscillations arising from the $\cos(qR_{cut})$ term in the

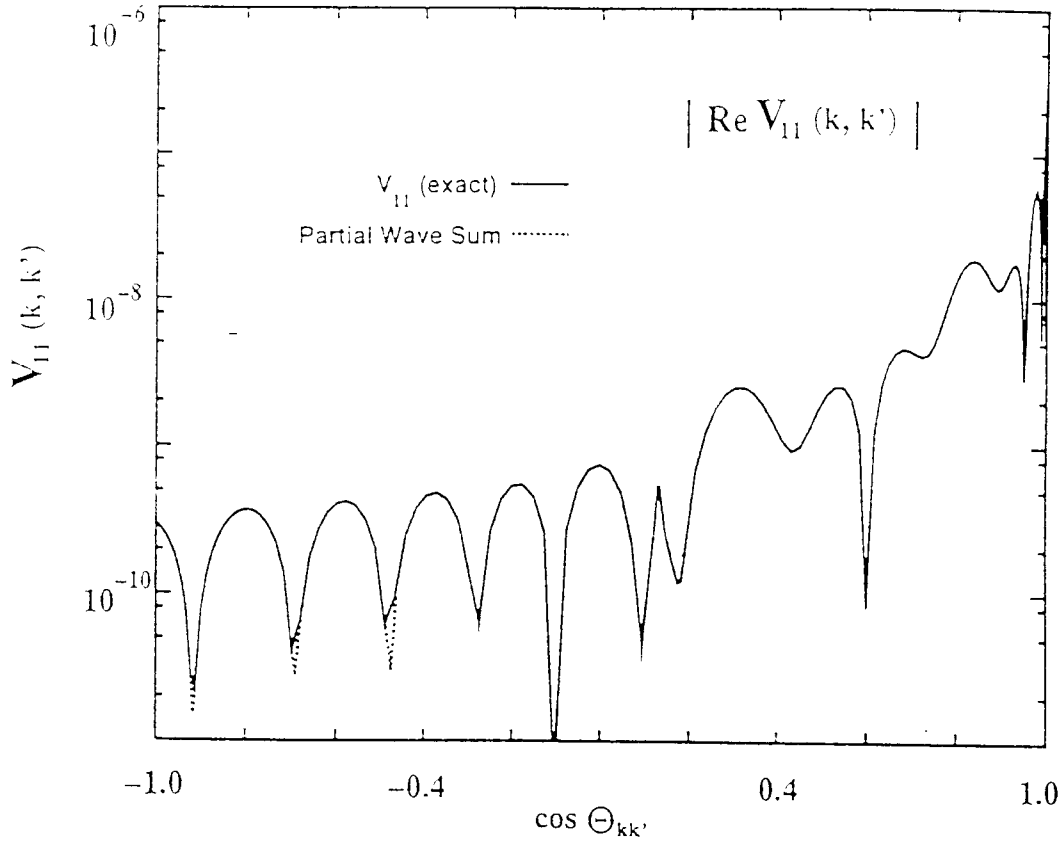

Figure 3.2. The nuclear plus Coulomb potentials in momentum space for the spin triplet state with $m_s = m_{s'} = 1$ as a function of the cosine of the angle between k and k'. The summation (3.73) of partial-wave potentials essentially overlaps the input potential.

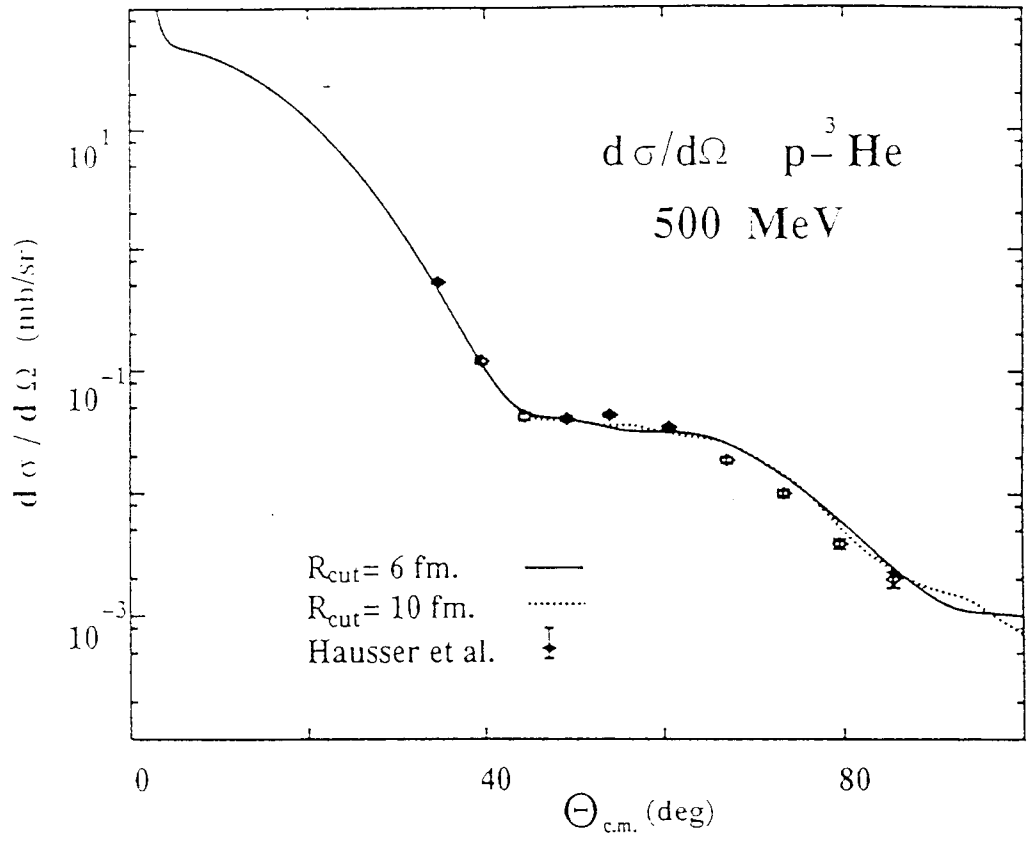

Figure 3.3. The differential cross section for 500 MeV proton scattering from ^{3}He. Calculations performed using a cutoff radius in the range 6 fm $\leq R_{cut} \leq$ 10 fm fall within the two curves. The experimental data are from Häusser et al. [50].

cut-off Coulomb potential (3.4) is evident. We obtained six-place reproduction of $V_c^{cut}(\mathbf{k}', \mathbf{k})$ using $l_{max} = 48$ partial waves and 96 integration points in the partial-wave projection (3.72). Ten-place reproduction demanded $l_{max} = 96$. We expect these number to scale as kR, and so larger nuclei or higher energies will require more partial waves and grid points. For these calculations we used analytic nuclear form factors, although we also were successful for ^{13}C using numerical Fourier transforms of Wood-Saxon densities [20]. However, we found that noise and instability appear for form factors which fall off slowly in q. In those cases, a cure is to impose a rapid fall off for q values beyond the limit of experimental measurements.

An important requirement on the VP method is that the matching radius, which we take equal to R_{cut}, be larger than the range of the nuclear force (in order to be able to express the intermediate region's wavefunction as a linear combination of pure Coulomb waves). However, increasing R_{cut} makes the cut-off Coulomb potential more oscillatory and more difficult to handle in momentum space. In fact, it was the sensitivity to changes in R_{cut} which led Ref. [39] to search for an alternative to the matching method. For p^3He at 500 MeV, we find that using $R_{cut} \leq 5$ fm produces unstable results (presumably cutting off some of the nuclear potential), but as seen in Fig. 3.3, we obtain stable results for $6\,\text{fm} \leq R_{cut} \leq 10\,\text{fm}$.

In Fig. 3.4 we compare the nuclear-plus-Coulomb cross section and polarization (solid curves) to those calculated without Coulomb (dashed curves). The exact handling of the Coulomb potential is seen to have a significant, although small, effect in the semi-logarithmic plot of $d\sigma/d\Omega$, and a more pronounced effect for A_{00n0}.

3.5. CONCLUSION

We have extended the Vincent-Phatak procedure for the exact inclusion of the Coulomb potential in momentum space to calculations of proton scattering from spin

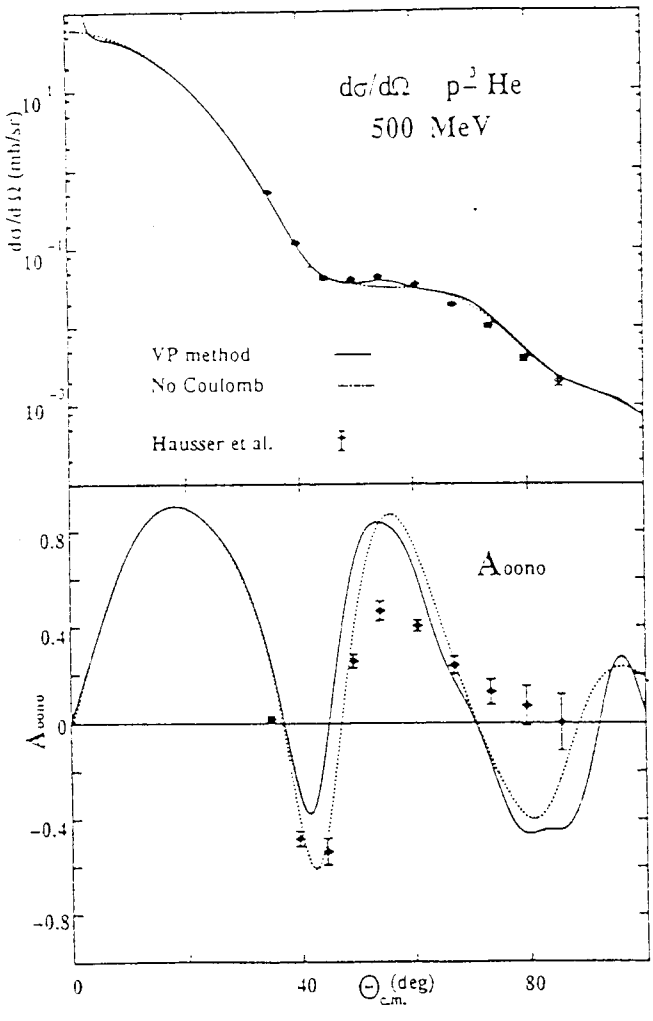

Figure 3.4. The differential cross section and analyzing power (unpolarized target, projectile polarized in normal direction) for 500 MeV proton scattering from ^{3}He. The solid curves gives the exact results using the VP method and the dashed curves gives the results if no Coulomb force is included. The experimental data are from Häusser et al. [50].

1/2 nuclei in which spin–dependent forces couple orbital and spin angular-momenta channels. As part of that extension we also generalized the Blatt-Biedenharn phase shift analysis for the scattering of two spin 1/2 particles to cases where the S matrix is no longer symmetric (optical potentials or complex phase shifts). Although our formulation and calculation is for a more complicated spin dependence than examined by Arrellano et al. [10], we confirm their finding that the VP procedure can be made sufficiently accurate for applications to intermediate-energy proton scattering by using high-precision partial-wave expansions and large numbers of partial waves.

3.6. ACKNOWLEDGMENTS

It is our pleasure to thank Shashi Phatak and Lanny Ray for helpful discussions and suggestions. We gratefully acknowledge support from the U.S. Department of Energy under Grant DE-FG06-86ER40283.

3.7. REFERENCES

[1] E. Hernàndez and A. Mondragon, Phys. Rev. C **29**, 722 (1984); G. Garcia–Calderon and R. Peierls, Nucl. Phys. **A265**, 443 (1976).

[2] V. Fock, Z. Physik **98**, 145 (1935).

[3] Y.R. Kwon and F. Tabakin, Phys. Rev. C **18**, 932 (1978); D.P. Heddle, Y.R. Kwon, and F. Tabakin, Comp. Phys. Comm. **38**, 71 (1985).

[4] A. Cieplý, M. Gmitro, R. Mach, S.S. Kamalov, Phys. Rev. C **44**, 713 (1991); M. Gmitro, S.S. Kamalov, and R. Mach, Phys. Rev. C **36**, 1105 (1987).

[5] C.M. Vincent and S.C. Phatak, Phys. Rev. **10**, 391 (1974).

[6] R.H. Landau, S.C. Phatak, and F. Tabakin, Ann. Phys. **78**, 299 (1973); R.H. Landau, Comp. Phys. Comm. **28** 109 (1982).

[7] R. Crespo and J.A. Tostevin, Phys. Rev. C **41**, 2615 (1990).

[8] A. Picklesimer, P.C. Tandy, R.M. Thaler, and D.H. Wolfe, Phys. Rev. C **30**, 2225 (1984).

[9] Ch. Elster, L.C. Liu, and R.M. Thaler, Los Alamos National Laboratory Report LA-OR-90-2126, 1990; C.R. Chinn, Ch. Elster, and R.M. Thaler, Phys. Rev. C. **44**, 1569 (1991).

[10] H.F. Arellano, F.A. Brieva, and W.G. Love, Phys. Rev. C **41**, 2188 (1990).

[11] R.A. Eisenstein and F. Tabakin, Phys. Rev. C **26**, 1 (1982).

[12] The Coulomb waves used here are consistent with a Lippmann-Schwinger equation (3.2) in which the nonrelativistic expression $E(p) = p^2/2\mu$ is used for the energy. In our applications we use the relativistic expression $E(p) = \sqrt{p^2 + m_P^2} + \sqrt{p^2 + m_T^2}$ which is not fully consistent with these Coulomb waves (although the forms for the Coulomb waves appropriate to the Klein-Gordon and Dirac equations are known, we are not aware of any discussion of the forms appropriate to the relativisic Schrödinger equation we use). While this introduces some inaccuracy into our calculation, it does not affect the thrust of this paper which is to outline the extensions to the VP method for two spin 1/2 particles and to demonstrate that the requisite precision is attainable. We suspect it would be a better approximation to use relativistic Coulomb waves.

[13] We use the conventions and normalizations found in R.H. Landau, Quantum Mechanics II, J. Wiley, New York, 1990.

[14] Since this Wronskian is a functional of the solutions from two different Schrödinger equations, it is *not* independent of r.

[15] L.S. Rodberg and R.M. Thaler, *Introduction to the Quantum Theory of Scattering*, Academic Press, New York (1967).

[16] M.J. Páez, M.E. Sagen, and R. H. Landau, Comp. Phys. Comm., **52**, 141 (1988). Note, the factorization of $exp(2i\sigma_l)$ was not made properly for all parts of the scattering amplitude in this code and this may lead to numerical problems.

[17] J. Bystricky, F. Lehar, and P. Winternitz, Le Journal de Physique,**39**,1, (1978).

[18] P. La France and P. Winternitz, Le Journal de Physique, **41**,1391 (1980); correction in L. Ray et al., Phys. Rev C **37**,1169 (1988).

[19] R.H. Landau, M. Sagen, and G. He, Phys. Rev. C **41**, 50 (1990).

[20] T. Mefford and R. H. Landau, accepted for publication, Phys. Rev. C.

[21] H.P. Stapp, T.J. Ypsilantis and N. Metropolis, Phys. Rev. **105**, 302 (1957).

[22] A. Gersten, Phys. Rev. C **18**, 2252 (1978); Phys. Rev. C **24**, 2174 (1981).

[23] J.M. Blatt, and L.C. Biedenharn, Revs. of Mod. Phys. **24**, 258 (1952).

[24] J.M Eisenberg and W. Greiner, *Nuclear Theory*, Vol. 3, 39 (1972).

[25] M.J. Paez and R. H. Landau, Phys. Rev. C **29**,2267 (1984); **30**, 1757 (1984); Phys. Lett. **142B**, 235 (1984).

[26] R.H. Landau and M. Sagen, Phys. Rev. C **33**, 447 (1986).

[27] O. Häusser, Colloque de Physique, **C6, supp. au 22**, C6-99 (1990) (7^th Int. Conf. on Polarization Phenom. in Nucl. Phys., Paris, 1990).

4. CHARGE SYMMETRY BREAKING IN 500 MEV NUCLEON-TRINUCLEON SCATTERING

Tim Mefford and Rubin H. Landau

Department of Physics, Oregon State University, Corvallis, OR 97331

(Submitted for Publication, Physical Review C)

Elastic nucleon scattering from the ^{3}He and ^{3}H mirror nuclei is examined as a test of charge symmetry violation. The differential cross sections at 500 MeV are calculated using a microscopic, momentum-space optical potential including the full coupling of two spin 1/2 particles and an exact treatment of the Coulomb force. The charge-symmetry-breaking effects investigated arise from a violation within the nuclear structure, from the p-nucleus Coulomb force, and from the mass differences of the charge symmetric states. Measurements likely to reveal reliable information are noted.

4.1. INTRODUCTION

Charge symmetry (CS) is an approximate symmetry of the strong force arising from the nearly equal masses of the up and down quarks. At the nuclear level this means that, apart from electromagnetic and weak effects, the interactions of nuclear systems must be the same as the interactions of their charge-symmetric counterparts as long as the spin-space states involved remain identical. Yet even if the nucleon-nucleon strong forces respected this symmetry, in an experimental measurement we would expect some CS violation to arise from the Coulomb force, from the different masses for the neutron and proton, and from the different masses of charge-symmetric (mirror) nuclei. If the nucleon-nucleon strong force does not obey CS [51], we would expect further violation within the nuclear structure and within the nucleon–nucleus interaction.

A useful approach to testing CS in scattering from the trinucleon system is to remove some experimental uncertainties by forming ratios of cross sections which

should be identically equal if CS were obeyed. For the pion-trinucleon system, charge symmetry predicts [2]

$$r1 = \frac{d\sigma/d\Omega(\pi^+ - {}^3\mathrm{H})}{d\sigma/d\Omega(\pi^- - {}^3\mathrm{He})} \equiv 1, \tag{4.1}$$

$$r2 = \frac{d\sigma/d\Omega(\pi^- - {}^3\mathrm{H})}{d\sigma/d\Omega(\pi^+ - {}^3\mathrm{He})} \equiv 1. \tag{4.2}$$

When Pillai *et al.* [56,57] measured these ratios they found large deviations from 1 and concluded that substantial CS violation must be occurring. The analysis by Kim *et al.* [58] showed that the π-trinucleon Coulomb force is largely responsible for these ratios differing from 1, specifically, the ratios get relatively large when $d\sigma/d\Omega(\pi^{\mp} - {}^3\mathrm{He})$ have minima, and these minima are sensitive to Coulomb-nuclear interference. In addition, Kim *et al.* concluded that meaningful predictions of these ratios required a theory which could reproduce accurately the individual cross sections, and not just the ratios.

In a further study, Gibbs and Gibson [59] concluded that the magnitude of the ratios $r1$ and $r2$ after the π-trinucleon Coulomb force is included arises from CS violation within the nuclear structure. They fit the pion scattering data by introducing differences in the root-mean-square nuclear radii,

$$R_n({}^3\mathrm{H}) - R_p({}^3\mathrm{He}) = -0.030 \pm 0.008 \text{ fm}, \tag{4.3}$$

$$R_n({}^3\mathrm{He}) - R_p({}^3\mathrm{H}) = 0.035 \pm 0.007 \text{ fm}, \tag{4.4}$$

differences which would vanish if CS were good within the nuclear structure [60]. While these differences are relatively small compared to the nuclear radius of ~ 2 fm, and probably close to the level of uncertainty in strong-interaction calculations, they are approximately the same size as the CS violation found by including the Coulomb force in Fadeev calculations of nuclear structure. It is, accordingly, interesting to see if other hadron probes can confirm this degree of CS violation.

For the nucleon-trinucleon system, charge symmetry demands equal cross sections for $p - {}^3\mathrm{H}$ and $n - {}^3\mathrm{He}$ reactions, and, independently, for the $p - {}^3\mathrm{He}$ and $n - {}^3\mathrm{H}$ reactions:

$$r1 \stackrel{def}{=} \frac{d\sigma/d\Omega(p - {}^3\mathrm{H})}{d\sigma/d\Omega(n - {}^3\mathrm{He})} \equiv 1, \tag{4.5}$$

$$r2 \stackrel{def}{=} \frac{d\sigma/d\Omega(n - {}^3\mathrm{H})}{d\sigma/d\Omega(p - {}^3\mathrm{He})} \equiv 1, \tag{4.6}$$

$$\mathcal{R} \stackrel{def}{=} r1 \times r2 \equiv 1, \tag{4.7}$$

where $\mathcal{R}$ is called a "superratio". It is the calculation of these ratios and the sensitivities of these ratios to several aspects of CS violation with which we are concerned in this paper. A direct CS violation within the nucleon-nucleon interaction [51] is not considered here.

4.2. THE CALCULATION

Our calculation is based on a solution of the Lippmann-Schwinger equation with a microscopic, nonlocal, momentum-space optical potential including all spin $\frac{1}{2} \times \frac{1}{2}$ couplings and an exact treatment of the Coulomb potential [3,47,25]. The potential is the sum of nuclear (nuc) and Coulomb ($coul$) parts:

$$V(\mathbf{k}', \mathbf{k}, E) = V^{nuc}(\mathbf{k}', \mathbf{k}, E) + V^{coul}(\mathbf{k}', \mathbf{k}), \tag{4.8}$$

$$\begin{aligned} V^{nuc}(\mathbf{k}', \mathbf{k}, E) \simeq N \Big\{ & (t^{Nn}_{a+b} + t^{Nn}_{e} \vec{\sigma}^N_n) \rho^n_{mt}(q = |\mathbf{k}' - \mathbf{k}|) + \\ & \left[t^{Nn}_{a-b} \vec{\sigma}^N_n \vec{\sigma}^3_n + t^{Nn}_{e} \vec{\sigma}^3_n + t^{Nn}_{c+d} \vec{\sigma}^N_m \vec{\sigma}^3_m + t^{Nn}_{c-d} \vec{\sigma}^N_l \vec{\sigma}^3_l + t^{Nn}_{c+d} (\vec{\sigma}^N_m \vec{\sigma}^3_l + \vec{\sigma}^N_l \vec{\sigma}^3_m) \right] \rho^n_{sp}(q) \Big\} \\ & + Z \Big\{ (t^{Np}_{a+b} + t^{Np}_{e} \vec{\sigma}^N_n) \rho^n_{mt}(q) + \\ & \left[t^{Np}_{a-b} \vec{\sigma}^N_n \vec{\sigma}^3_n + t^{Np}_{e} \vec{\sigma}^3_n + t^{Np}_{c+d} \vec{\sigma}^N_m \vec{\sigma}^3_m + t^{Np}_{c-d} \vec{\sigma}^N_l \vec{\sigma}^3_l + t^{Np}_{c+d} (\vec{\sigma}^N_m \vec{\sigma}^3_l + \vec{\sigma}^N_l \vec{\sigma}^3_m) \right] \rho^n_{sp}(q) \Big\}. \end{aligned} \tag{4.9}$$

Here the t's are elementary, two-nucleon T matrices with their superscripts indicating the nucleons involved, and with their subscripts indicating the spin dependences [11]. The σ's are Pauli spinors with their superscripts indicating the beam

nucleon and trinucleon target involved, and with their subscripts indicating σ's projections onto the three independent scattering vectors, $\hat{\mathbf{n}} \propto \mathbf{k} \times \mathbf{k}'$, $\hat{\mathbf{m}} \propto \mathbf{k} - \mathbf{k}'$, and $\hat{\mathbf{l}} \propto \mathbf{k} + \mathbf{k}'$. The ρ's are four independent form factors describing the distribution of matter (mt) and spin (sp) within the nucleus.

The nuclear form factors are a key ingredient of the optical potential and possibly the most interesting path upon which CS violation enters our calculation. If CS were good for the trinucleon structure, the form factors would obey the relation

$$\rho^p_\alpha(^3\mathrm{He}) = \rho^n_\alpha(^3\mathrm{H}), \quad \rho^p_\alpha(^3\mathrm{H}) = \rho^n_\alpha(^3\mathrm{He}), \quad (\alpha = mt,\, sp). \tag{4.10}$$

The relations (4.10) reflect the CS of mirror nuclei: the distribution of the two "like" nucleons is the same in both nuclei, as is the separate distributions of the "unlike" nucleons, and this is independent of whether the nucleons are neutrons or protons.

If we ignore meson-exchange currents, the matter and spin form factors are related to the charge (ch) and magnetic (mg) form factors of the trinucleon system with the finite proton size removed [3],

$$\rho^p_{mt}(\mathrm{He}) = F_{ch}(\mathrm{He})/f, \tag{4.11}$$

$$\rho^n_{mt}(\mathrm{He}) = F_{ch}(\mathrm{H})/f, \tag{4.12}$$

$$\rho^n_{sp}(\mathrm{He}) = [\mu_p^2 F_{mg}(\mathrm{H}) - \mu_n^2 F_{mg}(\mathrm{He})]/[f(\mu_p^2 - \mu_n^2)], \tag{4.13}$$

$$\rho^p_{sp}(\mathrm{He}) = \mu_p\mu_n[F_{mg}(\mathrm{H}) - F_{mg}(\mathrm{He})]/[2f(\mu_p^2 - \mu_n^2)]. \tag{4.14}$$

Here f is the charge form factor of an elementary proton and $\mu_{p,n}$ the nucleons' magnetic moments. In previous work we have applied (4.12)-(4.14) with realistic charge and magnetic form factors. For the present calculation, however, we make some simplifying assumptions which permit a more convenient variation of nuclear radii and which help eliminate noise from what is already a numerically challenging calculation. Specifically, we assume that the distribution of spin for the unpaired nucleon is the same as its distribution of matter,

Table 4.2. The rms radii of the matter distributions for the trinucleon system. The first row are the charge symmetric values, the others include CS breaking.

	$R_p(^3\mathrm{H})$	$R_n(^3\mathrm{H})$	$R_p(^3\mathrm{He})$	$R_n(^3\mathrm{He})$
CS	1.700	1.880	1.880	1.700
CSB1	1.700	1.850	1.880	1.735
CSB2	1.760	1.850	1.880	1.795

$$\rho^n_{sp}(\mathrm{He}) = \rho^n_{mt}(\mathrm{He}), \tag{4.15}$$

while the spin distribution for the paired nucleons vanish,

$$\rho^p_{sp}(\mathrm{He}) = 0. \tag{4.16}$$

To enable convenient variations of the nuclear radii, we use analytic expressions [62] for the form factors. (Performing the calculations with numerical, Fadeev form factors [63], changes the predictions somewhat, but not the conclusions.)

The nuclear RMS radii used in our calculation are given in Table 4.2. Row one gives the values used assuming charge symmetry, while rows two and three break CS. The 1.88 fm value derives from the ^{3}He charge form factor [62] and the 1.70 fm value from the ^{3}H charge form factor [64,65]. The value of 1.76 fm for $R_p(^3\mathrm{H})$ in row three arises from a recent measurement [66], and is significantly larger than the values of previous measurements. It would be valuable to have it confirmed with a nucleon probe.

To obtain sufficient numerical accuracy for the large momentum transfers which occur with protons, we discretized the coupled-channels Lippmann-Schwinger

equation over as many as 64 grid points, decomposed the potentials and T matrices into 64 partial waves, and included NN partial waves up to $l = 4$ (higher NN partial waves tend to introduce numerical noise). To include the singular, momentum-space Coulomb potential, we used a cutoff radius of 7 fm, and verified that our results are stable for small variations about this radius [25]. With all these effects included at the requisite high precision, the calculation is numerically intensive, and so we modified the computer code LPOTp to run on a parallel computer [67].

4.3. RESULTS

The calculations we report here are for 500 MeV nucleon scattering. Nearby energies yield similar predictions. In the top part of Fig. 4.1 we show the predicted differential cross sections for proton and neutron elastic scattering from ^{3}He and ^{3}H with all CS-breaking effects included. We see that the neutron scattering cross sections (dotted and long-dashed curves) do not exhibit a forward Coulomb peak. But aside from that, the $p\,^3$He and $n\,^3$H cross sections, and the $p\,^3$H and $n\,^3$He cross sections, respectively, are nearly equal (as expected from approximate CS). We also note that the proton scattering cross sections (solid and short-dashed curves) develop distinct oscillations for angles larger than $\sim 100°$. These oscillations are a consequence of Coulomb-nuclear interference, and in contrast to pion scattering where the large-angle ratios all equal one, nucleon oscillations occur because the nuclear cross section have fallen off to a level comparable to the background Coulomb cross section.

An important consequence of the backward-hemisphere oscillations in nucleon-trinucleon scattering is that the ratios (4.5)-(4.6) deviate considerably from 1, as we show in the bottom of Fig. 4.1. Unfortunately, while we really do expect this large an experimental CS-violation signal to occur, we suspect that the back-angle

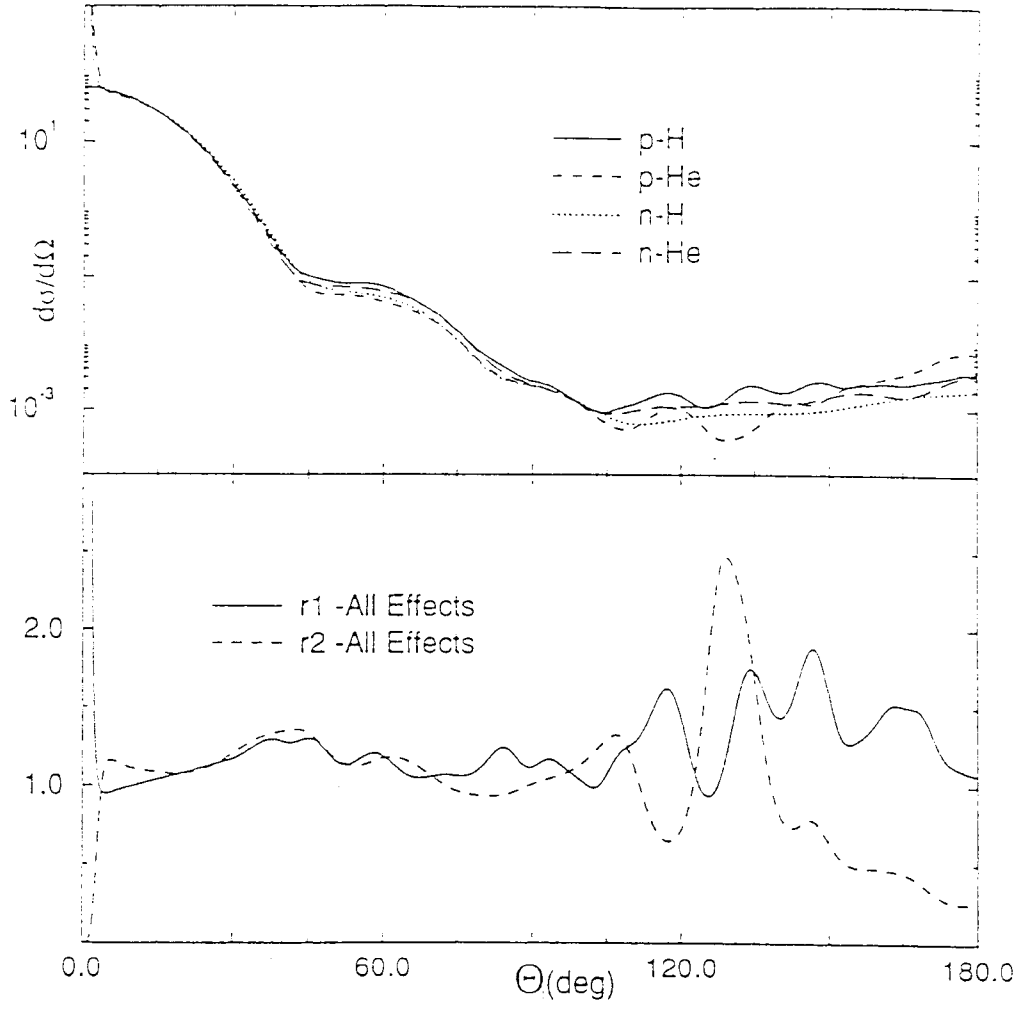

Figure 4.1. Top: Differential cross-sections for p and n scattering from ^{3}He and ^{3}H at 500 MeV as a function of CM scattering angle. Bottom: The ratios $r1$ and $r2$ given by equations (4.5) and (4.6). All CS-violating effects are included in this figure.

part is too sensitive to details of Coulomb-nuclear interference and to uncertainties in the numerical Coulomb procedure [25] to produce reliable information. Consequently, we consider only forward-hemisphere measurement of the ratios as reliable, and henceforth show only them. For example, we notice in the bottom of Fig. 4.1 that the forward-hemisphere ratios $r1$ and $r2$ differ smoothly and significantly from 1. Furthermore, as shown in Figs. 4.2-4.3, when the superratio $\mathcal{R}$ (4.7) is formed, we do obtain a large signal in the forward hemisphere, quite a bit larger in fact than the one for pion scattering.

In the the top of Fig. 4.2 we show the predicted superratio when all CS violation effects are included. The solid and dashed curves correspond to the smaller and larger nuclear radii given in rows 2 and 3 of Table 4.2. We see that the superratio is sensitive, but not overly sensitive, to the uncertainty in nuclear radii. If an experiment could measure the ratio to this level of precision, an independent measurement of nuclear size should be possible.

In the the bottom of Fig. 4.2 we show the predicted superratio including the CS violation arising from only the (n,p) and (^{3}He,^{3}H) mass differences (solid curve), and from only the nuclear structure (dashed curve). The mass difference effect essentially disappears in comparison to the nuclear structure one. Since a violation in the nuclear structure is of more interest than the mass difference one, this is an encouraging finding.

In the top of Fig. 4.3 we see the sensitivity of the superratio $\mathcal{R}$ to the use of nuclear form factors given by analytic fits to electron scattering data (solid curve) and given by numerical solutions to Fadeev equations (dashed curve). In the top part of this figure, CS violation from only the mass differences is included, and in the bottom violation from only the p-nucleus Coulomb force is included. This figure shows that the superratio in this angular region is not sensitive to details of the

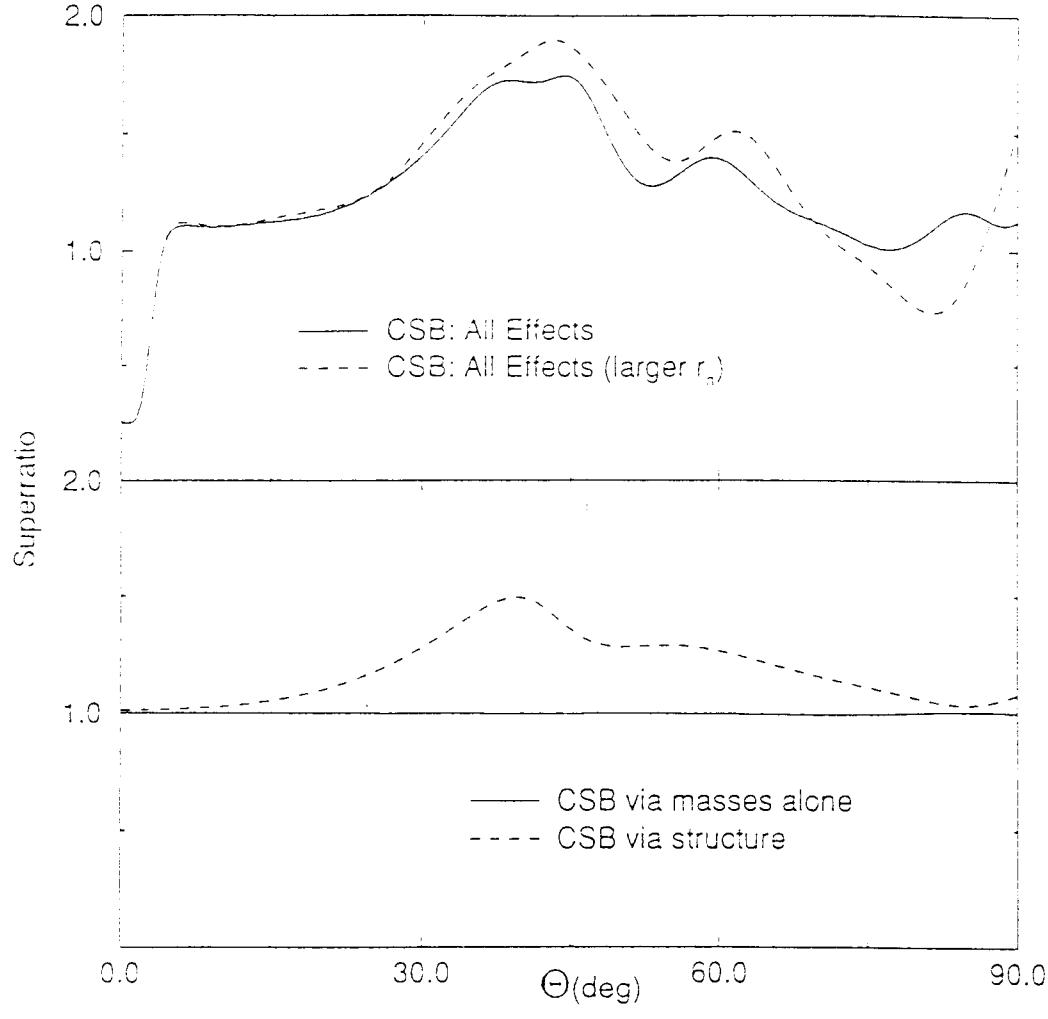

Figure 4.2. Top: The superratio R, (4.6), with all CS violating effects included. The solid and dashed curves correspond to smaller and large nuclear radii given in lines 2 and 3 respectively of Table 4.2. Bottom: The superratio R including the CS violation arising from only the (n,p) and (^{3}He,^{3}H) mass differences (solid curve), and from CS violation arising from only the nuclear structure (dashed curve).

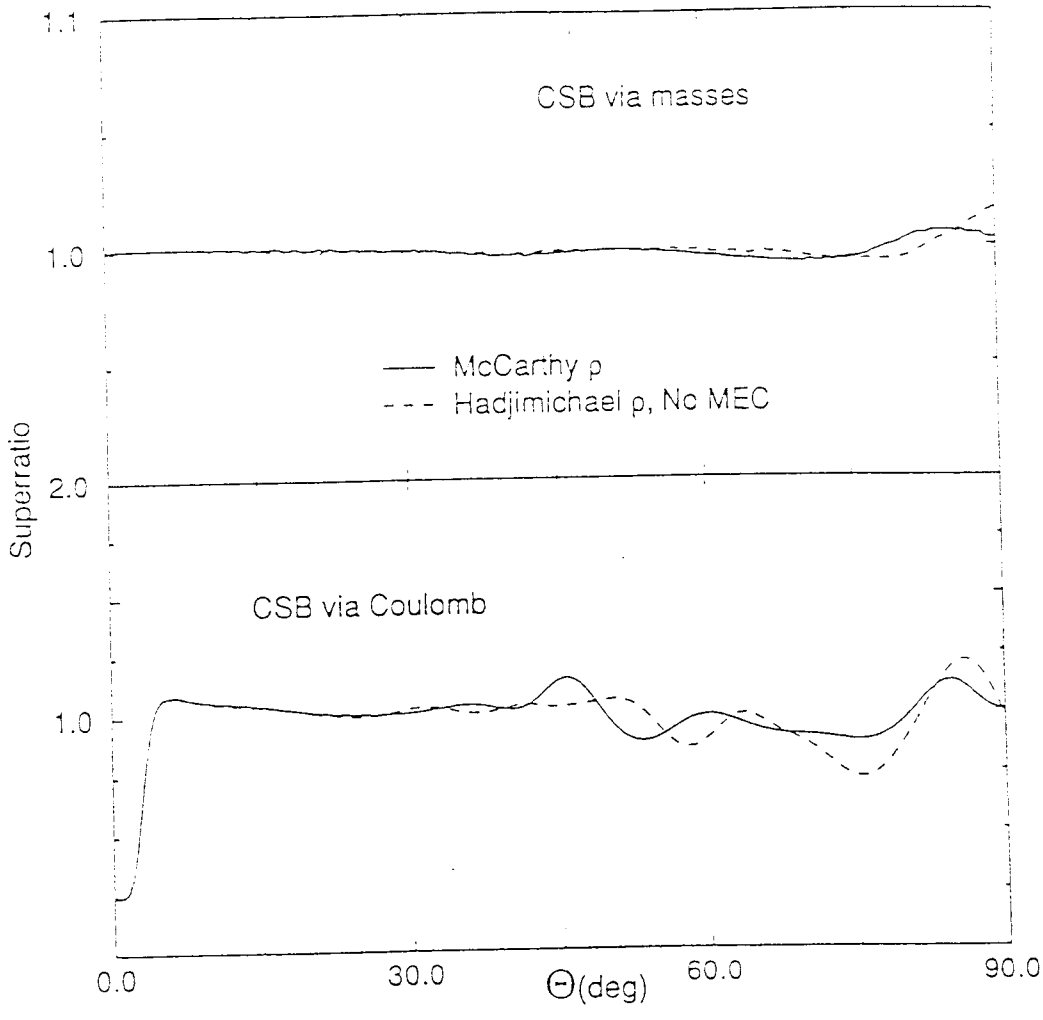

Figure 4.3. Top: The sensitivity of the superratio R to use of nuclear form factors given by analytic fits to electron scattering data (solid curve) and given by numerical solutions to Fadeev equations (dashed curve). In this case, CS violation from only the mass differences are included. Bottom: Same as on top, only now CS violation arises from only the p-nucleus Coulomb force.

nuclear form factors, but is sensitive to the nuclear size. In addition, by comparing Figs. 4.2 and 4.3 we see the main CS violation arises from the nuclear structure, with a somewhat smaller violation arising from the p-nucleus Coulomb force. The Coulomb and structure effects are seen to combine in the 40° region in Fig. 4.2 to produce a large effect.

4.4. CONCLUSION

We have calculated the ratios of differential cross sections for 500 MeV proton and neutron elastic scattering from ^{3}He and ^{3}H. We used a microscopic, momentum-space optical potential and included the Coulomb force and all spin couplings exactly. We found that at large angles the utility of these ratios as a measure of charge symmetry breaking is low due to highly sensitive Coulomb-nuclear interference. However, the forward-hemisphere ratio appears to be quite reliable yet still sensitive to the important CS violation mechanisms.

We predict that most of the CS violation in nucleon-trinucleon scattering should arise from CS violation at the nuclear structure level, with about 1/3 of the effect arising from the proton-nucleus Coulomb interaction. A measurement of the ratios of cross sections for nucleon-trinucleon scattering at the 10% level in the forward hemisphere would be a valuable adjoint to the analogous pion measurements.

4.5. ACKNOWLEDGMENTS

We gratefully acknowledge support from the U.S. Department of Energy under Grant DE-FG06-86ER40283 at Oregon State University. Some of the computations were conducted using resources of the Cornell Theory Center, which receives major funding from the National Science Foundation and New York State with additional support from Advanced Research Projects Agency, the National Center

for Research Resources at the National Institutes of Health, IBM Corporation and members of the Corporate Research Institute. We also thank Cherri Pancake for helpful conversations.

4.6. REFERENCES

[1] G. Krein, A.W. Thomas, A.G. Williams, Phys. Lett. **B317**, 293 (1993); G. Krein, A.G. Williams, Mod. Phys. Lett. **A5** 399 (1990); G.A. Miller, A.W. Thomas, A.G. Williams, Phys. Rev. Lett. **56**, 2567 (1986).

[2] R. H. Landau, Ann. Phys. **92**, 205 (1975); Phys. Rev. **15**, 2127 (1977).

[3] C. Pillai, D. B. Barlow, B. L. Berman, W. J. Briscoe, A. Mokhtari, B. M. K. Nefkens, and M. E. Sadler, Phys. Rev. C **43**, 1838 (1991).

[4] B. M. K. Nefkens, W. J. Briscoe, A. D. Eichon, D. H. Fitzgerald, J. A. Holt, A. A. Mokhtari, J. A. Wightman, M. E. Sadler, R. L. Boudrie, and C. L. Morris, Phys. Rev. Lett. **52**, 738 (1984).

[5] K. Y. Kim, Y. E. Kim, and R. H. Landau, Phys. Rev. C **36**, 2155 (1987).

[6] W. R. Gibbs and B. F. Gibson, Phys. Rev. C **43**, 1012 (1991).

[7] L. I. Schiff, Phys. Rev. **133**, B802 (1964); B. F. Gibson and Schiff, Phys. Rev. **138** B26 (1965).

[8] M.J. Paez and R. H. Landau, Phys. Rev. C **29**,2267 (1984); **30**, 1757 (1984); Phys. Lett. **142B**, 235 (1984).

[9] T. Mefford, R. H. Landau, L. Berge, and K. Amos, Phys. C **50**, 1648 (1994).

[10] D. Lu, T. Mefford, R. H. Landau, and G. Song, Phys. Rev. C **50**, 3037 (1994).

[11] At the NN level, we assume both charge symmetry, $t_\alpha(pp) = t_\alpha(nn)$, and charge independence (isospin symmetry), $t_\alpha(pp) = t_\alpha(pn)$, where α denotes the quantum state of the particles.

[12] J. S. McCarthy, I. Sick, and R. R. Whitney, Phys. Rev. C **15**, 1596 (1977).

[13] E. Hadjimichael, B. Goulard, and R. Bournais, Phys. Rev. C **27**, 831 (1983).

[14] H. Collard, R. Hofstader, E. B. Hughes, A. Johansson, M. R. Yearian, R. B. Day, and R. T. Magner, Phys. Rev. **138**, B57, (1965).

[15] D. H. Beck, S. B. Kowalski, M. E. Schulze, W. E. Turchinetz J. W. Lightbody, Jr., X. K. Maruyama, W. J. Stapor, H. S. Caplan, G. A. Retzlaff, D. M. Skopik, and R. Goloskie, Phys. Rev. C **30**, 1403 (1984).

[16] F.-P. Juster, S. Auffret, J.-M. Cavedon, J.-C. Clemens, B. Frois, D. Goutte, M. Huet, P. Leconte, J. Martino, Y. Mizuno, X.-H. Phan, S. Platchkov, S. Williamson, and I. Sick, Phys. Rev. Lett. **55**, 2261 (1985).

[17] T. Mefford, R.H. Landau, "A distributed memory, parallel code for polarized nucleon scattering from polarized nuclei", OSU preprint, submitted to *Computer Physics Communiations.*

5. PPP: A DISTRIBUTED MEMORY PARALLEL CODE FOR POLARIZED PROTONS SCATTERING FROM POLARIZED NUCLEI

Tim Mefford and Rubin H. Landau

Department of Physics, Oregon State University, Corvallis, OR 97331, USA

Supported in part by the US Department of Energy; computing performed using resources of the Cornell Theory Center, which receives major funding from the National Science Foundation and New York State, with additional support from IBM corporation.

(Submitted to Computer Physics Communications.)

PPP computes a microscopic, momentum-space optical potential and uses it as the driving term in the solution of coupled, Lippmann-Schwinger integral equations in momentum space. The solutions are used to predict all physical observables for the scattering of polarized nucleons from a polarized spin-1/2 nucleus. The inclusion of all spin degrees of freedom and the exact treatment of the Coulomb force leads to sufficient computational expense to make a parallel implementation of the previous LPOTp code attractive. This FORTRAN-77 code runs in parallel using the message passing library PVM.

Title of Program: PPP

Catalogue number: (supplied by Elsevier)

Program obtainable from: CPC Program Library, Queen's University of Belfast, N. Ireland (see application form in this issue)

Licensing provisions: none

Computer: IBM SP1; DEC 3000/500+DEC 200 4/166 + IBM RS6000/320.

Installations: Cornell Theory Center; Oregon State University.

Programming language used: FORTRAN 77, PVM

Memory required to execute with typical data: 20 MB

No. of processors used: 1-32; 1-3.

No. of lines in distributed program, including test data, etc.: 14,500

Nature of physical problem

Assuming the basic symmetries of nature, the scattering of a polarized nucleon from a polarized spin-1/2 nucleus can be described in terms of six complex amplitudes, each containing a different combination of the projectile's and the target's spin operators. These amplitudes, in turn, can be used to predict 36 experimental observables. To calculate these amplitudes we envision the scattering of the projectile nucleon from the nucleus as the coherent sum of multiple scatterings of the projectile from one, two, three, and so forth nucleons within the nucleus. We employ a theoretical optical potential (complex, nonlocal, and energy dependent) to describe the scattering of the projectile from a single nucleon bound within the nucleus. This potential incorporates the finite size of the projectile-nucleon interaction, proper kinematics to incorporate nucleon and nucleus recoil, modification of the elementary interactions due to binding effects, and Lorentz-invariant relations among the kinematic variables in different reference frames. We use the Lippmann-Schwinger equation (a momentum-space transform of the Schrödinger equation for scattering) to sum up all the multiple scatterings generated by the optical potential. While the total angular momentum is conserved in the scattering, the individual spins and orbital angular momenta of the nucleon and nucleus couple to each other, and this leads to coupled integral equations[1] and accordingly larger matrices. Further computational intensity arises from the high-precision inclusion of both the strong and Coulomb forces in momentum space[2][3].

Method of solution

PPP is a parallel extension of and a computational improvement to the serial code LPOTp[4]. It takes tables of the nucleon-nucleon (NN) phase shifts as input and uses them to generate the elementary NN scattering. It also takes as input nuclear form factors, that is, the Fourier transforms of densities describing the distribution of charge and magnetism within the target nucleus. The optical potential is constructed in the four-dimensional spin basis. The potential is calculated at the points on a grid in momentum space. Because of the large number of such points, we have calculated each row of the matrix on a different processor as the Phase I parallelization.

In order to reduce the dimensionality of the coupled integral equations to be solved, the equations and potentials are projected onto the angular momentum-energy basis. This "partial-wave" projection is computationally expensive, and so as Phase II of the parallelization, we solved the coupled-channels Lippmann-Schwinger integral equations for each orbital angular momentum value in parallel. This entails discretizing the integral equations into simultaneous linear equations and solving the linear equations via matrix inversion using the LAPACK routines *zgetrf* and *zgetri*. Although we have found that solutions of these equations with Gaussian elimination is ~30% faster than matrix inversion, we compute the inverse in order to permit a separate computation of the projectile-nucleus wave function. The resulting scattering amplitudes are used to predict the experimental observables.

References

[1] Mefford, Landau, Berge, and Amos, Phys. Rev. C **50**, 1648, (1994).

[2] Vincent and Phatak, Phys. Rev. **10**, 391, (1974).

[3] Lu, Mefford, Landau, and Song, Phys. Rev. C **50**, 3037, (1994).

[4] Paez, Sagen, and Landau, Comp. Phys. Comm., **52** (1988) 141-159.

5.1. INTRODUCTION

Recent experimental advances permit the precision measurement of the scattering of polarized proton beams from polarized nuclei, with the projectile polarization measured after, as well as before, the scattering. This has led to demands that the theory we have developed for nucleon-nucleus scattering be used to predict more and more spin observables and to predict them with greater accuracy. The resulting theoretical improvements have led to an increase in the size and complexity of the code LPOTp used for calculating proton scattering. For example, the larger number ($\sim$ 96) of partial waves required to include the Coulomb potential along with the nuclear one, the extra channel couplings arising from the mixing of the spin singlet and triplet states, and the larger numbers of grid points needed for high accuracy at large momentum transfers all combine to produce a calculation of significant computational intensity. For this reason, and to handle future order-of-magnitude longer calculations in which there is a complete average over the internal or Fermi momenta of nucleons within the nucleus, we have extended our serial code LPOTp into a parallel one PPP designed to run on a distributed memory computer. This FORTRAN-77 code runs in parallel using the message-passing Parallel Virtual Machine (PVM) library developed at Oak Ridge National Laboratory. [68] The test calculations were carried out on an IBM SP1 at the Cornell Theory Center and on a cluster of three workstations (DEC 3000/500 + DEC 200 4/166 + IBM RS6000/320) locally.

5.2. PROGRAM STRUCTURE

PPP performs three basic tasks. First it computes the momentum-space optical potential $V(\mathbf{k}', \mathbf{k})$. Second it solves the Lippmann-Schwinger equation, which for our problem reduces to 96 sets of coupled, 1D integral equations. Finally, the solutions to these integral equations are used to predict the 36 experimental observables describing the scattering of two spin-1/2 particles. Phase I of our parallelization corresponds to the first task and Phase II to the second. Although the equations for the observables are tedious to enumerate, they are easy to compute and would not benefit from a parallel treatment.

5.2.1. Optical Potential Construction (Phase I)

PPP inputs tables of the nucleon-nucleon (NN) phase shifts and uses them to generate elementary NN scattering matrices t_i^{NN}, or what we often refer to as the $a - f$ amplitudes. PPP also inputs nuclear form factors ρ's, which are the Fourier transforms of the density distributions of charge and magnetism within the target nucleus. From these ρ's PPP deduces the distributions of matter and spin within the nucleus, and then combines the ρ's and t's to form the optical potential.

If we assume rotation invariance, parity conservation, and time reversal invariance, the experimental observables needed to describe the scattering of two spin-1/2 particles all derive from a T matrix which has the spin-space structure:

$$\begin{aligned} 2\,T(\mathbf{k}', \mathbf{k}) = a + b + (a - b)\sigma_n^p \sigma_n^t + (c + d)\sigma_m^p \sigma_m^t \\ + (c - d)\sigma_l^p \sigma_l^t + e(\sigma_n^p + \sigma_n^t) + f(\sigma_n^p - \sigma_n^t). \end{aligned} \tag{5.1}$$

Here $\mathbf{k}$ and $\mathbf{k}'$ are momenta of the projectile prior to and after the scattering, $q = |\mathbf{k}' - \mathbf{k}|$ is the magnitude of the momentum transferred to the target nucleus,

and the σ's are Pauli spin operators. The superscripts on the Pauli spinors in (5.1) indicate whether they are the spin operator for the projectile p or target t, while the subscripts on σ indicate dot products with the three independent unit vectors which define the three-dimensional space of the scattering process,

$$\hat{\mathrm{n}} = \frac{\mathbf{k} \times \mathbf{k}'}{|\mathbf{k} \times \mathbf{k}'|}, \quad \hat{\mathrm{m}} = \frac{\mathbf{k} - \mathbf{k}'}{|\mathbf{k} - \mathbf{k}'|}, \quad \hat{\mathrm{l}} = \frac{\mathbf{k} + \mathbf{k}'}{|\mathbf{k} + \mathbf{k}'|}. \tag{5.2}$$

The first-order optical potential is constructed in the spin-momentum basis as the sum of products of NN scattering matrices, projectile and target spin operators, and nuclear forms factors [3,47]:

$$\begin{aligned} V(\mathbf{k}', \mathbf{k}) \simeq\ & N \Big\{ (t^{pn}_{a+b} + t^{pn}_{e} \sigma^{p}_{n}) \rho^{n}_{mt}(q) + \rho^{n}_{sp}(q) \times \\ & \Big[t^{pn}_{a-b} \sigma^{p}_{n} \sigma^{t}_{n} + t^{pn}_{e} \sigma^{t}_{n} + t^{pn}_{c+d} \sigma^{p}_{m} \sigma^{t}_{m} + t^{pn}_{c-d} \sigma^{p}_{l} \sigma^{t}_{l} + t^{pn}_{c+d} (\sigma^{p}_{m} \sigma^{t}_{l} + \sigma^{p}_{l} \sigma^{t}_{m}) \Big] \Big\} \\ & + Z \Big\{ (t^{pp}_{a+b} + t^{pp}_{e} \sigma^{p}_{n}) \rho^{p}_{mt}(q) + \rho^{p}_{sp}(q) \times \\ & \Big[t^{pp}_{a-b} \sigma^{p}_{n} \sigma^{t}_{n} + t^{pp}_{e} \sigma^{t}_{n} + t^{pp}_{c+d} \sigma^{p}_{m} \sigma^{t}_{m} + t^{pp}_{c-d} \sigma^{p}_{l} \sigma^{t}_{l} + t^{pp}_{c+d} (\sigma^{p}_{m} \sigma^{t}_{l} + \sigma^{p}_{l} \sigma^{t}_{m}) \Big] \Big\} \end{aligned} \tag{5.3}$$

where the subscripts on t indicate their origins in terms of the elementary NN amplitudes in (5.1), and the superscripts indicate whether proton-proton or proton-neutron scattering occurs. The potential (5.3) manifestly contains the projectile and target spin dependences weighted by four form factors (the ρ's) describing the distributions of spin (sp) and matter (mt) arising from the protons and neutrons within the nucleus.

Inclusion of the Coulomb potential in momentum space (in addition to the nuclear optical potential) for two spin-1/2 particles requires our extension [25] of the Vincent-Phatak technique to coupled angular-momentum channels and to much larger numbers of partial waves and grid points (both $\sim$ 96). The basis of the technique is a momentum-space Coulomb potential which is the Fourier transform of the coordinate-space potential arising from the actual nuclear charge distribution cut off at some radius R_{cut}:

$$V_{coul}(\mathbf{k}',\mathbf{k}) = \frac{Z_p Z_t e^2}{2\pi^2 q^2}\left[\rho(q) - \cos(qR_{cut})\right]. \tag{5.4}$$

Here Z_p and Z_t are the charge numbers of the projectile and target respectively, and the second term in (5.4) arises from the cutoff. The cut-off radius R_{cut} should be made as large as possible to guarantee that none of the nuclear force is cut off (R_{cut} equal to two times the nuclear radius seems about right). The final answers should be insensitive to a 1-2 fm variation of R_{cut}. In this way the short-range nuclear force and the short-range corrections which account for the finite extent of the nuclear charge distribution are included as input to the integral equations. The scattering from a point charge is included by adding the amplitude for scattering from a point charge f^c_{pt} to the final projectile-target a and b amplitudes of (5.1):

$$\begin{pmatrix} a(\theta) \\ b(\theta) \end{pmatrix} \rightarrow \begin{pmatrix} a(\theta) + f^c_{pt}(\theta) \\ b(\theta) + f^c_{pt}(\theta) \end{pmatrix}. \tag{5.5}$$

Many-body effects and relativity leads to a potential V which is a nonlocal operator, that is, an integration over all of space is required to determine the potential at any one point. Rather than treat such a potential in coordinate space and have to solve an integro-differential equation, we solve the Lippmann-Schwinger equation in momentum space:

$$T(\mathbf{k}',\mathbf{k}) = V(\mathbf{k}',\mathbf{k}) + \int \frac{d^3p}{E^+ - E(p)} V(\mathbf{k}',\mathbf{p})\, T(\mathbf{p},\mathbf{k}), \tag{5.6}$$

where $E(p) = E_p(p) + E_t(p)$ is the projectile plus target energy and the $+$ superscript on E indicates a $+i\epsilon$ has been added to the energy to move the zero of the denominator infinitesimally off the real axis.

In order not to deal with three-dimensional integral equations, the $T(\mathbf{k}',\mathbf{k})$ and $V(\mathbf{k}',\mathbf{k})$ in (5.6) are expanded as a series in spin-angle functions:

$$V(\mathbf{k}',\mathbf{k}) = \frac{2}{\pi} \sum_{jm_j ll' ss'} i^{(l'-l)}\, V^{j(s's)}_{l'l}(k',k)\, \mathcal{Y}^{jm_j}_{l's'}(\hat{k}')\, \mathcal{Y}^{\dagger jm_j}_{ls}(\hat{k}), \tag{5.7}$$

$$T(\mathbf{k}',\mathbf{k}) = \frac{2}{\pi} \sum_{jm_j ll' ss'} i^{(l'-l)}\, T_{l'l}^{j(s's)}(k',k)\, \mathcal{Y}_{l's'}^{jm_j}(\hat{k}')\, \mathcal{Y}_{ls}^{\dagger jm_j}(\hat{k}), \tag{5.8}$$

where l, s, and j are the orbital, spin, and total angular momenta for the target plus projectile. The determination of $T_{l'l}^{j(s's)}(k',k)$ requires the solution of an integral equation. The potential $V_{l'l}^{j(s's)}(k',k)$, which is the driving term in the integral equation, is determined by a two-step procedure [47]. First, we evaluate the potential in the momentum-spin basis, that is, we take the spin matrix elements of the potential in (5.3). After some manipulations, the sums in Eq. (5.7) reduce to the partial wave decompositions; for example,

$$V_{ss}(\mathbf{k}',\mathbf{k}) = \frac{1}{2\pi^2} \sum_{l=0} P_l(x)(2l+1)\, V_{ll}^{l(ss)}(k',k), \tag{5.9}$$

$$\begin{aligned} V_{01}(\mathbf{k}',\mathbf{k}) = \frac{\sqrt{2}}{4\pi^2} \sum_{l=1} P_l^1(x) \Bigg\{ & -\frac{l+2}{l+1} V_{ll}^{l+1(tt)}(k',k) + \frac{2l+1}{l(l+1)} V_{ll}^{l(tt)}(k',k) \\ & + \frac{l-1}{l} V_{ll}^{l-1(tt)}(k',k) + \sqrt{\frac{l+2}{l+1}} V_{ll+2}^{l+1(tt)}(k',k) - \sqrt{\frac{l-1}{l}} V_{ll-2}^{l-1(tt)} \Bigg\}. \end{aligned} \tag{5.10}$$

Note that the sums are over the orbital angular momentum l of the final state, and that we have combined matrix elements of different total angular momentum j values which multiply the same Legendre polynomial. We invert the partial-wave expansions for the potential to obtain $V_{l'l}^{j(s's)}(k',k)$ by multiplying the equation for each $V_{m'm}(\mathbf{k}',\mathbf{k})$ by $P_l^{|m'-m|}$, and then numerically evaluating the integral:

$$I_{m'm}(k',k) = \int_{-1}^{1} dx\, V_{m'm}(\mathbf{k}',\mathbf{k})\, P_l^{|m'-m|}(\cos\theta_{k'k}). \tag{5.11}$$

For cases in which only one $V_{l'l}^{j(s's)}(k',k)$ enters into the sum, this is simple; for example,

$$V_{ll}^{l(ss)}(k',k) = \pi^2 I_{ss}(k',k). \tag{5.12}$$

For cases in which only several $V_{l'l}^{j(s's)}(k',k)$'s for differing j and l values enters into the sum, the projection results in five, coupled equations:

$$\begin{pmatrix} I_{11}(k',k) \\ I_{00}(k',k) \\ I_{10}(k',k) \\ I_{01}(k',k) \\ I_{1-1}(k',k) \end{pmatrix} = \begin{pmatrix} \\ B_{l'l}^{m'm} \\ \\ \\ \end{pmatrix} \begin{pmatrix} V_{ll}^{l+1(tt)}(\mathbf{k}',\mathbf{k}) \\ V_{ll}^{l(tt)}(\mathbf{k}',\mathbf{k}) \\ V_{ll}^{l-1(tt)}(\mathbf{k}',\mathbf{k}) \\ V_{ll+2}^{l+1(tt)}(\mathbf{k}',\mathbf{k}) \\ V_{ll-2}^{l-1(tt)}(\mathbf{k}',\mathbf{k}) \end{pmatrix} \tag{5.13}$$

where the $B_{l'l}^{m'm}$ matrix is composed of the coefficients multiplying the V's as in equations (5.9) and (5.10). We solve the matrix equation (5.13) by numeric matrix inversion, $\mathbf{V} = B^{-1}\mathbf{I}$, and as a check we sum the partial-wave potentials according to Eqs. (5.9) and (5.10) and compare the sums to the original three-dimensional expressions.

This partial-wave projection is computationally expensive since we must do it for all values of k and k' on the grid $\{k_i | i = 1, N\}$ used to solve the integral equation (typically a 96×96 grid). Accordingly, as Phase I of the parallelization we evaluate each row of the potential matrices

$$V_{l,spin}(k,k') = \begin{pmatrix} V(k_1,k_1) & \dots & V(k_1,k_N) \\ V(k_2,k_1) & \dots & . \\ . & \dots & . \\ . & \dots & . \\ V(k_N,k_1) & \dots & V(k_N,k_N) \end{pmatrix} \tag{5.14}$$

in parallel, that is, each row is computed on a different processor.

The division of labor might have been made differently. Using N grid points for k and k', $lmax$ partial waves [number of values for subscript l in Eq. (5.14)], and eight spin channels (number of values for subscript $spin$ in Eq. (5.14))] requires calculating $N \times N \times lmax \times 8$ terms. The Phase I parallelization spawns N processes, each representing a row of Eq. (5.14), to calculate $N \times lmax \times 8$ terms apiece. Alternatively, We might have spawned $N \times N$ processes, one for each V element, to

calculate only $lmax \times 8$ terms each. This would have greatly increased my overhead; We chose instead to spawn a number as close to, without falling short of, the number of processors available as possible.

5.2.2. Lippmann-Schwinger Equation (Phase II)

Once the partial-wave expansions of the potentials have been determined, the scattering amplitudes are computed by substituting the potentials into the Lippmann-Schwinger equation (5.6), and solving the resulting integral equations. The integral equations reduce to coupled, one-dimensional equations of the form:

$$T_\alpha(k',k) = V_\alpha(k',k) + \sum_\gamma \int_0^\infty dp \frac{p^2 V_\gamma(k',p) T_\gamma(p,k)}{E + i\epsilon - E(k)}. \tag{5.15}$$

The subscript α represents the spin channel while the summation over γ spans the channels which couple to α.

The integrand in (5.15) contains an integrable singularity at the "on-shell" momentum k_0. To permit numerical integration, this singularity is removed by subtracting a term from the integrand which leaves the integrand nonsingular, and then adding in the integral of the subtracted term:

$$\begin{aligned}\int_0^\infty dp \frac{p^2 V(k',p) T(p,k)}{E - E(p) + i\epsilon} &= \int_0^\infty dp \left[\frac{p^2 V(k',p) T(p,k)}{E - E(p) + i\epsilon} - \frac{2\mu k_0^2 V(k',k_0) T(k_0,k)}{k_0^2 - p^2 + i\epsilon}\right] \\ &\quad + 2\mu k_0^2 V(k',k_0) T(k_0,k) \int_0^\infty dp \frac{1}{k_0^2 - p^2 + i\epsilon} \qquad (5.16) \\ &= \int_0^\infty dp \left[\frac{p^2 V(k',p) T(p,k)}{E - E(p)} - \frac{\pi\mu k_0^2 V(k',k_0) T(k_0,k)}{k_0^2 - p^2}\right] \\ &\quad - \pi i \mu k_0 V(k',k_0) T(k_0,k), \qquad (5.17)\end{aligned}$$

where the RHS of Eq. (5.16) is evaluated analytically and where μ is the relativistic "reduced mass":

$$\mu = \frac{1}{2}\frac{dp^2}{dE} = \frac{E_1(k_0) E_1(k_0)}{E_1(k_0) + E_1(k_0)}. \tag{5.18}$$

We solve the integral equations (5.15) by approximating the integrals as sums over N Gaussian grid points $\{p_i | i = 1, N\}$ with weights $\{w_i | i = 1, N\}$:

$$T_\alpha(k',k) = V_\alpha(k',k) - \sum 2i\mu k_0 V_\gamma(k',k_0)T_\gamma(k_0,k) + \frac{2}{\pi}\sum_{\gamma,i}\left[\frac{p_i^2 V_\gamma(k',p_i)T_\gamma(p_i,k)}{E - E(p_i)} - \frac{2\mu k_0^2 V_\gamma(k',k_0)T_\gamma(k_0,k)}{k_0^2 - p_i^2}\right]. \tag{5.19}$$

We convert (5.19) to a set of linear equations, such as

$$\begin{pmatrix} T_{jj}^{j(ss)}(m,n) \\ T_{jj}^{j(ts)}(m,n) \end{pmatrix} = \begin{pmatrix} V_{jj}^{j(ss)}(m,n) \\ V_{jj}^{j(ts)}(m,n) \end{pmatrix} + \begin{pmatrix} V_{jj}^{j(ss)}(m,n) & V_{jj}^{j(st)}(m,n) \\ V_{jj}^{j(ts)}(m,n) & V_{jj}^{j(tt)}(m,n) \end{pmatrix} \begin{pmatrix} G_{n=m} & 0 \\ 0 & G_{n=m} \end{pmatrix} \begin{pmatrix} T_{jj}^{j(ss)}(m,n) \\ T_{jj}^{j(ts)}(m,n) \end{pmatrix}. \tag{5.20}$$

by defining the supermatrix elements for G, V, and T with an $(N+1)$st, additional, "on-shell," point, such that $k_{N+1} = k_0$ and the sums over n and m now extend to $N+1$.

$$V_\alpha(m,n) = \begin{cases} V_\alpha(p_n,p_m) & (n = 1 \to N, \quad m = 1 \to N) \\ V_\alpha(k_0,p_m) & (n = N+1, \quad m = 1 \to N) \\ V_\alpha(p_n,k_0) & (n = 1 \to N, \quad m = N+1) \\ V_\alpha(k_0,k_0) & (n = N+1, \quad m = N+1) \end{cases}, \tag{5.21}$$

$$G_{n=m} = \begin{cases} 2w_n p_n^2/(\pi(E - E(p_n)) & (n = 1 \to N) \\ -2\mu\sum_{i=1}^{N}(2w_i k_0^2/(\pi(k_0^2 - p_i^2)) - ik_0 2\mu & (n = N+1). \end{cases} \tag{5.22}$$

We solve the $2\times(N+1)^2$ coupled equations (5.20) by rearranging the matrix equation:

$$[T] = [V] + [VG][T] \tag{5.23}$$

$$\Rightarrow \quad [1 - VG][T] = [V] \tag{5.24}$$

$$\Rightarrow \quad [T] = [1 - VG]^{-1}[V]. \tag{5.25}$$

Equation (5.25) is solved by matrix inversion using the LAPACK routines *zgetrf* and *zgetri*. Although we have found that solutions of these equations with Gaussian

Table 5.3. Notations for spin amplitudes.

$T_{ll'}^{j(ss')}$	$T_{jj}^{j(ss)}$	$T_{jj}^{j(ts)}$	$T_{j-1\,j-1}^{j(tt)}$	$T_{j+1\,j-1}^{j(tt)}$	$T_{j+1\,j+1}^{j(tt)}$	$T_{j-1\,j+1}^{j(tt)}$	$T_{jj}^{j(tt)}$	$T_{jj}^{j(st)}$
$\alpha \equiv N_{spin}$	1	2	3	4	5	6	7	8

elimination is ~30% faster than matrix inversion, we compute the inverse in order to permit a separate computation of the projectile-nucleus wave function with the same inverse matrix:

$$[\psi] = [1 - VG]^{-1}[\phi]. \tag{5.26}$$

As indicated in Table 5.3, there are eight spin channels (represented here as α or by the values of N_{spin}) for each value of l, with these spin channels coupled into pairs of two. (Note the special case, $T_{00}^{0(tt)} = T_{-1\,-1}^{0(tt)} = T_{1\,-1}^{0(tt)} = T_{-1\,1}^{0(tt)} = 0$.) In Phase II of our parallelization, the set of coupled integral equations for each of some 96 l values is solved as a separate process. Each solution is an ideally exportable parallel task since it requires little information, namely the V values, and performs many operations for each input datum while inverting the matrices.

5.2.3. Scattering Observables

Once we have solved the integral equations for the $T_{l'l}^{j(s's)}$'s, the matrix elements in the spin basis $\langle s'm_{s'}|T|sm_s\rangle$ are computed via equations such as (5.9)-(5.10) with the V's replaced by T's. The proton-nucleus $a - f$ amplitudes needed to compute experimental observables are then formed, for example,

$$a = \frac{1}{2}\left(T_{11} + T_{00} - T_{1-1}\right), \qquad f = i\sqrt{2}T_{s1}. \tag{5.27}$$

The amplitudes in Eq. (5.1) describing the scattering of two spin-1/2 particles can form 36 spin observables. For example, the differential cross section and analyzing power are:

$$\frac{d\sigma}{d\Omega} = \frac{1}{2}(|a|^2 + |b|^2 + |c|^2 + |d|^2 + |e|^2 + |f|^2), \tag{5.28}$$

$$A^{(2)}_{oono} = \frac{Re(a^*e + b^*f)}{d\sigma/d\Omega}. \tag{5.29}$$

5.3. PVM IMPLEMENTATION

The parallelization of PPP used the PVM package which functions by starting independent tasks on processors additional to the first and passing messages between the two. This message passing represents an overhead in computational resources because it requires additional operations beyond the algorithm and because any communication protocol is slower than the internal functioning of a serial CPU. Success in parallelization increases with the number of operations to be performed by the remote processor, but is inversely proportional to the amount of data which needs to be communicated between the master program and slave process.

A sample of code from the phase II parallelization shows the procedure. Once the potential has been calculated, the main program spawns slave processes to solve the LS equation. It must then transmit the potential values, along with other important variables, to the slaves by using the PVM communication protocol. Once that loop, addressing each slave in turn, has been completed, another loop, again adressing each slave in turn, must be initiated to receive the results of the calculations.

```
        call pvmfmytid( mytid )
        call pvmfcatchout(1)
c *****     Spawn slave processes        **************
        call pvmfspawn('Conquistador',PVMDEFAULT,'*',ldmax,tids,numt)

c   *************  Pack input data and send to slaves *************
       do 420 ldum = 1,ldmax
            call pvmfinitsend(PVMRAW,bufid)
            call pvmfpack( REAL8, ur(1,1,1), newdim, 1, info)
            call pvmfpack( REAL8, ui(1,1,1), newdim, 1, info)
                 .
                 .
            call pvmfsend( tids(ldum), 1, info)
 420     continue
c  **********   Receive output from slaves    ******************
       do 425 ld = 1,ldmax

           call pvmfrecv(tids(ld), ld, bufid)
           call pvmfunpack( REAL8, ttr(1), 8, 1, info)

 425  continue
```

The slave process program will have mirror coding to receive the input data message and to send the output back to the master program. The PVM subroutines handle all the data encoding and communication protocols. The slave program, called conquistador.f here, includes other subroutines at compile time. It might run

on a different processor of the same machine as the main program, or it might exist on a separate computer connected only via network.

```
      program conquistador
      include '/usr/local/include/fpvm3.h'
      implicit real*8 (a-h, o-z)
      integer info, nproc, nhost, mytid, bufid, consti
         ...
      dimension   den(194) , gp(96) , wt(96) , sigbrn(361)
         ...
c **** Determine Process ID number for this slave and its parent**
               call pvmfmytid( mytid )
               call pvmfparent( mtid )
c **** Receive input data and parameters from parent  ************
          call pvmfunpack( INTEGER4, consti(1), 5, 1, info)
          newdim = consti(5)
          call pvmfunpack( REAL8, ur(1,1,1), newdim, 1, info)
             .
             .
c **** Loop over nspin values in which LS equation is solved *****
         do 410 nspin = 1,8
            call Fmatrx( den , n1 , nmax , nspin , ldum, psfac)
               .
               .
 410     continue
c **** Transmit results back to parent process ******************
        call pvmfinitsend(PVMRAW, bufid)
```

```
call pvmfpack( REAL8, tr(1), 8, 1, info)
call pvmfpack( REAL8, ti(1), 8, 1, info)
call pvmfsend( mtid, ld, info)
 call pvmfexit(info)
end
```

The subroutines called by the slave process perform the computationally involved solution of the LS equation as well as the Coulomb matching [25]. The main processor has moved on to instructing other slaves while the work proceeds on the slave processor.

5.4. RESULTS

It is important to remember that the only goal of parallelizing a code is a realtime speed-up. Traditionally, the goal of optimization has been to reduce CPU time; the fewer the operations, the faster the code. As we have seen, the message passing between processes represents an unavoidable increase in the number of operations. Success, therefore, can only be judged in realtime running length. Fortunately, the IBM SP1 is a single threaded machine. This means that each processor will not be sharing resources with other programs during successive runs of the same calculation, which would lead to widely disparate runtimes. Another consideration unnecessary here is a consideration of varying speeds in the processors making up the virtual machine. The SP1 consists of identical RS-6000 processors connected by fiber optic links. These direct links also help to reduce the latency time in message passing.

Figure 1 plots the phase I parallelization running time of a typical calculation versus the number of processors made available to it. The overhead of the parallel

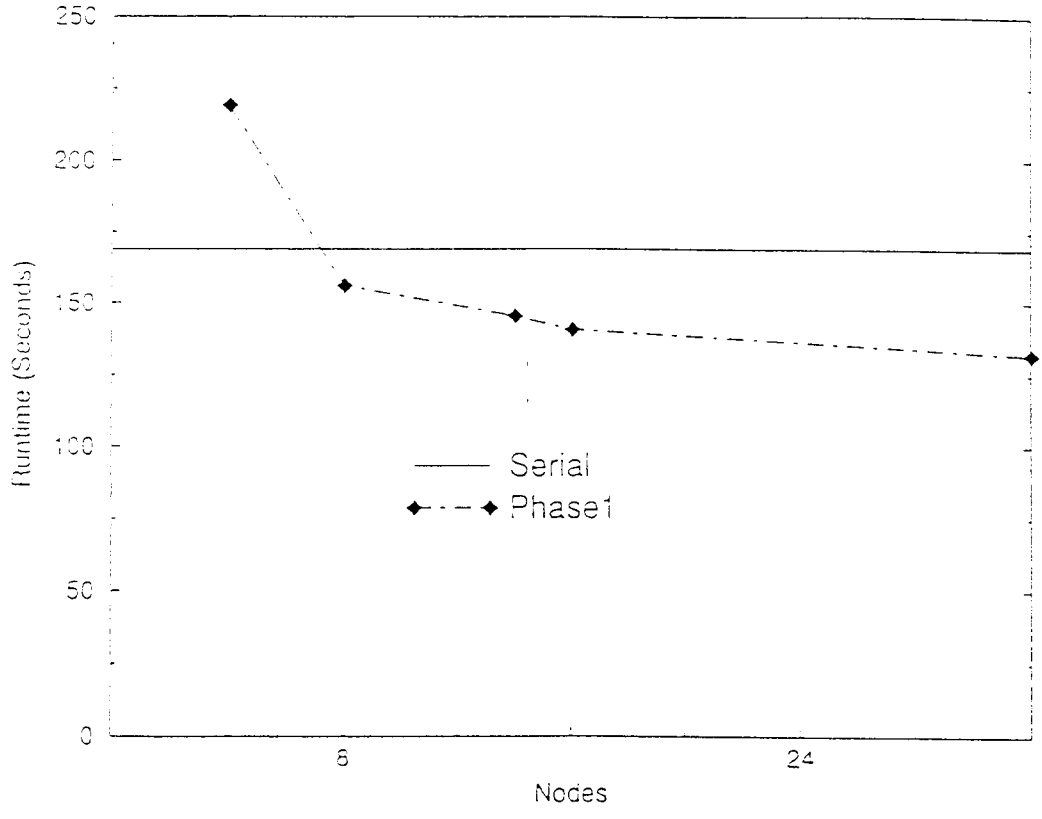

Figure 5.1. Running time versus number of nodes for phase I.

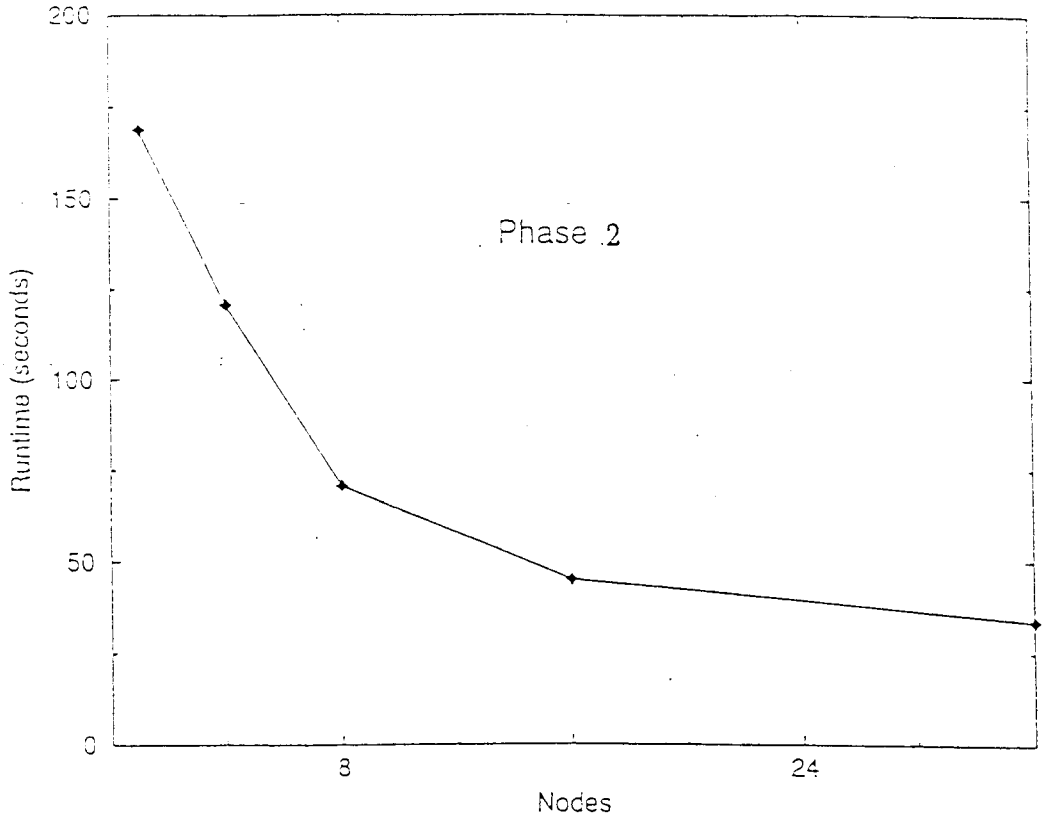

Figure 5.2. Running time versus number of nodes for phase II.

calculation is apparent for small numbers of processors. The serial calculation, at 169 seconds of running time, outperforms the four processor parallel version, using 219 seconds to complete the same calculation.

Figure II plots the same variables for the phase II parallelization. The improvement in running time is immediate and dramatic. The greater ratio of operations performed by slave tasks to messages passed makes this parallel version more effective than serial even for small numbers of processors. Had greater computing resources, allowing us to perform a calculation for every possible number of nodes, been available, this graph would contain discontinuities where the average number of slave tasks per processor crossed an integer number. For instance, a 22 node calculation, corresponding to exactly two slave processes per node, would show a discontinuously smaller running time than calculations using 21 or fewer nodes, which would require at least some nodes to handle three slave tasks.

5.5. CONCLUSION

The use of PVM to parallelize PPP has resulted in a factor of five improvement in running time. The unavoidable processes of loading phase shifts and storing results cannot be optimized; therefore, any additional attempts to speed the calculation promise to present a case of diminishing returns. This speedup makes it possible to run larger calculations with more grid points and greater numbers of partial waves. This should provide for increased accuracy sufficient to make further more sensitive calculations feasible.

5.6. REFERENCES

[1] A. Geist, A. Beguelin, J. Dongarra, W. Jiang, R. Manchek, and V. Sunderam, *PVM 3 User's Guide and Reference Manual* ORNL/TM-12187, (1994).

[2] M. Paez and R. H. Landau, Phys. Rev. C **29**, 2267 (1984).

[3] T. Mefford, R. H. Landau, L. Berge, and K. Amos, Phys. Rev. C **50**, 1648 (1994).

[4] D. Lu, T. Mefford, R. H. Landau, and G. Song, Phys. Rev. C **50**, 3037 (1994).

6. CONCLUSIONS

The theory of the momentum space optical potential for spin $\frac{1}{2} \times \frac{1}{2}$ scattering has been improved significantly over previous versions. [17] We can now calculate a scattering amplitude previously set to zero or included in first Born approximation and we no longer need to treat the Coulomb potential approximately. Running time has been reduced, calculation size has been increased, and in the process, the code has been simplified. The door is now open to further improvements.

Agreement between prediction and data for specific variables has improved dramatically, yet others retain a disparity. [47] In part, this seemingly continual gap between theory and experiment is due to the ever-increasing number of observables for which data is becoming available. The need for greater accuracy and improved theory remains.

The charge-symmetry violation reflected in differences between the up and down quark masses is very small. Seeing it reflected in a gap between a measured observable and a theoretical curve will require a great deal of accuracy and an improvement in theory. The present code is in a position to help determine the accuracy of physical parameters, such as the neutron radii in trinucleons, which are currently insufficiently known to draw any conclusions about charge-symmetry violation. [59]

Further experiments would make such conclusions possible. If they are performed, more accurate theoretical calculations will be required. The groundwork laid

here, with further advances, possibly full-Fermi averaging, inclusion of the second order optical potential, Dirac degrees of freedom, or better nucleon-nucleon phase shifts, will enable agreement between theory and experiment sufficiently accurate to isolate quark-level effects.

BIBLIOGRAPHY

[1] O. Häusser, B. Larson, W.P. Alford, C. Chan, P.P.J. Delheij, R.S. Henderson, K. P. Jackson, R.H. Landau, T. Mefford, C.A. Miller, A. Rahav, L. Ray, A. Trudel, and M.C. Vetterli, Phys. Lett. B **343** 36, (1995).

[2] E. Brash, O. Häusser, W. Cummings, M. Bahrami, P.P.J. Delheij, R. Henderson, M.C. Vetterli, D. Whittal, B. Larson, R.H. Landau, T. Mefford, and L. Ray. submitted for publication, Phys. Rev. C.

[3] M.J. Paez and R. H. Landau, Phys. Rev. C **29**,2267 (1984); **30**, 1757 (1984); Phys. Lett. **142B**, 235 (1984).

[4] R.H. Landau, S.C. Phatak, and F. Tabakin, Ann. Phys. **78**, 299 (1973).

[5] S.J. Seestrom–Morris, M.A. Franey, D. Dehnhard, D.B. Holtkamp, R.L. Bourdie, J.F. Amann, G.C. Idzorek, and C.A. Goulding, Phys. Rev. C **30**, 270 (1984).

[6] L. Ray, G.W. Hoffmann, M.L. Barlett, J.D. Lumpe, B.C. Clark, S. Hama, and R.L. Mercer, Phys. Rev C **37**,1169 (1988).

[7] G.W. Hoffmann, M.L. Barlett, D. Ciskowski, G. Pauletta, M. Purcell, L. Ray, J.F. Amann, J.J. Jarmer, K.W. Jones, S. Penttilä, N. Tanaka, M.M.Gazzaly, J.R. Comfort, B.C. Clark,and S. Hama, Phys. Rev. C **41**, 1651 (1990).

[8] G.W. Hoffmann, M.L. Barlett, W. Kielhorn, G. Pauletta, M. Purcell, L. Ray, J.F. Amann, J.J. Jarmer, K.W. Jones, S. Penttilä, N. Tanaka, G. Burleson, J. Faucett, M. Gilani, G. Kyle, L. Stevens, A.M. Mack, D. Mihailidis, T. Averett, J. Comfort, J. Görgen, J. Tinsley, B.C. Clark, S. Hama, and R.L. Mercer, Phys. Rev. Letters, **65**, 3096 (1990).

[9] G.R. Goldstein and M.J. Moravcsik, Ann. Phys. (N.Y.) **142**, 219 (1982).

[10] M. Goldberger and K. Watson *Collision Theory*, Wiley, New York, 1964.

[11] H.P. Stapp, T.J. Ypsilantis, and N. Metropolis, Physical Review, **105**, 302 (1957).

[12] A. Gersten, Phys. Rev. C **18**, 2252 (1978); Phys. Rev. C **24**, 2174 (1981).

[13] A.G. Williams, A.W. Thomas, and G.A. Miller, Phys. Rev. C **36**, 1956 (1987).

[14] J. Bystricky, F. Lehar, and P. Winternitz, Le Journal de Physique,**39**,1, (1978).

[15] P. La France and P. Winternitz, Le Journal de Physique, **41**,1391 (1980).

[16] P.L. Csonka, Rev. Mod. Phys **37**, 177 (1965).

[17] R.H. Landau, M. Sagen, and G. He, Phys. Rev. C **41**, 50 (1990).

[18] R.H. Landau and M. Sagen, Phys. Rev. C **33**, 447 (1986).

[19] C.W. DeJager, H.DeVries, and C. DeVries, Atomic Data and Nuclear Data Tables **14**, 479 (1974).

[20] B.Bartoli, F. Felicetti, and V.S. Silvestrini, Rev. Nuov. Cim. **2**, 241 (1972).

[21] R.F. Frosch, R. Hofstadter, J.S. McCarthy, G.K. Nöldeke, K.J. vanOostrum, M.R. Yearian, B.C. Clark, R. Herman, and D.G. Ravenhall, Phys. Rev. **174**, 1380 (1968).

[22] R.A. Arndt, L.D. Roper, R.A. Bryan, R.B. Clark, B.J. VerWest, and P. Signell, SAID dial up system, IP no. 128.173.176.61, userid=physics, password=quantum.

[23] K. Schwarz, J. Haidenbauer, and J. Frohlich, Phys. Rev. C **86**, 456 (1986).

[24] C.M. Vincent and S.C. Phatak, Phys. Rev. **10**, 391 (1974).

[25] D. Lu, T. Mefford, R. H. Landau, and G. Song, Phys. Rev. C **50**, 3037 (1994).

[26] H.F. Arellano, F.A. Brieva, and W.G. Love, Phys. Rev C **41**, 2188 (1990).

[27] H.F. Arellano, F.A. Brieva, W.G. Love, and K. Nakayama, *ibid* **43**, 1875 (1991).

[28] L. Ray, Phys. Rev. C 41, 2816 (1990).

[29] L. Ray, Phys. Rev. C 47, 2990 (1993).

[30] B.C. Clark, *Relativstic Dynamics and Quark-Nuclear Physics*, M.B. Johnson and A. Pickelseimer, eds., New York, Wiley, p.302 (1986).

[31] E. Hernàndez and A. Mondragon, Phys. Rev. C **29**, 722 (1984)

[32] G. Garcia-Calderon and R. Peierls, Nucl. Phys. **A265**, 443 (1976).

[33] V. Fock, Z. Physik **98**, 145 (1935).

[34] Y.R. Kwon and F. Tabakin, Phys. Rev. C **18**, 932 (1978).

[35] D.P. Heddle, Y.R. Kwon, and F. Tabakin, Comp. Phys. Comm. **38**, 71 (1985).

[36] A. Cieplý, M. Gmitro, R. Mach, S.S. Kamalov, Phys. Rev. C **44**, 713 (1991).

[37] M. Gmitro, S.S. Kamalov, and R. Mach, Phys. Rev. C **36**, 1105 (1987).

[38] R.H. Landau, Comp. Phys. Comm. **28** 109 (1982).

[39] R. Crespo and J.A. Tostevin, Phys. Rev. C **41**, 2615 (1990).

[40] A. Picklesimer, P.C. Tandy, R.M. Thaler, and D.H. Wolfe, Phys. Rev. C **30**, 2225 (1984).

[41] Ch. Elster, L.C. Liu, and R.M. Thaler, Los Alamos National Laboratory Report LA-OR-90-2126, 1990.

[42] C.R. Chinn, Ch. Elster, and R.M. Thaler, Phys. Rev. C. **44**, 1569 (1991).

[43] R.A. Eisenstein and F. Tabakin, Phys. Rev. C **26**, 1 (1982).

[44] R.H.Landau, Quantum Mechanics II, J. Wiley, New York, 1990.

[45] L.S. Rodberg and R.M. Thaler, *Introduction to the Quantum Theory of Scattering*, Academic Press, New York (1967).

[46] M.J. Páez, M.E. Sagen, and R. H. Landau, Comp. Phys. Comm., **52**, 141 (1988).

[47] T. Mefford, R. H. Landau, L. Berge, and K. Amos, Phys. C **50**, 1648 (1994).

[48] J.M. Blatt, and L.C. Biedenharn, Revs. of Mod. Phys. **24**, 258 (1952).

[49] J.M Eisenberg and W. Greiner, *Nuclear Theory*, Vol. 3, 39 (1972).

[50] O. Häusser, Colloque de Physique, **C6, supp. au 22**, C6-99 (1990) (7^th Int. Conf. on Polarization Phenom. in Nucl. Phys., Paris, 1990).

[51] G. Krein, A.W. Thomas, A.G. Williams, Phys. Lett. **B317**, 293 (1993).

[52] G. Krein, A.G. Williams, Mod. Phys. Lett. **A5** 399 (1990).

[53] G.A. Miller, A.W. Thomas, A.G. Williams, Phys. Rev. Lett. **56**, 2567 (1986).

[54] R. H. Landau, Ann. Phys. **92**, 205 (1975).

[55] Phys. Rev. **15**, 2127 (1977).

[56] C. Pillai, D. B. Barlow, B. L. Berman, W. J. Briscoe, A. Mokhtari, B. M. K. Nefkens, and M. E. Sadler, Phys. Rev. C **43**, 1838 (1991).

[57] B. M. K. Nefkens, W. J. Briscoe, A. D. Eichon, D. H. Fitzgerald, J. A. Holt, A. A. Mokhtari, J. A. Wightman, M. E. Sadler, R. L. Boudrie, and C. L. Morris, Phys. Rev. Lett. **52**, 738 (1984).

[58] K. Y. Kim, Y. E. Kim, and R. H. Landau, Phys. Rev. C **36**, 2155 (1987).

[59] W. R. Gibbs and B. F. Gibson, Phys. Rev. C **43**, 1012 (1991).

[60] L. I. Schiff, Phys. Rev. **133**, B802 (1964).

[61] B. F. Gibson and Schiff, Phys. Rev. **138** B26 (1965).

[62] J. S. McCarthy, I. Sick, and R. R. Whitney, Phys. Rev. C **15**, 1596 (1977).

[63] E. Hadjimichael, B. Goulard, and R. Bournais, Phys. Rev. C **27**, 831 (1983).

[64] H. Collard, R. Hofstader, E. B. Hughes, A. Johansson, M. R. Yearian, R. B. Day, and R. T. Magner, Phys. Rev. **138**, B57, (1965).

[65] D. H. Beck, S. B. Kowalski, M. E. Schulze, W. E. Turchinetz J. W. Lightbody, Jr., X. K. Maruyama, W. J. Stapor, H. S. Caplan, G. A. Retzlaff, D. M. Skopik, and R. Goloskie, Phys. Rev. C **30**, 1403 (1984).

[66] F.-P. Juster, S. Auffret, J.-M. Cavedon, J.-C. Clemens, B. Frois, D. Goutte, M. Huet, P. Leconte, J. Martino, Y. Mizuno, X.-H. Phan, S. Platchkov, S. Williamson, and I. Sick, Phys. Rev. Lett. **55**, 2261 (1985).

[67] T. Mefford, R.H. Landau, "A distributed memory, parallel code for polarized nucleon scattering from polarized nuclei", OSU preprint, submitted to *Computer Physics Communiations.*

[68] A. Geist, A. Beguelin, J. Dongarra, W. Jiang, R. Manchek, and V. Sunderam, *PVM 3 User's Guide and Reference Manual* ORNL/TM-12187, (1994).